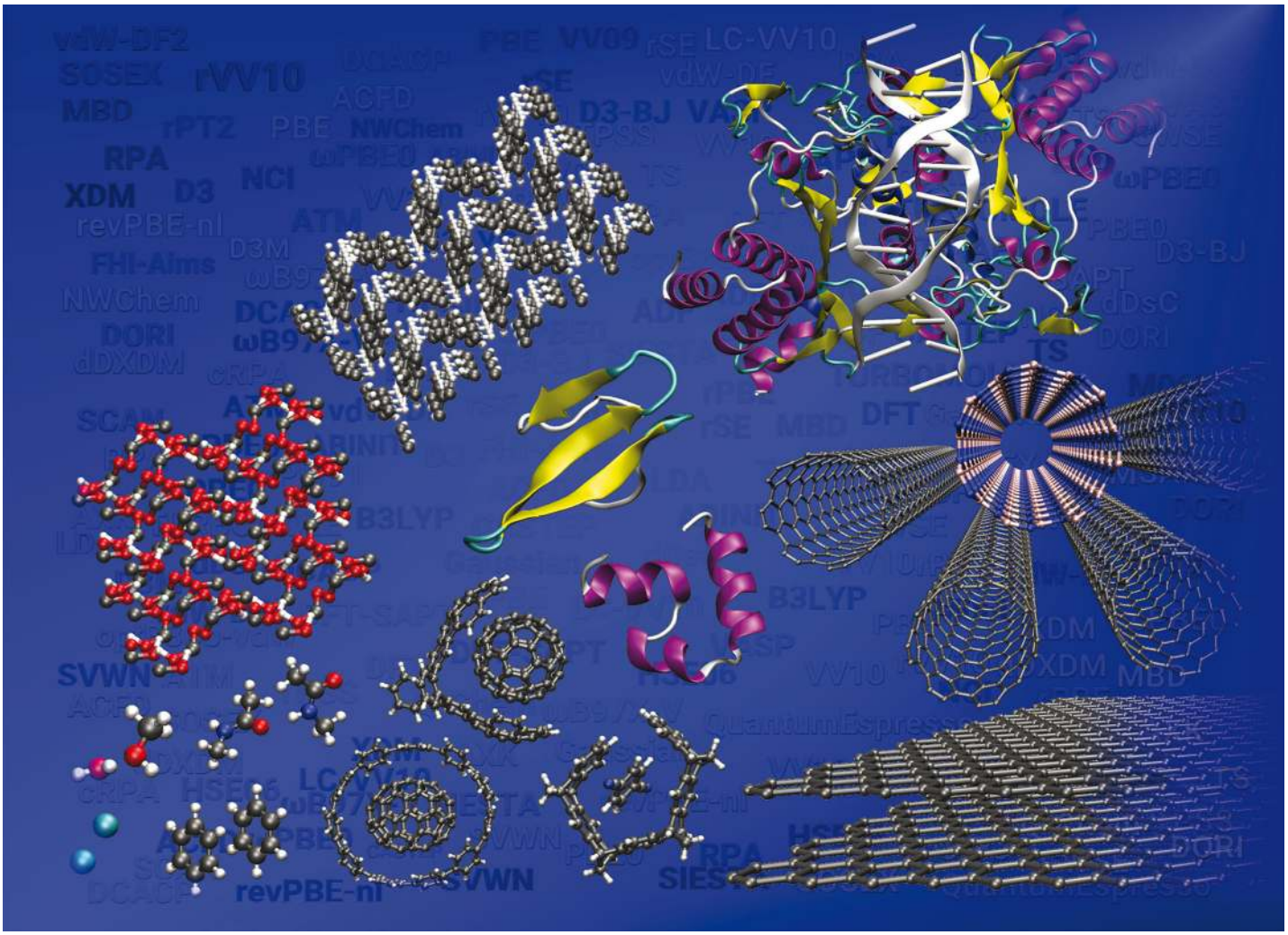

Showcasing a review from the laboratories of Professor Tkatchenko (Physics and Materials Science Research Unit, University of Luxembourg, Luxembourg) and Professor Van Voorhis (Department of Chemistry, Massachusetts Institute of Technology, Cambridge, MA, United States).

Theory and practice of modeling van der Waals interactions in electronic-structure calculations

Van der Waals-inclusive electronic structure theory: a tutorial-style guide through the quantum-mechanical foundations, state-of-the-art methods in computational modeling and their practical application including an introduction to recent methodological developments and complementary experimental techniques for a broad and general audience.

As featured in:

See Alexandre Tkatchenko *et al.*, *Chem. Soc. Rev.*, 2019, **48**, 4118.

ROYAL SOCIETY OF CHEMISTRY | Celebrating IYPT 2019

rsc.li/chem-soc-rev

Registered charity number: 207890

Chem Soc Rev

REVIEW ARTICLE

Cite this: *Chem. Soc. Rev.*, 2019, **48**, 4118

Theory and practice of modeling van der Waals interactions in electronic-structure calculations

Martin Stöhr,[a] Troy Van Voorhis[b] and Alexandre Tkatchenko *[a]

The accurate description of long-range electron correlation, most prominently including van der Waals (vdW) dispersion interactions, represents a particularly challenging task in the modeling of molecules and materials. vdW forces arise from the interaction of quantum-mechanical fluctuations in the electronic charge density. Within (semi-)local density functional approximations or Hartree–Fock theory such interactions are neglected altogether. Non-covalent vdW interactions, however, are ubiquitous in nature and play a key role for the understanding and accurate description of the stability, dynamics, structure, and response properties in a plethora of systems. During the last decade, many promising methods have been developed for modeling vdW interactions in electronic-structure calculations. These methods include vdW-inclusive Density Functional Theory and correlated post-Hartree–Fock approaches. Here, we focus on the methods within the framework of Density Functional Theory, including non-local van der Waals density functionals, interatomic dispersion models within many-body and pairwise formulation, and random phase approximation-based approaches. This review aims to guide the reader through the theoretical foundations of these methods in a tutorial-style manner and, in particular, highlight practical aspects such as the applicability and the advantages and shortcomings of current vdW-inclusive approaches. In addition, we give an overview of complementary experimental approaches, and discuss tools for the qualitative understanding of non-covalent interactions as well as energy decomposition techniques. Besides representing a reference for the current state-of-the-art, this work is thus also designed as a concise and detailed introduction to vdW-inclusive electronic structure calculations for a general and broad audience.

Received 21st February 2019

DOI: 10.1039/c9cs00060g

rsc.li/chem-soc-rev

[a] *Physics and Materials Science Research Unit, University of Luxembourg, L-1511 Luxembourg, Luxembourg. E-mail: alexandre.tkatchenko@uni.lu*

[b] *Department of Chemistry, Massachusetts Institute of Technology, Cambridge, MA, USA*

1 Introduction

The basic challenge when modeling molecules or materials from first principles of quantum mechanics is that it is impossible to exactly solve the many-body problem for a system with many electrons.

Martin Stöhr

Martin Stöhr received a BSc and MSc in Chemistry from the Technical University of Munich. Under the supervision of Karsten Reuter and Reinhard J. Maurer and as a visiting assistant in research with John C. Tully at Yale University, he worked on hybrid organic–inorganic interfaces and methods for efficient van der Waals-inclusive modeling. Now as an AFR PhD fellow with Alexandre Tkatchenko at the University of Luxembourg, his research focuses on dispersion forces in large-scale systems and their interplay with nuclear dynamics.

Troy Van Voorhis

Troy Van Voorhis earned his BS in Chemistry and Mathematics from Rice University in 1997 and his PhD in Chemistry from UC Berkeley in 2001. After a postdoctoral fellowship at Harvard University, he joined the faculty at MIT where he is now the Haslam and Dewey Professor of Chemistry. His research focuses on the study of electron and energy transfer in molecular systems and he has a long standing interest in the development of electronic structure tools for these applications.

The vast majority of practical methods in electronic structure theory approaches this problem by reformulating the *N*-electron problem to *N* effective independent-particle problems. Examples of this are the Hartree–Fock (HF) equations in wavefunction-based methods or the Kohn–Sham (KS) reference system in density functional theory (DFT). This seminal reformulation paves the way to first-principles modeling of molecules and materials and already captures, depending on the system, 99 per cent or more of the total electronic energy.† Unfortunately, the remaining fraction of the total electronic energy can be crucial for various observables and properties of interest, such as relative energies,[1–4] binding properties,[5–9] and structural features[3,4,10,11] as well as the mechanical,[12,13] thermodynamic,[4,14] kinetic,[15–17] and electronic[18,19] signatures of a given system. In the simple case of an Argon dimer for instance, KS-DFT calculation with the hybrid PBE0 functional captures about 99.95% of the total energy, but it gives no more than roughly 15% of the interaction energy. HF does not even bind an Argon dimer. The major part of the missing electronic energy is due to the correlated motion of electrons, or correlated quantum-mechanical fluctuations of the average electron distribution in the DFT picture. It is thus referred to as (long-range) electron correlation energy.‡ In particular, the long-range correlation energy represents a challenging task in electronic structure calculations due to its highly non-local character. The main component of this long-range contribution is what is known as the van der Waals (vdW) dispersion interaction. As such, vdW interactions are inherently quantum-mechanical and many-body ("collective") in nature and, moreover, they are ubiquitous in molecular systems and materials. The strongly non-linear scaling with size in polarizable systems[2,23] presents further challenges for modeling such long-range correlation forces.

Describing (long-range) electron correlation has been a central topic in the quantum chemistry community, which since the early days mainly focused on wavefunction-based methods typically starting from the HF mean-field picture. Thanks to extensive methodological developments a number of asymptotically correct and to some extent practical methods have been devised. Among those the coupled cluster technique has established itself as one of the most prevalent post-HF methods in quantum chemistry. Coupled cluster theory starts from a Slater determinant based on the mean-field HF orbitals and includes excitations by the use of the exponential cluster operator. Such intrinsic electronic excitations represent the analogue of electron density fluctuations in a perturbation picture. Accounting for up to double excitations together with a perturbative treatment of triple excitations, labeled as CCSD(T), is usually referred to as the gold standard and often relied upon as a reference method for more approximate models. However, CCSD(T) and comparably accurate methods are still limited to small- and medium-sized systems (typically less than $\sim$200 atoms) due to the immense computational costs characterized by a scaling of the computation time with the number of electrons to the power of 7. A quite different, yet similarly accurate, approach is Quantum Monte-Carlo (QMC). Here, one solves the many-body Schrödinger equation in a stochastic manner. The most relevant flavors of QMC in the context of modeling molecules and materials are: Variational Monte-Carlo, Green's Function Monte-Carlo and Diffusion Monte-Carlo, which exploits the similarity between Schrödinger's equation and a diffusion equation in imaginary time. Thanks to its stochastic character one can even estimate the expected deviation from the exact solution. Parallelization of this approach is straightforward and tractable system sizes have reached a few hundreds of atoms,[24] which has boosted its use as a benchmark method in recent years. In the end, both CCSD(T) and QMC are typically only used to benchmark (interaction) energies based on a given structure, as force evaluation can become extremely intricate as a result of their perturbative or stochastic character.

In contrast to accurate quantum-chemical methods, density functional approximations (DFAs) require less computational workload and offer access to atomic forces. Since the first successful applications of DFT, however, the lack of explicit electron correlation has proven itself an important issue when modeling molecular systems and gave rise to numerous developments. As of today, a vast number of possible remedies has been proposed. Thereby, an *a posteriori* inclusion of long-range correlation forces is the most widely used approach.

† Even though the KS equations in DFT are, in principle, exact, the universal exchange–correlation functional is yet unknown and the (semi-)local approximations to it based on the uniform electron gas give rise to similar shortcomings.
‡ For completeness: electron correlation is often divided into dynamic and static (or non-dynamic) correlation.[20,21] The dynamic correlation energy, to which vdW interactions can be assigned, represents the energy difference due to approximating the instantaneous interaction of electrons by the interaction of each electron with the average field due to all other electrons (mean field formalism).[20] The energy difference arising when a system cannot be described by a single, pure electronic state *e.g.*, due to (near-)degeneracies of electronic states, is referred to as static (non-dynamic) correlation energy. Proper description of this effect requires so-called multi-reference methods and is beyond the scope of this work, see ref. 22, for instance. In this work, correlation energy shall refer to dynamic correlation only.

Alexandre Tkatchenko

Alexandre Tkatchenko is a Professor and Chair of Theoretical Chemical Physics at the University of Luxembourg. He obtained his bachelor degree in Computer Science and a PhD in Physical Chemistry in Mexico City. Between 2008 and 2016, he was an Alexander von Humboldt Fellow at the Fritz Haber Institute of the Max Planck Society in Berlin and then led an independent research group there. Tkatchenko has given more than 200 invited talks and colloquia worldwide, published more than 140 articles in peer-reviewed academic journals, and serves on the editorial boards of Science Advances and Physical Review Letters. He has received a number of awards, including the Gerhard Ertl Young Investigator Award of the German Physical Society in 2011, and two leadership grants from the European Research Council: a Starting Grant in 2011 and a Consolidator Grant in 2016.

Nevertheless, it is worthwhile to point out that long-range correlation is, in principle, part of the electronic Hamiltonian and can thus also affect the solution of the self-consistent field procedure.[18,19]

In this work, we review the origin of vdW forces and particularly focus on practical approaches how to qualitatively understand and quantitatively model dispersion interactions in electronic structure calculations. We start out by giving an exact formulation based on the non-local electron correlation energy and the approximate reduction to additive two-body interaction potentials and its fundamental limitations in Section 2. Section 3 gives a brief overview of relevant experimental techniques and observations. We then present analysis tools for understanding vdW interactions in Section 4 before describing quantitative and practical approaches for calculating dispersion forces in Section 5. In Section 6, we showcase the performance and some of the strengths and weaknesses of the most widely-used models and Section 7 gives a summary and conclusion of current methods and a short outlook on open problems and future developments. Throughout this work we will focus on approaches within the scope of DFT, being the main workhorse in first-principles modeling of molecules and materials, but we draw connections to wavefunction-based techniques where applicable.

2 van der Waals interactions: formulation from non-local electron correlation

The electron correlation energy, E_{corr}, is typically defined as the difference between the exact (non-relativistic) solution of the Schrödinger equation and the effective mean-field description such as the HF or KS reference system. Hence, it depends on the definition of the mean-field description and can be rigorously formulated in multiple ways.[21] In this work, we rely on the so-called adiabatic-connection fluctuation–dissipation (ACFD) theorem, as it provides a common basis for the majority of methods presented in this article. The ACFD theorem provides an exact formulation of the non-relativistic (non-retarded) exchange and correlation energy of a system in terms of the Coulomb-coupled density response on top of an independent-particle framework such as the HF or KS reference system. Relativistic effects such as retardation and scattering as well as thermal field fluctuations can play an important role for extended, mesoscopic systems (*cf.* Casimir forces), but will not be covered in this work. For reviews on this topic, see ref. 25 or 26, for instance.

2.1 Exact formulation from the adiabatic-connection fluctuation–dissipation theorem

The ACFD formula originates from linear response theory§ and relies on the non-local, time-dependent density–density response function, $\chi(\mathbf{r},\mathbf{r}',t,t')$, which describes the response of an electron density at point $\mathbf{r}$ and time t to a perturbation at position $\mathbf{r}'$ at time t'. Under the assumption of time invariance, which holds for stationary states in quantum mechanics, the time-dependent density response can be Fourier-transformed to the frequency domain yielding the non-local, frequency-dependent, and complex-valued density response, $\chi(\mathbf{r},\mathbf{r}',\omega)$. Thereby, the imaginary part describes the contribution due to dissipation.[28] Hence, integrating over the Coulomb-coupled imaginary part of $\chi(\mathbf{r},\mathbf{r}',\omega)$ gives the energy due to dissipation of a (scalar) perturbation.

In quantum mechanics, any charge density is subject to instantaneous fluctuations, which gives rise to intrinsic fluctuations of the electric field within the system (or *vice versa*). The electron correlation energy is the dissipation energy of this fluctuating electric field. The ACFD theorem states that the energy due to dissipation of such internal perturbations is the same as for external perturbations and can thus be calculated *via* the imaginary part of $\chi(\mathbf{r},\mathbf{r}',\omega)$. Evaluation of the correlation energy on top of an independent-particle formalism is then carried out by means of the adiabatic theorem,[29,30] meaning *via* coupling parameter integration from the non-correlated system to the fully correlated density response (atomic units used throughout this work):

$$E_{\mathrm{corr}} = -\frac{1}{2\pi}\int_0^\infty \mathrm{d}\omega \int_0^1 \mathrm{d}\lambda \iint \mathrm{d}\mathbf{r}\mathrm{d}\mathbf{r}' [\chi_\lambda(\mathbf{r},\mathbf{r}',i\omega) - \chi_{\lambda=0}(\mathbf{r},\mathbf{r}',i\omega)]\mathscr{V}_{\mathrm{Coul}}(\mathbf{r},\mathbf{r}') \quad (1)$$

with λ as the coupling constant, where $\lambda = 1$ corresponds to the real, fully correlated system and $\lambda = 0$ to the non-correlated system of independent electrons, *e.g.*, the KS (or HF) reference system. $\mathscr{V}_{\mathrm{Coul}} = 1/\|\mathbf{r}-\mathbf{r}'\|$ is the Coulomb potential, with $\|\mathbf{r}-\mathbf{r}'\|$ being the (Euclidean) distance between the points $\mathbf{r}$ and $\mathbf{r}'$. For the integration of the imaginary part of $\chi(\mathbf{r},\mathbf{r}',\omega)$ we have used:[28]

$$\int_0^\infty \mathrm{Im}\chi(\mathbf{r},\mathbf{r}',\omega)\mathrm{d}\omega = \int_0^\infty \chi(\mathbf{r},\mathbf{r}',i\omega)\mathrm{d}\omega. \quad (2)$$

To further simplify the derivation and explanation of the practical approaches outlined below, we may also reformulate the ACFD formula (1) in terms of the non-local, frequency-dependent polarizability tensor $\boldsymbol{\alpha}(\mathbf{r},\mathbf{r},i\omega)$, which is connected to the density response *via* $\chi(\mathbf{r},\mathbf{r}',i\omega) = \nabla_{\mathbf{r}}\nabla_{\mathbf{r}'}\boldsymbol{\alpha}(\mathbf{r},\mathbf{r}',i\omega)$. Introducing the dipole coupling tensor $\mathbf{T}(\mathbf{r},\mathbf{r}') = -\nabla_{\mathbf{r}} \otimes \nabla_{\mathbf{r}'}\mathscr{V}_{\mathrm{Coul}}(\mathbf{r},\mathbf{r}')$, one can rewrite eqn (1) as,

$$E_{\mathrm{corr}} = \frac{1}{2\pi}\int_0^\infty \mathrm{d}\omega \int_0^1 \mathrm{d}\lambda \iint \mathrm{d}\mathbf{r}\mathrm{d}\mathbf{r}' \mathrm{Tr}\{[\boldsymbol{\alpha}_\lambda(\mathbf{r},\mathbf{r}',i\omega) - \boldsymbol{\alpha}_{\lambda=0}(\mathbf{r},\mathbf{r}',i\omega)]\mathbf{T}(\mathbf{r},\mathbf{r}')\}, \quad (3)$$

where $\mathrm{Tr}\{\cdot\}$ denotes the trace operator over Cartesian components.[27] The non-local polarizability within the independent-particle framework ($\boldsymbol{\alpha}_{\lambda=0}$) can be directly calculated based on the single-particle states *via* the Adler–Wiser formula[31,32] and the polarizability tensor of the correlated system can be defined *via*

§ We point out, that while the response of a material can be highly non-linear, the electron correlation energy can be fully recovered solely based on linear response functions, which allows linear response theory and the ACFD theorem to be exact.[27]

the self-consistent Dyson equation,

$$\begin{aligned}\boldsymbol{\alpha}_\lambda(\mathbf{r},\mathbf{r}',i\omega) &= \boldsymbol{\alpha}_{\lambda=0}(\mathbf{r},\mathbf{r}',i\omega) - \iint \boldsymbol{\alpha}_{\lambda=0}(\mathbf{r},\mathbf{r}'',i\omega) \\ &\quad \times \lambda \mathbf{T}_{\mathrm{xc},\lambda}(\mathbf{r}'',\mathbf{r}''',i\omega)\boldsymbol{\alpha}_\lambda(\mathbf{r}''',\mathbf{r}',i\omega)\mathrm{d}\mathbf{r}''\mathrm{d}\mathbf{r}''' \\ &\equiv \boldsymbol{\alpha}_0 - \left\langle \lambda \boldsymbol{\alpha}_0 \mathbf{T}_{\mathrm{xc},\lambda}\boldsymbol{\alpha}_\lambda \right\rangle_{\mathbf{r}'',\mathbf{r}'''} \\ &= \sum_{n=0}^{\infty} \left\langle \boldsymbol{\alpha}_0 \left(-\lambda \mathbf{T}_{\mathrm{xc},\lambda}\boldsymbol{\alpha}_0\right)^n \right\rangle_{\mathbf{r}'',\mathbf{r}'''},\end{aligned} \tag{4}$$

where we have introduced the shorthand $\langle\cdot\rangle_{\mathbf{r}'',\mathbf{r}'''}$ for the integration over spatial coordinates, $\mathbf{r}''$ and $\mathbf{r}'''$, and skipped the explicit notion of the variables of $\boldsymbol{\alpha}$ and $\mathbf{T}_{\mathrm{xc},\lambda}$ for clarity. The coupling tensor $\mathbf{T}_{\mathrm{xc},\lambda}$ is defined for each coupling constant λ as,[27]

$$\mathbf{T}_{\mathrm{xc},\lambda}(\mathbf{r}'',\mathbf{r}''',\omega) = \mathbf{T}(\mathbf{r}'',\mathbf{r}''') - \frac{1}{\lambda}\nabla_{\mathbf{r}''} \otimes \nabla_{\mathbf{r}'''} f_{\mathrm{xc},\lambda}(\mathbf{r}'',\mathbf{r}''',\omega). \tag{5}$$

In practice, the exact exchange–correlation kernel, $f_{\mathrm{xc},\lambda}$, in eqn (5) is not known. Thus, direct evaluation of the ACFD formula, both in terms of χ and $\boldsymbol{\alpha}$, is not possible. Practical approaches that directly involve the ACFD formulation therefore involve the neglect of the explicit dependence on λ and additional approximations for the exchange–correlation kernel. The most prominent method among those relies on the random phase approximation and is covered in further detail in Section 5.1.

For the purpose of discussing vdW interactions, *i.e.*, long-range correlation forces, and especially for comparing the various approaches to describe vdW interactions, it is worthwhile to further separate the above exact formulation of the electron correlation energy into short- and long-range contributions as detailed in ref. 27 and 33. For this, we split the coupling tensors in eqn (3) and (4) by means of a range-separating function $g_{\mathrm{rs}}(\|\mathbf{r}-\mathbf{r}'\|)$, which satisfies $g_{\mathrm{rs}}(0) = 0$ and $g_{\mathrm{rs}}(\|\mathbf{r}-\mathbf{r}'\| \to \infty) = 1$. This separates the total electron correlation energy into a short- and a long-range contribution, where the latter can be seen as an analogue to the original definition of vdW dispersion interactions based on a perturbative picture of intermolecular interactions.[27] In the Dyson eqn (4), we may range-separate the full coupling tensor, $\mathbf{T}_{\mathrm{xc},\lambda}$, into a short- and a long-range screening tensor ($\mathbf{T}^{(\mathrm{sr})}_{\mathrm{xc},\lambda}$ and $\mathbf{T}^{(\mathrm{lr})}_{\mathrm{xc},\lambda}$, respectively) according to

$$\begin{aligned}\mathbf{T}_{\mathrm{xc},\lambda} &= \underbrace{[1 - g_{\mathrm{rs}}(\|\mathbf{r}-\mathbf{r}'\|)]\mathbf{T}_{\mathrm{xc},\lambda}} + \underbrace{g_{\mathrm{rs}}(\|\mathbf{r}-\mathbf{r}'\|)\mathbf{T}_{\mathrm{xc},\lambda}} \\ &= \qquad \mathbf{T}^{(\mathrm{sr})}_{\mathrm{xc},\lambda} \qquad + \qquad \mathbf{T}^{(\mathrm{lr})}_{\mathrm{xc},\lambda},\end{aligned} \tag{6}$$

which in turn account for short- and long-range screening of the non-local polarizability, respectively. Inserting this into eqn (4) and subsequently contracting all short-range screening components lets us define an effective, non-local polarizability, $\boldsymbol{\alpha}^{(\mathrm{sr})}$, which already includes short-range screening. By the use of this definition, eqn (4) becomes

$$\boldsymbol{\alpha}_\lambda = \sum_{n=0}^{\infty} \left\langle \boldsymbol{\alpha}^{(\mathrm{sr})} \left(-\lambda \mathbf{T}^{(\lambda)}_{\mathrm{xc,lr}} \boldsymbol{\alpha}^{(\mathrm{sr})}\right)^n \right\rangle_{\mathbf{r}'',\mathbf{r}'''}. \tag{7}$$

Finally, combining eqn (7) and the long-range part of the ACFD formula (3) gives the long-range electron correlation energy,

$$\begin{aligned}E^{(\mathrm{lr})}_{\mathrm{corr}} &= -\sum_{n=1}^{\infty} \frac{1}{2\pi}\int_0^\infty \mathrm{d}\omega \int_0^1 \mathrm{d}\lambda \\ &\quad \times \left\langle \mathrm{Tr}\left\{ \left[\left\langle \boldsymbol{\alpha}^{(\mathrm{sr})} \left(\lambda \mathbf{T}^{(\mathrm{lr})}_{\mathrm{xc},\lambda} \boldsymbol{\alpha}^{(\mathrm{sr})}\right)^n \right\rangle_{\mathbf{r}'',\mathbf{r}'''} \right] \mathbf{T}_{\mathrm{lr}}(\mathbf{r},\mathbf{r}') \right\} \right\rangle_{\mathbf{r},\mathbf{r}'},\end{aligned} \tag{8}$$

where $\mathbf{T}_{\mathrm{lr}}$ is the long-range part of the bare dipole coupling tensor and the $n = 0$ term cancels out. Note that we have not introduced any approximations up to this point and the sum of eqn (8) and its short-range analogue still equals the exact total correlation energy as defined by eqn (3). In this work, we use the above definition of the long-range correlation energy (8) as the vdW energy for all non-perturbative approaches to dispersion interactions and as we shall see, many widely-used vdW models can be traced down to this form of the ACFD formula, where each flavor involves a given approximation for the effective polarizability after short-range screening, $\boldsymbol{\alpha}^{(\mathrm{sr})}$, and the exchange–correlation kernel in $\mathbf{T}^{(\mathrm{lr})}_{\mathrm{xc},\lambda}$ or combinations thereof.

2.2 Approximate reduction to interaction coefficients

As can be seen from the definitions in Section 2.1, the polarizability and the electron correlation energy have a highly complex, non-local character. As of today, numerous experimental and theoretical works have clearly shown the many-body nature of dispersion forces. Nonetheless, one of the most common approaches to model vdW interactions is by the use of pairwise-additive potentials. In this section, we sketch the approximations and basic steps leading to the fundamental form of pairwise potentials for long-range correlation forces based on the long-range ACFD formula (8). At this point, we would like to note that the functional form derived below can be, and was obtained, in multiple ways including (many-body) perturbation theory and other approximations to the ACFD formula.

One of the most successful and common approximations is the so-called random phase approximation (RPA), which corresponds to the neglect of the unknown exchange–correlation kernel ($f_{\mathrm{xc},\lambda} = 0$). Within the range-separated ACFD formula, we may apply that approximation only in the long-range part, where $f_{\mathrm{xc},\lambda}$ indeed barely contributes, such that $\mathbf{T}^{(\mathrm{lr})}_{\mathrm{xc},\lambda}$ in eqn (8) no longer explicitly depends on λ and reduces to $\mathbf{T}_{\mathrm{lr}}$. This allows us to analytically carry out the integration over the coupling constant, which leads to the series

$$\begin{aligned}E^{(\mathrm{lr,RPA})}_{\mathrm{corr}} &= -\sum_{n=2}^{\infty} \frac{(-1)^n}{n}\frac{1}{2\pi}\int_0^\infty \mathrm{d}\omega \\ &\quad \times \left\langle \mathrm{Tr}\left\{ \left\langle \left(\boldsymbol{\alpha}^{(\mathrm{sr})}\mathbf{T}_{\mathrm{lr}}\right)^n \right\rangle_{\mathbf{r}'',\mathbf{r}'''} \right\} \right\rangle_{\mathbf{r},\mathbf{r}'}\end{aligned} \tag{9}$$

where the index n is shifted by +1 due to integration over λ.

Next, we approximate the non-local polarizability by a sum of point-like, local polarizabilities situated at the N atomic positions, $\{\mathbf{R}_A\}$, by the use of the three-dimensional Dirac delta-function, $\delta^3(\mathbf{r})$:

$$\boldsymbol{\alpha}^{(\mathrm{sr})} \approx \sum_{A=1}^{N} \boldsymbol{\alpha}_A^{(\mathrm{sr})}(i\omega)\delta^3(\mathbf{r}-\mathbf{R}_A)\delta^3(\mathbf{r}-\mathbf{r}') \equiv \sum_{A=1}^{N} \boldsymbol{\alpha}_A^{(\mathrm{sr})}. \tag{10}$$

Inserting this into the long-range RPA correlation energy gives,

$$E_{\mathrm{corr}}^{(\mathrm{lr,RPA})} \approx -\sum_{n=2}^{\infty} \frac{(-1)^n}{n} \frac{1}{2\pi} \int_0^{\infty} \mathrm{d}\omega \times \left\langle \mathrm{Tr}\left\{ \left\langle \left(\sum_{A=1}^{N} \boldsymbol{\alpha}_A^{(\mathrm{sr})} \mathbf{T}_{\mathrm{lr}} \right)^n \right\rangle_{\mathbf{r}'',\mathbf{r}'''} \right\} \right\rangle_{\mathbf{r},\mathbf{r}'} . \tag{11}$$

It can be seen that we get $\boldsymbol{\alpha}_A^{(\mathrm{sr})}\mathbf{T}_{\mathrm{lr}}\boldsymbol{\alpha}_B^{(\mathrm{sr})}\mathbf{T}_{\mathrm{lr}}$ for $n = 2$, $\boldsymbol{\alpha}_A^{(\mathrm{sr})}\mathbf{T}_{\mathrm{lr}}\boldsymbol{\alpha}_B^{(\mathrm{sr})}\mathbf{T}_{\mathrm{lr}}\boldsymbol{\alpha}_C^{(\mathrm{sr})}\mathbf{T}_{\mathrm{lr}}$ for $n = 3$, and so on. Thus, the expansion series (11) is a series of all the n^{th}-order correlation terms. As such, the order n does not represent a pure n-body (in this work, body refers to atom) vdW interaction term, as for instance defined in the perturbational approach. For example, $n = 3$ contains non-vanishing terms with $C = A$, which correspond to screened two-body interactions.

$n = 2$, on the other side, only involves non-vanishing terms with two different polarizability centers A and B and is therefore a pure (yet incomplete) two-body vdW interaction. If we limit ourselves to this second-order term, $E_{\mathrm{corr}}^{(2)}$, we can carry out the integration over spatial coordinates to arrive at,

$$E_{\mathrm{corr}}^{(2)} = -\frac{1}{2}\frac{1}{2\pi}\int_0^{\infty} \mathrm{d}\omega \mathrm{Tr}\left\{ \sum_{A,B} \boldsymbol{\alpha}_A^{(\mathrm{sr})} \mathbf{T}_{AB}^{(\mathrm{lr})} \boldsymbol{\alpha}_B^{(\mathrm{sr})} \mathbf{T}_{BA}^{(\mathrm{lr})} \right\}, \tag{12}$$

where $\mathbf{T}_{AB}^{(\mathrm{lr})} \equiv \mathbf{T}_{\mathrm{lr}}(\mathbf{R}_A,\mathbf{R}_B)$. As a final approximation, we assume the point polarizabilities to be isotropic, *i.e.*, $\boldsymbol{\alpha}_A^{(\mathrm{sr})} = \alpha_A^{(\mathrm{sr})}\mathbf{1}$, with $\mathbf{1}$ being (3×3) unity. As a result, the polarizabilities and dipole tensors commute and

$$E_{\mathrm{corr}}^{(2)} = -\frac{1}{2}\sum_{A,B}\frac{3}{\pi}\int_0^{\infty} \alpha_A^{(\mathrm{sr})}\alpha_B^{(\mathrm{sr})}\mathrm{d}\omega \frac{1}{6}\mathrm{Tr}\left\{ \mathbf{T}_{AB}^{(\mathrm{lr})}\mathbf{T}_{BA}^{(\mathrm{lr})} \right\}. \tag{13}$$

The integral in the above equation is known as the Casimir–Polder integral[34] and corresponds to the so-called C_6-interaction coefficient (Hamaker constant for macroscopic spherical bodies[35]). Noting that $\mathbf{T}_{AB}^{(\mathrm{lr})} = g_{\mathrm{rs}}(\|\mathbf{R}_A - \mathbf{R}_B\|)\mathbf{T}_{AB}$, $\mathbf{T}_{AA} = \mathbf{0}$, and $\mathrm{Tr}\{\mathbf{T}_{AB}\mathbf{T}_{BA}\} = 6/\|\mathbf{R}_A - \mathbf{R}_B\|^6$ leads to

$$\begin{aligned} E_{\mathrm{corr}}^{(2)} &= -\frac{1}{2}\sum_{A\neq B}\underbrace{\frac{3}{\pi}\int_0^{\infty} \alpha_A^{(\mathrm{sr})}\alpha_B^{(\mathrm{sr})}\mathrm{d}\omega}_{C_{6,AB}^{(\mathrm{eff})}} \frac{g_{\mathrm{rs}}(\|\mathbf{R}_A - \mathbf{R}_B\|)^2}{\|\mathbf{R}_A - \mathbf{R}_B\|^6} \\ &= -\frac{1}{2}\sum_{A\neq B} C_{6,AB}^{(\mathrm{eff})} \frac{f_{\mathrm{damp}}(R_{AB})}{{R_{AB}}^6}, \end{aligned} \tag{14}$$

where we have used $R_{AB} = ||\mathbf{R}_A - \mathbf{R}_B||$ and introduced the damping function $f_{\mathrm{damp}}(R_{AB}) = g_{\mathrm{rs}}(R_{AB})^2$. This is the well-known formula for the vdW dispersion interaction between two microscopic bodies within the dipole approximation as first derived by London.[36] As of today, a manifold of pairwise-additive vdW models has been devised and widely used.[37–45] The general difference between those models lies in the damping function, f_{damp}, and how effective, short-range screened interaction coefficients are obtained. It is worthwhile to point out that the same functional form can be derived based on a full-range RPA of eqn (3), by invoking the so-called full potential approximation, *i.e.*, $\boldsymbol{\alpha}_\lambda = \boldsymbol{\alpha}_1$,[46] from a model system of Quantum Drude Oscillators[47] or in various ways from (second-order) perturbation theory invoking a multipole expansion and subsequent dipole approximation for the interaction potential.[47]

2.3 Non-additive aspects of van der Waals interactions

The above derivations show the theoretical foundation of vdW dispersion interactions and with eqn (14) we have derived an approximated expression. However, no seamless way of obtaining the damping function, the short-range screened polarizabilities, or the resulting C_6-interaction coefficients has been put forward as of the time of this article. In addition, the expansion (or corresponding perturbation) series is truncated at second order and one has to invoke an additional approximation for the – at least long-range part of the – coupling potential, $\mathbf{T}_{\mathrm{xc},\lambda}$, to arrive at the pairwise formula (14). As classified by Dobson, effects beyond this pairwise-additive expression for vdW interactions can, in general, be understood in terms of three types of non-additivity,[48]

- Type A: the effect of the local chemical environment on the polarizability apart from short-range screening. One often relies on partitioning the system into its constituent atoms for the construction of the polarizability of the (sub)system. Type A non-additivity can be understood by the fact that the polarizability in the KS reference system does not correspond to a superposition of $\boldsymbol{\alpha}_0$ of isolated atoms. This type of non-additivity is accounted for in almost all modern vdW models.
- Type B: electron correlation and screening are defined by multi-center integrals. This enters the ACFD formalism both in form of the electrodynamic screening in the Dyson-like eqn (4) as well as in the expansion series of the (long-range) correlation energy to finite orders of n in eqn (8), *i.e.*, many-body interactions and higher-order correlation terms. The difference of coupled N-center interactions and a sum of pairwise terms is illustrated in Fig. 1: in the pairwise formula, the energy arises as the sum of the interaction of pairs of instantaneous dipoles, which fluctuate in ideal alignment. However, all fluctuations are coupled simultaneously (multi-center interaction), which does not necessarily correspond to a sum of ideally correlated dipoles as shown by select collective density fluctuation patterns for the simple example of an Argon trimer in Fig. 1 (right). This type of non-additivity manifests itself particularly in (sub)systems with strong anisotropy, complex geometrical arrangements, or reduced symmetry (1D, 2D materials) and can substantially alter the scaling laws for vdW interactions.[2,23,27,48–50]
- Type C: assigned to systems with extremely large delocalization lengths, basically corresponding to intrinsic electron hopping between atomic centers. Such phenomena cannot fully be described within an atom-centered framework of polarizability and electronic fluctuations. Understandably, type C non-additivity almost exclusively appears in systems with a

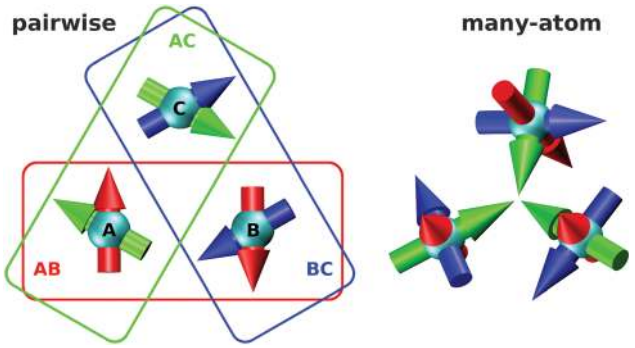

Fig. 1 Illustrative comparison of the (assumed) physics behind pairwise-additive (left) and many-atom (right) van der Waals interactions in an interatomic picture for an Argon (cyan) trimer. The arrows of a given color each depict an "eigenmode" of simultaneous electron density fluctuations. In the dipole-limit, these represent the alignment of fluctuating, instantaneous dipoles. See text for further discussion.

(near-)zero band (or HOMO–LUMO) gap, which allow for quantum-mechanical fluctuations to cause instantaneous electron hopping.[48]

3 van der Waals forces in experiment

3.1 Experimental assessment

As a result of the non-additive and non-pairwise effects outlined above, the simplified additive description in eqn (14) has been found to be insufficient for a variety of systems and an increasing number of experiments showcase the non-local and non-additive character of vdW dispersion interactions. In this regard, it has to be mentioned that direct experimental assessment of vdW interactions is intrinsically difficult as they are typically intertwined with several other (non-covalent) interactions and appear on all scales including intra- as well as intermolecular forces. This, obviously, complicates a clear-cut direct analysis from experimental observables. A very successful approach to disentangle non-covalent interactions is *via* competition methods (see *e.g.*, ref. 51 and 52), where one relies on a comparison of the binding energies among well-controlled complementary systems or interaction mechanisms. Such complementary systems include structural mutations, varying binding partners, or different solvents. This, however, has the disadvantage that the molecule or material must not exhibit significant structural distortions or different interaction mechanisms among the modifications, which is mostly not given for complex systems like biopolymers, for example. In addition, measurements require highly accurate force measurements under well-defined experimental conditions on a microscopic level,[26] which ideally involves accurate control over position and balancing potentials on the level of individual atoms or molecules. For instance, Chemical Force Microscopy (CFM),[53] which relies on chemical functionalization of Atomic Force Microscopy (AFM) probes, represents a very promising technique to directly measure non-covalent interactions, but requires special position control of one of the binding partners.[54]

The common experimental techniques to study vdW interactions can be categorized into measurements of binding affinities and kinetics of vdW-bound systems and spectroscopy. Among others, the former group includes AFM/CFM, Surface Plasmon Resonance experiments, as well as (spectroscopic) titration techniques and sublimation experiments like (micro-)calorimetry. On the one side, these methods by now undoubtedly provide highly accurate results and vital insights into the properties and behavior of the system under consideration. On the other side, the computational costs of most electronic structure methods prohibit a sufficiently complete description of the thermodynamics to be directly compared to these experiments. Comparisons to this kind of experiment therefore usually rely on "experimentally derived" interaction energies, where approximate models are used to estimate the effect of experimental conditions such as finite temperature and solvent (see *e.g.*, the S12L and X23 benchmark set introduced in Section 6.1). Of course, this can introduce considerable uncertainties in the experimental reference.[8,55]

Spectroscopic techniques like Nuclear Magnetic Response measurements, Terahertz (THz) experiments, or X-ray spectroscopy, for example, mostly provide information on the system's structure and (roto-)vibrational response. THz spectroscopy thereby represents a versatile and particularly promising approach in our view as it probes more collective vibrations, for which long-range interactions naturally play a pivotal role. Non-linear, *i.e.*, multi-dimensional, THz spectroscopy then even allows to investigate long-range dynamics and non-local response properties as shown in ref. 56, for instance. In general, multi-dimensional approaches, also including 2D electronic spectroscopy, can provide insights into long-range and long-timescale (relaxation) dynamics, where we expect an important role of non-local interactions for the dynamics and dissipation channels of a system. Disentangling the spectroscopic features for complex systems beyond a few atoms usually poses a very challenging task, however. The increased population of rotationally and vibrationally excited states due to temperature further complicates this problem. To limit this aspect, spectroscopic measurements are typically combined with jet-cooling techniques.[57] In addition, the analysis of experimental spectra is usually performed in conjunction with computationally demanding simulations and thus limited to small- or medium-sized systems.[54] This, of course, limits the exploration of the highly non-trivial behavior of electron correlation at increased system size and complexity.

Despite or maybe even due to the challenges and limitations, the experimental assessment of vdW forces represents a rapidly progressing field, in which probably three classes of systems have emerged as main work horses: hybrid inorganic–organic systems (non-covalent surface bonding), supramolecular complexes, and layered materials (multiple two-dimensional systems bound by vdW forces – often even referred to as vdW materials). Obviously, the main characteristic is that within these classes one can realize systems that are predominantly or almost exclusively vdW-bound. In addition, hybrid inorganic–organic systems are naturally predestined for AFM/CFM measurements and therefore allow for accurate and direct probing of non-covalent interactions. (Synthetic) supramolecular complexes are most often stable

over a wide range of conditions including varying temperature and solvents and can easily be mutated, which enables reliable competition methods.[54] Layered materials offer a wide range of hetero- and homo-structures, which can be realized on various length scales. This allows to observe interlayer (vdW) interactions for a variety of mono-layer properties and different contact areas through mechanical or chemical exfoliation, for instance. This feature, which is also true for hybrid inorganic–organic systems, enables studies on the scaling behavior of vdW forces with increasing "interaction area". Additionally, the interlayer interaction is almost exclusively due to dispersion forces, which reduces the otherwise complicated disentanglement from other non-covalent contributions.

Ultimately, vdW forces play a significant role for the stability, dynamics, and response of a molecular system or material. Thus, they can be readily observed indirectly from a variety of experimental measurements in combination with complimentary vdW-inclusive modeling. Deviations from an experimental reference in terms of such (indirect) manifestations of vdW interactions, however, represent a conglomeration of potential errors and a seamless conclusion about dispersion forces is often very limited. For further details on the experimental assessment of vdW interactions and non-covalent forces in general, we refer the interested reader to the rich set of reviews on this topic.[54,57,58]

3.2 Non-additivity in experiment

Following up on the discussion of effects beyond pairwise additivity in Section 2.3, we will conclude this section by highlighting some of the experimental observations of the non-additive nature of dispersion forces. One of the most well-known deviations from pairwise additivity thereby appears when a single atom or molecule is interacting with a metallic surface. Since the early theoretical works by Lifshitz[59] and Zaremba and Kohn[60] it is known that, at larger separations, the interaction energy follows a D^{-3} power law, where D is the distance of the atom or molecule to the surface. AFM measurements by Wagner *et al.*[61] confirmed this scaling law and quantified the non-additivity. Also between adsorbed molecules, several experiments observed strongly non-additive long-range interactions.[62–64]

In a study on the adsorption of gold nanoparticles on multi-walled carbon nanotubes, Rance *et al.* showed that the adsorption affinity scales quadratically with the accessible surface area of the nanotubes and is highly non-linear for more complex nanostructures.[65] In constrast, pairwise-additive vdW models, neglecting molecular anisotropy and collective behavior, predict a simple linear dependence in those cases. Batista *et al.* emphasize that the non-additivity of interactions, including dispersion forces, arise particularly at the nanoscale[66] due to complex geometrical arrangements and the resulting polarizability anisotropy. Such behavior beyond pairwise additivity, however, also extends from the nano-scale to the meso- and macro-scale as shown by the interaction range of proteins, bacteria, and gecko feet with bulk silicon. By separating the respective adhesive partner and the silicon substrate with an increasing layer of silicon dioxide, Loskill *et al.* showed that the interaction extends up to a separation of 10–20 nm,[67,68] while a pairwise formalism predicts only 1 nm. On the other side, covering dielectric bulk materials with strongly anisotropic monolayers can also screen the vdW interaction between the surface and an adsorbed molecule. Using AFM, it has been shown that the D^{-3}-dependence predicted by Lifshitz–Zaremba–Kohn theory holds for the interaction of the metallic AFM tip with pristine silicon dioxide. When the surface is covered by a 2D-material, such as graphene or molybdenum disulfide, the tip seems to only interact with the adsorbed 2D-material.[69] This unexpected behavior could be explained by in-plane electronic fluctuations within the 2D-material being decoupled from the fluctuations at the surface and within the bulk and with that screening electronic fluctuations perpendicular to it, *i.e.*, those responsible for the interaction of the AFM tip with the surface through the adsorbed monolayer.

As most of our experience and understanding of vdW interactions is based on rather small systems, where a pairwise approximation tends to be qualitatively sufficient, many of the phenomena arising at larger length-scales are still not entirely understood. This and the growing interest in nano-structured and low-dimensional materials motivate on-going studies including a quantum-mechanical many-body treatment of vdW interactions. The ability to reliably model and understand the interactions in such systems is of utmost importance for the design of composite nanostructures[65] and future (nano)technological developments.

4 Qualitative description and analysis of non-covalent interactions

In the field of covalent and electrostatic interactions, conceptual understanding of molecules and materials has largely benefited by the aid of qualitative models, ranging from the basic concept of chemical bonding dating back to Frankland, Kekulé, Erlenmeyer, and Lewis structures[70] to more advanced, electronic structure-based descriptions like the quantum theory of atoms in molecules (QTAIM),[71] the electron localization function,[72,73] the orbital-free single exponential decay detector (SEDD),[74,75] or electrostatic potential maps.[76] As of today, also a few insightful models for the description and analysis of non-covalent interactions have been devised to aid our understanding. These models can, in general, be separated into two main categories: electron density-based approaches and energy decomposition methods. Below we will shortly outline the most prominent examples from both categories and showcase how they can help to analyze, illustrate, and understand non-covalent interactions.

4.1 Density descriptors

According to the seminal work by Hohenberg and Kohn,[77] the electronic charge density, $\rho(\mathbf{r})$, provides all chemical information of a system. It, thus, represents the starting point for DFT and numerous qualitative and quantitative *a posteriori* analysis models. For non-covalent interactions, the (reduced) density

gradient, as also utilized in advanced density functionals and some QTAIM approaches, is particularly useful. Electron density-based approaches are usually employed to obtain a spatial illustration of the relevant interactions, which can be vital to understand supra- or macro-molecular systems and to design novel compounds. However, these models typically do not discriminate between vdW interactions and other (intermolecular) forces.

The first approach filling the gap of the abovementioned models to characterize physical interactions, was put forward by Johnson *et al.* and termed non-covalent interaction index (NCI).[78,79] In their study, the authors realized that the predominant region of non-covalent interaction is characterized by a peak in the regime of low electron densities and a low reduced density gradient, which is a unit-less measure for the deviation from an homogeneous electron gas[77] given by

$$s = \frac{\|\nabla_{\mathbf{r}}\rho(\mathbf{r})\|}{2\rho(\mathbf{r})[3\pi^2\rho(\mathbf{r})]^{\frac{1}{3}}} = \frac{\|\nabla_{\mathbf{r}}\rho(\mathbf{r})\|}{2\rho(\mathbf{r})k_{\mathrm{F}}}, \quad (15)$$

where $\|\cdot\|$ is the (L2-)norm and k_{F} is the Fermi wave vector in the homogeneous electron gas. This can be explained by the fact that density tails are mainly responsible for intermolecular interactions and the reduced gradient approaches zero upon formation of a bond. This feature is also used to identify atomic fragments in the QTAIM approach by Bader.[71]

To further characterize the type of interaction occurring in such low-density, low-reduced gradient regions, Johnson *et al.* found an intriguing connection between the sign of the second-largest eigenvalue of the Hessian of the electron density and bonding/non-bonding interactions. This connection initially seems *ad hoc*, but can be rationalized by concepts from the analysis of chemical bonds.[78] Combining their approach to locate non-covalent interactions together with the discriminator for attractive and repulsive interaction with the absolute value of the electron density as a measure of the strength of the interaction, ultimately yields an insightful tool to analyze intermolecular interactions. Curiously, both a self-consistently obtained electron density from DFT and a crude promolecular density (superposition of atomic densities) lead to qualitatively the same results in most cases. Hence, the NCI approach often does not necessarily require a full DFT calculation[78] and has been successfully applied also to large-scale systems including porous crystalline materials, metal and guest–host complexes, OH-π interactions, and proteins.[78–83] Especially regarding repulsive interactions, we would like to point out that care must be taken when using a non-self-consistent density. In a promolecular density there is no Pauli-repulsion between the atomic densities to cause charge depletion. As a result, the NCI approach does not capture the repulsive character in those cases and in contrast to the authors original conclusion[78] relying on a self-consistent density can in fact be essential (see the simple case of a water dimer in Fig. 2). The necessary level of theory in obtaining the self-consistent density and the resulting limitations for the applicability of the NCI method to large-scale systems remains to be investigated.

The connection between the geometric signatures of the electron density and the energetic features of the corresponding system is also exploited in the SEDD approach and its adaption to reliably illustrate also non-covalent interactions called Density Overlap Regions Indicator (DORI).[84] Being a modification of the SEDD, the DORI model by construction provides a description of both covalent and non-covalent interactions within the same framework and thanks to renormalization within the same scalar range. The basic idea behind DORI and SEDD is to identify areas, where the electron density shows a (nearly) singly exponential decay, which is characteristic of electrons close to nuclei and in the long-range limit.[85,86] Based on this idea, de Silva *et al.* proposed the unitless descriptor

$$\mathrm{DORI}(\mathbf{r}) = \frac{\theta(\mathbf{r})}{1+\theta(\mathbf{r})}, \theta(\mathbf{r}) = \frac{\left\|\nabla_{\mathbf{r}}\|\mathbf{k}\|^2\right\|^2}{\|\mathbf{k}\|^6} \text{ and } \mathbf{k} = \frac{\nabla_{\mathbf{r}}\rho(\mathbf{r})}{\rho(\mathbf{r})}, \quad (16)$$

which can be interpreted in terms of the local wave vector, $\mathbf{k}$. In fact, DORI($\mathbf{r}$) approaches 1 in bonding regions, where the reduced density gradient (15) goes to 0, *i.e.*, at the zero curl of (overlapping) densities. Close to nuclei and far from any atom in the molecule, on the other side, the electron density shows (nearly) singly-exponential decay and DORI($\mathbf{r}$) approaches 0. Combining this approach with the sign of the second-largest eigenvalue of the Hessian of the electron density to distinguish attractive and repulsive interactions and the absolute magnitude of the electron density as a measure for the strength of the interaction as done for the NCI (*vide supra*), allows for a comprehensive description of both covalent and non-covalent interactions within the same framework and on the same scale. It has been shown to provide conceptual insight into the relevant interactions in molecular dimers, complex organic molecules, supramolecular complexes,[84,87–89] and an adaptive QM/MM approach making use of both SEDD and DORI to tessellate the system into QM and MM regions.[90]

The NCI as well as the DORI rely on identifying bonding regions based on the (reduced) gradient of the electronic charge density. As a result, they do not capture electrostatic interactions of non-overlapping fragments nor secondary effects like accumulation and especially depletion of electron density or its intrinsic quantum-mechanical fluctuations. For this matter it is sometimes useful to combine these qualitative techniques with electrostatic potential maps (for electrostatic interactions) or differences in the electron density between the full system and its fragments (charge accumulation/depletion, *i.e.*, charge transfer and induction/polarisation). For the visualization of both NCI and DORI the MULTIWFN package[91] can be used. For the NCI approach there also exists a separate program NCIPLOT,[79,92] which has been used here together with VMD[93] to create Fig. 2.

4.2 Energy decomposition analysis

The second category, in its idea, is rooted in the description of intermolecular interactions in terms of the various energy contributions as formulated in perturbation theory. The aim is to decompose the total interaction energy into contributions from electrostatic interactions, induction (also referred to as polarisation),

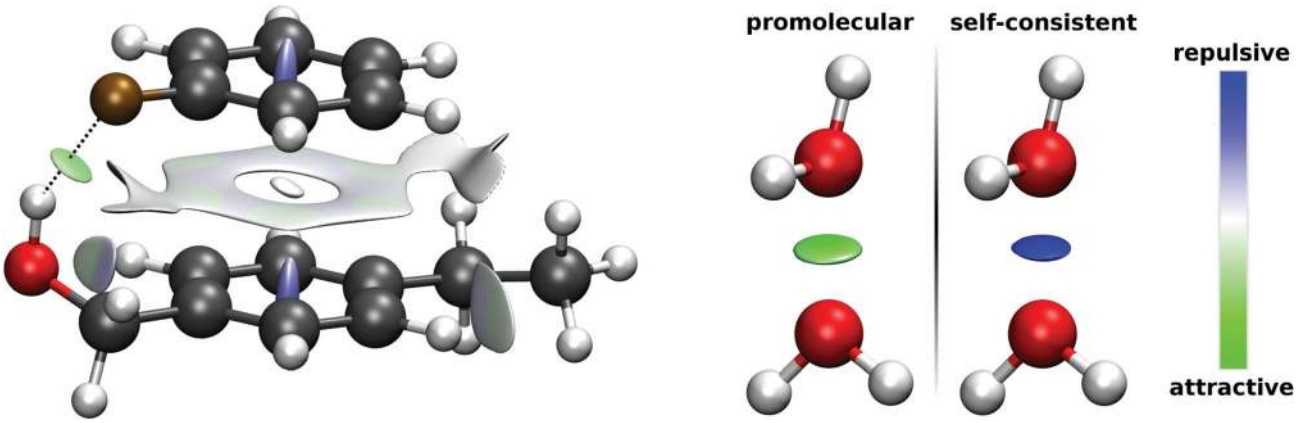

Fig. 2 Intermolecular interactions within the non-covalent interaction index (NCI) approach. Left: Visualizing the hydrogen bond between hydrogen (white) and fluorine (ocher) and weak van der Waals interactions between functionalized benzene molecules. Right: Correctly describing the repulsive character of intermolecular interactions illustrates a so far unnoticed importance of using self-consistent densities.

exchange-repulsion, dispersion interactions, and higher-order terms. So, in contrast to the models outlined in Section 4.1, these methods do not provide a spatial representation of the relevant interactions, but rather give a measure of how much a given type of interaction contributes. This can also provide essential insights for the development of force field approaches.[94,95] It has to be mentioned that there is no unique way of decomposing interaction energies and albeit qualitative agreement different models yield different numerical results. In general, energy decomposition techniques can be classified according to two fundamental approaches: variational or perturbational. In principle, energy decomposition methods provide a quantitative analysis of intermolecular interactions. Variational approaches, however, represent a decomposition of energies calculated within a given framework, contrary to explicit modeling of vdW interactions. The majority of perturbational approaches are highly limited in terms of tractable system sizes and rarely used in the modeling of molecular systems and materials. Thus, we do not consider energy decompositions among the practical methods for vdW modeling described in Section 5.

4.2.1 Variational energy decomposition techniques. Variational energy decomposition approaches, as first developed by Morokuma and Kitaura[96,97] and Ziegler,[98] are formulated within a molecular orbital picture of intermolecular interactions: first, the independent-particle states of the individual monomers are obtained at a given level of theory and then a variational space is constructed on those to obtain the intermolecular interaction between the monomers. The original formalism was based on the HF reference system, but has been adapted to the KS picture of DFT. The different energy contributions are finally obtained by calculating the interaction energy *via* constrained SCF calculations, keeping some of the monomer states frozen (unchanged) during the SCF procedure. Depending on which states are frozen or which terms in the Fock operator are neglected, one can extract the individual contributions to the total interaction energy.[94]

The variational category involves methodologies such as Constrained Space Orbital Variation,[99] Restricted Variational Space,[100] or the self-consistent field method for molecular interactions.[101–103] The different flavors are distinguished by which integrals or elements in the construction of the KS equivalent of the Fock operator from the monomer states are neglected or by which number of monomer orbitals are kept frozen throughout the calculation. This approach has also been employed using intermediate single-particle states based on the natural bond orbital approach to avoid problems with basis set superposition and the Pauli exclusion principle in the original Morokuma–Kitaura scheme.[104,105] The general framework set by Morokuma and Kitaura is formulated in terms of only two interacting fragments. Chen and Gordon[106] later extended the original framework to an arbitrary number of fragments.

In contrast to the above molecular orbital-based models, Wu *et al.*[107] proposed a purely density-based energy decomposition method, which employs constrained DFT to also account for charge transfer effects, and allows for a clean decomposition of the interactions captured by the underlying density functional.[95,107] This already hints at a very important point: In order to obtain the contribution of vdW interactions, the underlying method used for the constrained SCF procedure must explicitly account for dispersion forces and desirably, higher-order terms too. Because of this, many schemes have been re-expressed at higher levels of theory, such as coupled cluster[108–110] or dispersion-corrected DFT.[111–113] As of today, a vast number of methodologies and flavors of variational energy decomposition techniques has been devised and above we only presented a few, select examples. For a more comprehensive list, see *e.g.*, ref. 114 and references therein.

4.2.2 Perturbational energy decomposition. Perturbational approaches treat intermolecular interaction as a perturbation to the Hamiltonian of non-interacting subsystems. With increasing order of the perturbation, one can identify the classic definitions of the different types of intermolecular interactions including electrostatics, induction, and dispersion interactions. The typically covered terms are given in Table 1 and Fig. 3. As known from basic perturbation theory this expansion reaches the exact limit at infinite order given that the perturbation, *i.e.*, the intermolecular

Table 1 Interaction terms covered by (DFT-based) Symmetry-Adapted Perturbation Theory (SAPT). The order of the perturbation expansion in which the term appears is indicated as superscript[47]

Term$^{(order)}$		Physical interpretation
$E_{es}^{(1)}$		Electrostatics
$E_{ex}^{(1)}$		Exchange-/Pauli-repulsion
$E_{ind}^{(2)}$, $E_{ex\text{-}ind}^{(2)}$	E_{ind}	Typically combined into induction (“polarization”)
$E_{disp}^{(2)}$, $E_{ex\text{-}disp}^{(2)}$	E_{disp}	Typically combined into (second-order) dispersion
δ_{HF}		Estimate of higher-order contributions to induction

$E_{int} = E_{es}^{(1)} + E_{exch}^{(1)} + E_{ind} + E_{disp} + \delta_{HF}$

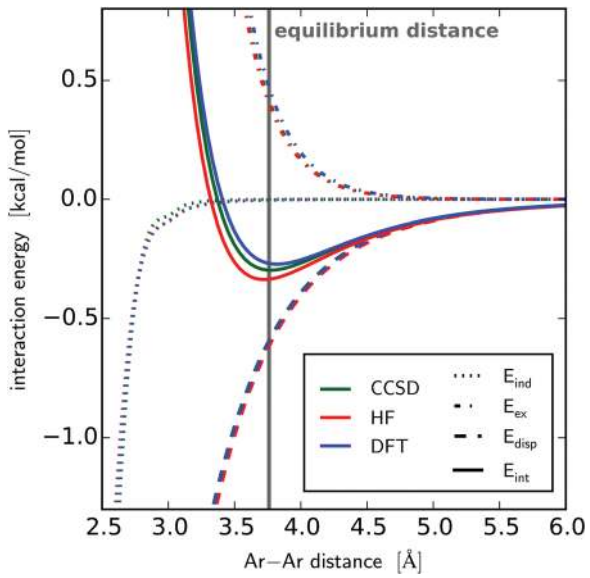

Fig. 3 Energy contributions along dissociation curve of Argon dimer as obtained by SAPT when based on CCSD, HF, or DFT description of monomers. Data taken from ref. 115.

interaction, is small. With that, it also represents a well-defined *ab initio* method for modeling vdW interactions. Nevertheless, for practical calculations and especially in the context of DFT, the series is truncated at second order. Due to the still large computational workload associated with such approaches, however, they are typically less commonly used in practical electronic structure calculations. Mostly they serve as a benchmark for the development and parametrization of more approximate models and in energy decomposition analysis for a quantitative understanding of intermolecular interactions.

The main problem when starting from non-interacting subsystems is the neglect of anti-symmetry of the total wavefunction with respect to particle exchange: the total wavefunction for non-interacting subsystems is the Hartree-product of the respective subsystem wavefunctions, which does not obey the Pauli principle. To account for this shortcoming, a variety of symmetry-forcing methods have been put forward.[47] The most successful and well-established approach among those is the so-called (intermolecular) symmetry-adapted perturbation theory (SAPT),[116,117] which accounts for the Pauli principle in form of using an anti-symmetrization operator. SAPT has traditionally been employed in conjunction with wavefunction-based methods, but has also been formulated in the context of KS-DFT, which allows to study larger molecular systems.[118] After this initial formulation, Heßelmann and Jansen[119–121] and Misquitta *et al.*[122–124] independently devised the nowadays practical methods termed SAPT(DFT)[119] and DFT-SAPT,[122] respectively. Both approaches are essentially identical and rely on asymptotically corrected density functionals, *e.g.*, PBE0-AC,[125] and density–density response functions (susceptibilities). For the remainder of this section, we will collectively refer to these methods as SAPT@DFT.

In the DFT-based SAPT formalism, the monomers are calculated within DFT and the respective (anti-symmetrized) KS determinants serve as a starting point for the perturbation expansion. Thereby using asymptotically corrected functionals especially improves the otherwise poorly reproduced exchange-repulsion term in SAPT@DFT.[122] The second-order induction (polarization) and dispersion energies are calculated from charge density susceptibilities, which are obtained by time-dependent DFT. For this, it is often recommended to also include response effects, *i.e.*, the effect of the perturbing intermolecular potential on the density–density response, which ultimately leads to coupled susceptibilities.[126] In many cases, the error associated with using uncoupled susceptibilities has been found to cancel out with errors in the charge penetration contribution.[124,127] Especially at large monomer separations, however, usage of uncoupled susceptibilities often leads to larger errors in interaction energies,[124] while using coupled susceptibilities yields excellent agreement with accurate results from coupled cluster theory.[128] The difference of dispersion interactions from coupled and uncoupled KS theory is also exploited in the so-called MP2C method based on second-order Møller–Plesset perturbation theory.[129] In MP2C, the dispersion energy based on uncoupled HF of KS states is replaced with the dispersion components calculated in the corresponding coupled perturbation formalism, which has been shown to significantly improve interaction energies for dispersion bound systems.[130–132] Another successful application is the use of SAPT-derived potential energy surfaces (PESs), where the PES is calculated on a representative grid using SAPT(@DFT). This PES is then interpolated at runtime to perform, *e.g.*, extended molecular dynamics simulations with quantum-chemical accuracy nearly at the cost of molecular mechanics, which has been proven a viable tool for studying simple biomolecular assemblies, vdW complexes, crystal structures, or condensed phase systems, for instance.[133–136]

For practical calculations, the wavefunctions are represented in a basis set. In SAPT@DFT, the monomer wavefunctions can be described in a monomer-centered basis set or in a dimer-centered basis. In the former both monomers are represented as if they were isolated molecules. Perturbed states are then constructed from the orbitals of each monomer individually. This excludes excitations from monomer *A* to monomer *B* in perturbed states, which excludes charge transfer – a possible significant contribution to the interaction energy. To further avoid basis set superposition

errors, one can use the dimer-centered basis, in which both monomers are described in the full basis set of the dimer including ghost orbitals situated on the other monomer in dimer configuration. In addition, so-called mid-point functions placed in between the monomers can considerably improve accuracy and convergence by augmenting the representation of the bonding region.[124] Besides this fundamental choice of representation, the actual basis sets are of utmost importance. As intermolecular interactions are particularly sensitive to the outer regions of the wavefunction, *i.e.*, the density tails, this region has to be properly described. One measure is using asymptotically correct density functionals as mentioned above. Another important point is a sufficiently large basis set to describe the density tails. Typically, augmentation with additional diffuse basis functions is recommended.[47] The need for large basis set sizes is one reason for the high computational work load in SAPT(@DFT). As an additional ramification, the calculations can be very memory-demanding and can cause severe limitations in terms of tractable system sizes. A typical problem when trying to obtain the total interaction energy from intermolecular SAPT, and perturbation theory in general, is the slow convergence of the induction energy due to consecutive polarization terms at increasing orders.[47] The most common approach to deal with this is by obtaining an estimate for the higher-order contributions to the induction energy, δ_{HF}, from HF calculations for the dimer,[137,138] which can however further limit the applicability due to the associated computational costs of a self-consistent dimer calculation.

One of the central drawbacks of the well-established intermolecular SAPT approaches is that they are formulated in terms of two separated, *i.e.*, not covalently-bond, fragments such that their interaction can be treated as a small perturbation of the individual fragments. Calculating many-fragment interactions represents a difficult and especially time-consuming task within such an perturbational approach. Significant progress has been made for three-body corrections.[139,140] This has allowed the investigation of three-fragment contributions in the benzene crystal, endohedral fullerene complexes, or water clusters, for example.[141–143] Three-fragment SAPT calculations considerably increase the already high computational demands of SAPT and the impact of many-fragment interactions beyond three is rarely reported. One approach to go beyond these limitations in terms of system size and the number of fragments is the Extended SAPT (XSAPT) family.[144,145] While originally accounting only for many-fragment polarization, the XSAPT framework has recently been extended to also incorporate many-fragment dispersion *via* an adaption of the Many-Body Dispersion formalism (*cf.* Section 5.4).[146]

Another limitation is the modeling of non-covalent intramolecular interactions in the perturbational framework. In conventional wavefunction-based SAPT, this is tackled in form of a three-perturbation expansion, where one is the intermolecular interaction and the other two are intra-fragment electron correlation.[47] In SAPT@DFT, on the other hand, one typically performs a single perturbation with the intermolecular electron–electron interaction and the DFT-functional is meant to capture intra-fragment exchange and correlation. Systems with strong, yet non-covalent, intramolecular interactions, such as extended biomolecules for instance, cannot be cut at covalent bonds and treated as individual fragments, which complicates calculations in a perturbational framework. Based on the Chemical Hamiltonian approach,[147] this issue has recently been addressed by Corminboeuf and co-workers, who devised a SAPT methodology for intramolecular interactions.[148,149] In this intramolecular SAPT variant, the system under consideration is partitioned into non-covalently interacting molecular fragments by means of strictly localized orbitals.[148,150] The starting wavefuctions for the fragments are obtained while being embedded in the HF-wavefunction of a covalent linker, which connects the two fragments. The intramolecular interaction ultimately is obtained in a perturbation expansion ontop of the fragments' starting wavefunctions.[148,149] This has allowed to accurately decompose intramolecular interactions among functional groups, in hairpin-configurations of extended alkanes, stacked aromatic residues, and ionic guest–host complexes.[148,149,151] It is worthwhile to point out, that this method remains ill-defined in the complete basis set limit[151] and, to the best of our knowledge, has not been formulated in the context of DFT. For the latter, subsystem DFT with three-partition frozen density embedding (3-FDE)[152–154] might represent a promising framework to provide the necessary fragment KS determinants.

For SAPT(@DFT), there also exists a derived formalism, known as A/F-SAPT,[155] which maps intermolecular forces to the interaction of pairs of atoms/fragments. This provides an insightful, conceptual analysis and also spatial illustration of individual contributions to intermolecular interactions and can help to significantly boost the derivation of *ab initio*-based molecular mechanics force field approaches.

In general, an accurate, quantitative energy decomposition analysis for vdW interactions is usually limited to small-sized systems due to the computational cost given by the required level of theory or basis set size.[114] For larger-scale systems, this calls for more efficient, practical models, which we will present in the section below (in particular Sections 5.2–5.5).

5 Practical methods for van der Waals interactions

In Section 4, we introduced some qualitative and quantitative tools, which can guide our understanding of vdW interactions and serve as benchmark reference, but are limited in terms of system size and complexity due to the associated computational costs. As discussed above, the inclusion of vdW interactions is essential to obtain quantitatively and even qualitatively correct results for a variety of molecular systems and materials. This realization together with the limitations of higher-level approaches, motivated the development of more practical methods, that allow us to describe and understand long-range correlation forces in more realistic and practically relevant systems. In the following section, we outline some of the currently widely-used vdW models,

their theoretical background as well as some direct consequences for practical applications connected to the individual methodologies. A short, but by no means complete, overview of the availability and usage of each method in electronic structure codes is given at the end of each subsection.

5.1 Random-phase approximation of the ACFD formula

A first, rigorous approach to model long-range correlation forces is to directly evaluate the ACFD formula, for clarity repeated from eqn (1):

$$E_{\mathrm{corr}} = -\frac{1}{2\pi}\int_0^\infty \mathrm{d}\omega \int_0^1 \mathrm{d}\lambda \iint \mathrm{d}\mathbf{r}\mathrm{d}\mathbf{r}' [\chi_\lambda(\mathbf{r},\mathbf{r}',i\omega) - \chi_{\lambda=0}(\mathbf{r},\mathbf{r}',i\omega)]\mathscr{V}_{\mathrm{Coul}}(\mathbf{r},\mathbf{r}') \tag{17}$$

where the density–density response for the non-correlated system, $\chi_{\lambda=0}(\mathbf{r},\mathbf{r}',i\omega)$, can be obtained from the KS (or HF) independent-particle orbitals, ϕ_i, with corresponding eigenenergies, ε_i, and occupation numbers, f_i, *via* the Adler–Wiser formula,[31,32]

$$\chi_{\lambda=0}(\mathbf{r},\mathbf{r}',i\omega) = \sum_{i,j}(f_i - f_j)\frac{\phi_i^*(\mathbf{r})\phi_i(\mathbf{r}')\phi_j(\mathbf{r}')\phi_j^*(\mathbf{r})}{\varepsilon_i - \varepsilon_j + i\omega}. \tag{18}$$

Just as the definition of the non-local polarizability according to the self-consistent Dyson eqn (4), the interacting density response function χ_λ depends on the exact exchange–correlation kernel, f_{xc}, which is in general not known. A widely employed and successful approximation that allows evaluation of the ACFD formula is the random phase approximation (RPA). In the RPA, we neglect the exchange–correlation kernel in the Dyson-equation ($f_{\mathrm{xc}} = 0$). This leads to the RPA-variant of the Dyson equation (here we skip the notion of the $i\omega$-dependency for reasons of clarity),

$$\chi_\lambda^{(\mathrm{RPA})}(\mathbf{r},\mathbf{r}') = \chi_{\lambda=0}(\mathbf{r},\mathbf{r}') + \lambda\iint \mathrm{d}\mathbf{r}''\mathrm{d}\mathbf{r}''' \times \chi_{\lambda=0}(\mathbf{r},\mathbf{r}'')\mathscr{V}_{\mathrm{Coul}}(\mathbf{r}'',\mathbf{r}''')\chi_\lambda(\mathbf{r}''',\mathbf{r}'). \tag{19}$$

Within the framework of RPA, the ACFD formula (17) is typically not reformulated in terms of the non-local polarizability as done in Section 2.1, but stated in terms of the non-local density–density response, which according to eqn (19) is now fully defined by $\chi_{\lambda=0}$. Solving eqn (19) and inserting the result into the ACFD formula (17) allows to analytically integrate over the coupling constant, λ, and gives the expansion series for the full-range RPA correlation energy,

$$E_{\mathrm{corr}}^{(\mathrm{RPA})} = -\frac{1}{2\pi}\int_0^\infty \mathrm{d}\omega \sum_{n=2}^\infty \frac{1}{n}\iint \mathrm{d}\mathbf{r}\mathrm{d}\mathbf{r}' \times [\chi_{\lambda=0}(\mathbf{r},\mathbf{r}',i\omega)\mathscr{V}_{\mathrm{Coul}}(\mathbf{r},\mathbf{r}')]^n. \tag{20}$$

In order to get a complete description of a system, the RPA correlation energy is then combined with KS-DFT, usually further augmented by using exact exchange (EXX). This combination of the RPA correlation energy from the ACFD formula and EXX[156,157] is long known as a promising avenue in electronic structure theory and was also adapted[158–160] and explored[161–169] in combination with DFT. This combined approach is referred to as "exact exchange with correlation from RPA" (EXX/cRPA) and the total energy functional in that case is composed of the kinetic energy of the non-interacting KS reference system, the external (nuclear) potential energy, and the Hartree energy just as in conventional KS-DFT. Exchange and correlation, on the other side, are treated *via* RPA of the ACFD formula instead of an approximate exchange–correlation functional at the Local Density Approximation (LDA), Generalized Gradient Approximation (GGA), or Hybrid level. In modern implementations, the RPA approach and many of its flavors discussed below typically scale between $\mathcal{O}(N^4)$ and $\mathcal{O}(N^5)$ with the number of basis functions N (comparable to canonical, second-order Møller–Plesset perturbation theory) and are usually employed in an *a posteriori* fashion.[164,170–172] Also, analytical nuclear gradients, *i.e.*, interatomic forces, and many other first-order molecular properties are available in modern codes.[172]

As can be seen more easily when reformulated in terms of the non-local polarizability, the RPA essentially corresponds to a saddle point approximation (*cf.* eqn (5) in Section 2.1). In addition, RPA does not rely on a full multi-electron wavefunction and therefore the resulting correlation energy is not necessarily based on antisymmetric states, which in particular affects the short-range. As a consequence, the RPA formalism tends to show significant deficiencies especially in the description of short-range correlation, where it tends to overestimate the correlation energy.[173,174] Despite the shortcomings of the original formulation, the EXX/cRPA approach has been established as a reliable, yet computationally demanding, method for total (interaction) energies within the context of KS-DFT thanks to appropriate reformulations, which we will shortly summarize below after discussing the connections of the RPA correlation energy and electron correlation in wavefunction-based methods.

5.1.1 ACFD/RPA and wavefunction-based methods. Besides forming the basis for the variety of vdW models used in the context of DFT, the ACFD theorem also allows to connect the two fundamental approaches of describing electron correlation: post-HF methods in the form of coupled cluster theory and the ACFD/RPA formalism including the models derived thereof. Scuseria *et al.*[164] were able to show that the ground-state ACFD/RPA correlation energy mathematically equals the result from a particle-hole ring diagram approximation to the coupled cluster doubles (rCCD) theory. In the particle-hole ring approximation, one only considers a single excitation with corresponding creation of a hole and subsequent deexcitation into the original state, thus representing a ring diagram.[164,175] This can also be seen as electron density fluctuations within dipole approximation, where the dipole is spanned by the particle and the hole and the fluctuation corresponds to continuous excitation–deexcitation. It can further be concluded that, in the RPA, the corresponding fermionic product operator for excitation–deexcitation is approximated by a single effective bosonic excitation operator.[175] The equivalence of the resulting correlation energies has been shown to hold between direct RPA and direct rCCD, *i.e.*, neglecting the effect of exchange on the correlation energy, as well as for the full RPA and full rCCD correlation energies.[164] Based on this

connection a myriad of rCCD-derived RPA flavors has been proposed[175–178] and further connections between ACFD/RPA and rCCD, such as between amplitudes and densities,[179] can be drawn. In fact, many of the general extensions to the original EXX/cRPA formalism outlined below, which particularly address the improvement of the description of short-range correlation, have been motivated or can even be expressed in terms of this connection.[179]

5.1.2 ACFD/RPA and density functional theory. A first approach to reduce the deficiency in describing short-range correlation in RPA, was put forward by Perdew and co-workers.[180,181] In their scheme, termed RPA+, the short-range correlation energy is adapted by a local correction *via* the corresponding energy of the homogeneous electron gas as given by DFT in the LDA or GGA, such that

$$E_{\mathrm{corr}}^{(\mathrm{RPA+})} = E_{\mathrm{corr}}^{(\mathrm{RPA})} - \left(E_{\mathrm{corr}}^{(\mathrm{LDA/GGA-RPA})} - E_{\mathrm{corr}}^{(\mathrm{LDA/GGA})}\right), \quad (21)$$

where $E_{\mathrm{corr}}^{(\mathrm{LDA/GGA-RPA})}$ is the LDA/GGA of the RPA correlation energy and $E_{\mathrm{corr}}^{(\mathrm{LDA/GGA})}$ is the correlation energy for the system as obtained by LDA/GGA-DFT.[174,180,181] This modified approach converges to the correct solution for the homogeneous electron gas and already significantly improves total correlation energies,[162,165,182] but can still show considerable shortcomings for binding properties.[183]

Another approach is to avoid spurious one-electron self-correlation arising from using a not necessarily antisymmetric many-electron wavefunction as basis of the RPA treatment. This can be achieved *via* the inclusion of second-order screened exchange (SOSEX).[166,170] Despite being numerically more demanding, EXX/cRPA with SOSEX correction usually performs well for molecules and solids.[166,170] However, adding SOSEX can lead to a reduced accuracy of the calculated height of reaction barriers,[184–186] which can be explained in terms of a less accurate treatment of static correlation.[187] Within the EXX/cRPA + SOSEX framework, this issue has recently been addressed by introducing a short-range SOSEX correction.[187] The spurious overestimation of short-range correlation by the original EXX/cRPA scheme can also be avoided in the spirit of range-separated Hybrid DFT. Here, the RPA-ACFD formula, together with the HF exchange kernel[167] or coupled cluster theory,[168] is only employed in the long-range (as was also introduced in eqn (9) in Section 2.2), while the short-range correlation (and exchange) is treated by a short-range density functional.[167–169] This approach yields reliable and accurate results for thermochemical properties and vdW dimers,[168,169] yet introduces an empirical range-separation and scaling parameter,[167–169,171] which might affect generality and transferability.

Ren *et al.* presented a slightly different approach to go beyond the original EXX/cRPA model motivated by considerations from perturbation theory.[171] Most RPA flavours described above, when based on KS-DFT or HF, can also be interpreted in terms of many-body perturbation theory based on the corresponding (generalized) KS or HF reference states, respectively. Thereby, within Rayleigh–Schrödinger perturbation theory, the RPA correlation energy corresponds to the sum of all zeroth and first-order terms of the perturbation expansion independent of whether one starts from a (generalized) KS or HF reference state.[129,171] For the exchange energy, however, RPA and SOSEX miss single excitation (SE) terms, when based on DFT. This term can easily be obtained based on the independent-particle KS states and including the SE term has been shown to lead to significant improvements for weakly interacting systems.[171] Later, a renormalization based on higher-order terms (→rSE) and Coulomb screening in the form of self-energies as obtained within the GW approximation (→GWSE) have been introduced to avoid problems in (nearly) zero band gap systems.[185,188] Keeping most of the improvements of the SE term, the combined approach of EXX/cRPA + SOSEX + rSE also provides a remarkable transferability and has been shown to yield highly accurate results for atomisation, binding, and reaction energies as well as for reaction barrier heights.[184,185] For hydrogen-bond systems, on the other side, the combination of RPA with both SOSEX and (r)SE turned out to be unprofitable.[185] Employing the EXX/cRPA + GWSE formalism, Klimeš obtained remarkably accurate lattice energies for molecular solids.[189] A similar route was taken by Bates and Furche, who devised a renormalized many-body perturbation theory directly starting from RPA.[186] Account for the resulting leading-order term, referred to as "approximate exchange kernel" (AXK), considerably improves RPA energies and has been found to provide a more balanced correction to RPA than the SOSEX approach, when treating main-group compounds.[190]

5.1.3 ACFD/RPA in electronic structure codes. As a general remark, it has unanimously been found that EXX/cRPA calculations are more reliable when based on KS states obtained from GGA-DFT calculations rather than Hybrid density functionals. Also, proper testing with respect to convergence of the basis set size is highly recommended and if possible corrections to potential basis set superposition errors should be included. Calculation of the RPA correlation energy is available in the following codes (this does not represent a complete list, but covers most major electronic structure codes):

- ABINIT:[191–193] the total and long-range RPA correlation energy can be calculated for periodic systems in a plane-wave basis set in the GW-module. It allows to specify the number of states/bands to be used to obtain χ_0 *via* eqn (18) (large values recommended for convergence) and the cut-off energy of the plane-wave basis set for the representation of the dielectric matrix. Additional speed-up can be obtained when taking advantage of time-reversal symmetry or using an extrapolation scheme with respect to the number of empty states/bands.
- CP2K[186,194] features EXX/cRPA calculations within the resolution-of-identity (RI) approximation for gas-phase and periodic calculations. In addition, the AXK correction to RPA is available.
- FHI-aims:[195] following the EXX/cRPA scheme the total energy is calculated *via*

$$E_{\mathrm{tot}}^{(\mathrm{RPA})} = E_{\mathrm{tot}}^{(\mathrm{DFT})} - E_{\mathrm{xc}}^{(\mathrm{DFT})} + E_{\mathrm{x}}^{(\mathrm{EXX})} + E_{\mathrm{corr}}^{(\mathrm{RPA})}. \quad (22)$$

Currently, FHI-aims allows for plain cRPA, cRPA + SOSEX, RPA + (r)SE, and cRPA + rSE + SOSEX (≡rPT2) calculations for

non-periodic systems relying on the RI approximation. These "RPA and beyond"-methods are prone for considerable basis set superposition errors. Hence, using counterpoise correction is recommended for accurate energies. Using a correlation consistent basis set is in general recommended for use in RPA calculations. For the number of empty states, large values, typically beyond the basis set size to include all available states, is recommended. Due to a significant loss in accuracy, usage of the accelerated RI method is not recommended. Calculation of the RPA correlation energy along the coupling constant, λ, and output of the (linear) dielectric tensor within RPA is also implemented.

• TURBOMOLE:[196] calculation of the RPA correlation energy and gradients within RI is available. Additional options such as the frequency grid-size for numerical integration and skipping of the EXX calculation can be set manually. Orbitals can be excluded from correlation treatment (recommended for inner-level orbitals) and usage of high angular momentum (diffuse) basis function and inclusion of auxiliary basis (for the calculation of HF exchange) is required.

• VASP[197–201] allows for direct ACFD/RPA calculations for periodic systems in plane-wave basis. This however, requires several individual calculations and can not be obtained in a single run as of the time of this publication. After performing a standard DFT calculation, obtaining EXX from the resulting KS states, and running a refined DFT calculation using the maximum number of plane-waves, one can obtain the ACFD/RPA correlation energy. Thereby, using the maximum number of plane-waves is recommended. For convergence tests with respect to reciprocal space summation and basis set size, the energy cutoff should be changed already in the first standard DFT calculation and all four steps are to be repeated.

5.2 Non-local density functionals

5.2.1 Theory and connection to ACFD formula. The maybe most obvious way to approximate vdW interactions within DFT would be to modify the underlying energy functional to include the proper physics for describing weak, dispersive interactions. The general idea is to begin with the ACFD formula of eqn (1), postulate an approximate form for $\chi_\lambda(\mathbf{r},\mathbf{r}',i\omega)$ and then simplify the integrals. Invariably, the goal is to avoid the summation over unoccupied states that is explicit in the full RPA expression of eqn (20). Functionals of this type have the appealing feature of potentially being computationally less demanding compared to RPA or EXX calculations, while still being seamless in the sense of not requiring any partitioning of the system into fragments.

In order to simplify the ACFD formula, one might naively try a local density approximation to the response function:

$$\chi_\lambda(\mathbf{r},\mathbf{r}',i\omega) \approx \tilde{f}(\rho(\mathbf{r}),i\omega)\delta^3(\mathbf{r}-\mathbf{r}'), \quad (23)$$

for some appropriate function $\tilde{f}(\rho(\mathbf{r}),i\omega)$. However, as shown by Dobson,[202] this corresponds to unphysical fluctuations in the total number of electrons rather than the number-conserving fluctuations implied by the ACFD formula of eqn (1). To make a proper local approximation, one must instead approximate the polarizability:

$$\boldsymbol{\alpha}_\lambda(\mathbf{r},\mathbf{r}',i\omega) \approx \boldsymbol{f}(\rho(\mathbf{r}),i\omega)\delta^3(\mathbf{r}-\mathbf{r}'), \quad (24)$$

which can be used to construct the ACFD correlation energy *via* eqn (3). The first explicit density functional to successfully apply these ideas was proposed by Dobson.[203] The resulting functional was only applicable to jellium-like systems, but seamlessly connected short- and long-range interactions.

To extend this idea to general systems, one requires a more general ansatz for the local polarizability of eqn (24). A tremendous amount of effort has been devoted to this topic,[204–207] much of which has centered around plasmon-pole-type approximations to the local polarizability:

$$\alpha(\mathbf{r},\mathbf{r}',i\omega) = \frac{1}{4\pi}\frac{\omega_\mathrm{p}^2(\mathbf{r})\delta^3(\mathbf{r}-\mathbf{r}')}{\omega_\mathrm{p}^2(\mathbf{r})-\omega^2} \quad \text{with} \quad \omega_\mathrm{p}^2(\mathbf{r}) = 4\pi\rho(\mathbf{r}), \quad (25)$$

which is thought to be a good approximation for uniform systems. The big breakthrough came with the development of the vdW-DF functional in the Rutgers–Chalmers group.[208,209] Here, in order to simplify the algebra, one truncates the Dyson equation for α_λ in eqn (4) at second order so that¶

$$\alpha_\lambda \approx \alpha_0 - \langle\lambda\alpha_0\mathbf{T}_{\mathrm{xc},\lambda}\alpha_0\rangle_{\mathbf{r}'',\mathbf{r}'''}. \quad (26)$$

This truncation has the unfortunate side effect of discarding screening effects (type B non-additivity), but otherwise the algebra becomes too cumbersome to be tractable for practically relevant systems. One then proceeds to make a semi-local, plasmon-pole-like approximation to α_0, constructed to satisfy several exact constraints: (1) the *f*-sum rule (Thomas–Reiche–Kuhn), (2) the short wave-vector (small q) limit, (3) time reversal symmetry, and (4) the volume of the xc hole. The resulting functional can be expressed in non-local form as,

$$E_\mathrm{corr}^{(\mathrm{nl})} = \frac{1}{2}\iint\rho(\mathbf{r})\phi(\mathbf{r},\mathbf{r}')\rho(\mathbf{r}')\mathrm{d}\mathbf{r}\mathrm{d}\mathbf{r}', \quad (27)$$

where ϕ is itself an integral that is in practice approximated numerically *via* interpolation of a dense grid of pre-computed values. The vdW-DF functional is in principle non-empirical and seamless and produced an explosion of activity applying density functional theory to weakly interacting systems.[6,210–213] Numerous variants of vdW-DF have arrived in the intervening years, including the vdW-DF2 functional,[214] which improves upon the accuracy of the original functional for a variety of systems. A recent review nicely summarizes the important progress in this area.[215]

The original non-local vdW-DF was intended to be used with a semi-local exchange functional that was close to HF exchange (or EXX). However, a number of initial studies noted that the results were extremely sensitive to the choice of semi-local exchange[216] and a number of authors proposed re-parameterizing

¶ It should be noted that most of the literature on the vdW-DF is formulated in terms of the dielectric permittivity, ε, rather than the polarizability, α. In the context of the present work, however, we will phrase the discussion in terms of polarizability for consistency with the other sections.

the semi-local exchange functional for the specific purpose of producing good intermolecular forces when paired with vdW-DF.[212,217] This approach has the obvious negative consequence that re-parameterizing the exchange will also have a significant impact on intramolecular forces and on the molecular electron density itself. A more natural approach would be to re-parameterize the vdW-DF to match the semi-local exchange functional, but the extremely complicated nature of the vdW-DF functional makes this a daunting task.

Vydrov and Van Voorhis made progress in this direction[218] by dropping the constraint that the approximation to α_0 has to be correct in the short wave vector limit. That limit is not relevant for long-range intermolecular interactions and introduces a numerically troublesome short-range divergence of the integral kernel ϕ in eqn (27). Proposing a new approximate α_0 that ignores this constraint, the resulting VV09 functional takes the form

$$E_{\mathrm{corr}}^{\mathrm{VV09}} \equiv \frac{3}{64\pi^2}\int\int \frac{\omega_{\mathrm{p}}^2(\mathbf{r})\omega_{\mathrm{p}}^2(\mathbf{r}')D(K)\mathrm{d}\mathbf{r}\mathrm{d}\mathbf{r}'}{\omega_0^2(\mathbf{r})\omega_0^2(\mathbf{r}')[\omega_0^6(\mathbf{r})+\omega_0^6(\mathbf{r}')]\|\mathbf{r}-\mathbf{r}'\|^6}, \quad (28)$$

where ${\omega_0}^2 = {\omega_{\mathrm{p}}}^2/3 + {\omega_{\mathrm{g}}}^2$ is the plasmon response with band gap determined by ω_{g} and $D(K)$ is a non-empirical damping function. While eqn (28) may look more complicated than the original vdW-DF, it is in practice easier to deal with because the function $D(K)$ is an explicit, analytic function of the local density variables. Subsequently, VV09 was simplified further[219] by discarding the semi-local model for α_0 altogether and instead directly proposing a form for ϕ in eqn (27):

$$\phi^{\mathrm{VV10}} \equiv \frac{-3}{2g(\mathbf{r})g(\mathbf{r}')(g(\mathbf{r})+g(\mathbf{r}'))}, \quad (29)$$

where g is a function of the local density variables. The resulting VV10 functional is equivalent to VV09 as the fragment separation approaches infinity, but is manifestly simpler in construction and in practice seems to be significantly more accurate than the original VV09 functional.[220] Because of the semi-empirical nature of its construction, VV10 contains two parameters (C and b) that must be chosen in practice. The first, C, controls the effective local band gap and is typically chosen such that the non-local functional gives accurate C_6 coefficients, which are very sensitive to the size of the gap. The second parameter, b, controls the strength of the damping function and thus has no impact on long-range properties like the C_6 coefficients. Instead, b is typically chosen differently for different semi-local functionals so that the short-range repulsion from exchange and the damping of dispersion interactions in $E_{\mathrm{corr}}^{(\mathrm{nl})}$ balance appropriately. The flexibility implied by the choice of b has allowed VV10 to be paired with a wide array of different semi-local exchange–correlation functionals – GGAs,[219,221] hybrids,[221] meta-GGAs[222,223] and range-separated hybrids[219,223,224] have all been successfully combined with VV10.

5.2.2 Practical aspects. The six dimensional integral implied by eqn (27) is typically the computational bottleneck in evaluating non-local xc-functionals, having a formal scaling of $\mathcal{O}(N^2)$ with system size and a large prefactor. The complicating element is that the kernel, ϕ, is a function not only of $R \equiv \|\mathbf{r}-\mathbf{r}'\|$ but also of the local density and density gradient values at $\mathbf{r}$ and $\mathbf{r}'$. If it only depended on R, the integral could be done rapidly by convolution. Fortunately, $\phi(\mathbf{r},\mathbf{r}')$ only depends on the density through a single function, $q[\rho,\|\nabla\rho\|]$ evaluated at the points $\mathbf{r}$ and $\mathbf{r}'$. As a result, one can write:[225]

$$\phi(q,q',R) \approx \sum_{i,j}\phi(q_i,q_j,R)p_i(q)p_j(q'), \quad (30)$$

where q_i is a mesh of points and p_i is some complete set of functions. For each fixed pair $\{q_i,q_j\}$ the six dimensional integral in eqn (27) can be evaluated *via* convolution. Therefore, for some fixed number of grid points, G, eqn (30) allows one to compute the energy and forces for vdW-DF in $\mathcal{O}(N\log N)$ time – a huge speed-up relative to the brute force implementation. In practice, relatively modest values of G ($\sim$20) suffice, in which case the vdW interactions in a typical vdW-DF simulation do not noticeably affect the overall timing, making vdW-DF and its derivatives modern workhorses for the simulation of weakly bound solids.[215]

Unfortunately, the non-local kernels for VV09 and VV10 do not share the same structure as vdW-DF: instead of depending on one function (q), VV09 and VV10 depend on two functions (ω_0 and ω_{p}). As a result, eqn (30) cannot easily be applied to VV10. However, one can introduce an approximation in which the damping factor in g is assumed to be the same at both $\mathbf{r}$ and $\mathbf{r}'$, resulting in the revised VV10 (rVV10) kernel:[226]

$$\phi^{\mathrm{rVV10}} \equiv \frac{-3}{2(hR^2+1)(h'R^2+1)(hR^2+h'R^2+2)}, \quad (31)$$

where h is a function of the local density and its gradient. This revised functional is numerically very similar to VV10, but has the distinct advantage that it can be expanded using eqn (30) and thus evaluated in $\mathcal{O}(N\log N)$ time.

5.2.3 Non-local (vdW) density functionals in select electronic structure codes. vdW-DF, VV10 and their variants are available in a wide array of electronic structure codes. Broadly speaking, plane-wave codes tend to implement the convolution approximation to speed up the evaluation of the xc energy and thus implement only rVV10. Gaussian orbital-based codes sometimes implement the full six dimensional integral either by quadrature or by Monte Carlo, leading to facile implementation of VV10. In the latter case, the evaluation of the non-local energy can become prohibitive for very large systems. Some examples of electronic structure codes featuring non-local vdW-DFs include:

- Q-Chem:[227] calculation of vdW-DF, vdW-DF2, VV10 and rVV10 energies and forces. Note that the C and b parameters for VV10 and rVV10 have to be specified *via* additional keywords.
- Quantum espresso[228] allows for calculation of dispersion-inclusive electronic energies and forces as obtained by vdW-DF, vdW-DF2 and rVV10.[226,229,230]
- SIESTA[231] features vdW-DF, vdW-DF2 and rVV10 energies and forces.
- VASP:[197–201] The vdW-inclusive functionals vdW-DF, vdW-DF2 and rVV10 are implemented.[212,213] Manual specification of b parameter for rVV10 and switch between vdW-DF and vdW-DF2 required.

5.3 Effective non-local core potentials

Above (Section 5.2), we introduced non-local density functionals as a promising approach to model vdW interactions. It is aimed to include non-local, long-range correlation interactions directly in the form of the potential of the density functional instead of using post-processing of any sort. While the above vdW-DF models use a physically motivated two-point potential between positions in the electronic charge density, such a path can also be pursued in a data-driven manner, *i.e.*, by adding a non-local two-point or core potential, which can be optimized to comply with accurate reference results.

The basic idea and framework of optimizing the core potential referred to as optimized effective potential (OEP) is due to Sharp and Horton[232] and has later been picked up in the context of describing electron correlation within DFT as an alternative to common density functional approximations (DFAs).[233–236] von Lilienfeld *et al.* generalized the previously still first principles-based framework to so-called dispersion-corrected atom-centered potentials (DCACPs), which aim at accurately reproducing dispersion interactions and other complex molecular properties as predicted from higher-level theoretical methods (or experiment).[237] In their approach they include angular momentum-dependent non-local effective core potentials, as also used in norm-conserving pseudo-potentials in DFT calculations with a plane wave basis set,[238] composed of spherical harmonics and Gaussian-type radial projectors.[237] To model dispersion interactions, the parameters, $\{\sigma_i\}$, entering the effective non-local core potential are then optimized by minimizing the penalty functional,

$$\begin{aligned}\mathscr{P}[\rho(\mathscr{M}_{\mathrm{ref}})] &= |E_{\mathrm{ref}}[\rho(\mathscr{M}_{\mathrm{ref}})] - E[\rho(\mathscr{M}_{\mathrm{ref}});\{\sigma_i\}]|^2 \\ &\quad + \sum_A c_A \|\mathbf{F}_A[\rho(\mathscr{M}_{\mathrm{ref}});\{\sigma_i\}]\|^2\end{aligned} \tag{32}$$

via a second Gaussian-type projector. Above, $E_{\mathrm{ref}}[\rho(\mathscr{M}_{\mathrm{ref}})]$ and $E[\rho(\mathscr{M}_{\mathrm{ref}});\{\sigma_i\}]$ are the energy obtained for the reference system $\mathscr{M}_{\mathrm{ref}}$ using the reference method and the parametrically dependent DCACP energy, respectively, and $\mathbf{F}_A$ is the nuclear force on atom A as obtained in the DCACP method. For the evaluation of the penalty functional, one chooses reference systems, $\mathscr{M}_{\mathrm{ref}}$, which are minima on the potential energy surface in the reference method. Thus, $\mathbf{F}_{\mathrm{ref}} = \mathbf{0}$. c_A, finally, is a weighting factor, which allows to exclude the nuclear gradient A in the optimization.[237,239] Using the gradient of the penalty function with respect to $\{\sigma_i\}$, this procedure can be used to variationally tune common DFAs to (re-)produce accurate results for a given molecular property. It has to be kept in mind though, that a given application requires a given choice of reference systems, the penalty function(al) and the weighting factors,[237] which adds a certain degree of empiricism and potentially limits transferability.[6]

Typically, second-order Møller–Plesset theory or more recently also CCSD(T) serves as a reference method and it has been shown that DFT+DCACP can be used to accurately reproduce the binding properties of noble gases, a variety of hydrocarbon complexes as well as condensed matter systems like graphite, multilayer graphene, molecular crystals, liquid water, and adsorption phenomena.[237,239–243] Approaches to include vdW dispersion interactions *via* effective core potentials are, in general, available in pseudo-potential DFT codes, such as CPMD,[244] for instance. As the DCACP approach relies on optimizing effective core potentials, one can use the obtained potentials in the form of pseudo-potentials in a variety of electronic structure codes.

5.4 Interatomic many-body method from ACFD/RPA: many-body dispersion formalism

The most common and successful approach to model electron correlation in realistic systems in the context of DFT is to combine a (semi-)local DFA for the short-range exchange and correlation contribution with a model for long-range correlation (vdW interactions) as a post-processing step.

5.4.1 Theoretical background. Typically, post-DFT vdW models are based on a dipole approximation or RPA and written in an interatomic framework. The latter can be interpreted as coarse-graining the response functions entering the long-range ACFD/RPA formula (9), which we will repeat here for reasons of clarity:

$$\begin{aligned}E_{\mathrm{corr}}^{(\mathrm{lr,RPA})} &= -\sum_{n=2}^{\infty}\frac{(-1)^n}{n}\frac{1}{2\pi}\int_0^{\infty}\mathrm{d}\omega \\ &\quad\times\left\langle \mathrm{Tr}\left\{\left\langle\left(\boldsymbol{\alpha}^{(\mathrm{sr})}\mathbf{T}_{\mathrm{lr}}\right)^n\right\rangle_{\mathbf{r}'',\mathbf{r}'''}\right\}\right\rangle_{\mathbf{r},\mathbf{r}'}.\end{aligned} \tag{33}$$

The coarse-graining is usually chosen such that the spatial integrations in eqn (33) can be performed analytically, which significantly reduces the computational cost. In Section 2.2, we already introduced such a coarse-grained polarizability in terms of atomic point polarizabilities, see eqn (10). In the Many-Body Dispersion (MBD) formalism,[49,245] a less approximate approach is chosen. Here, the total polarizability is contracted to a sum of effective isotropic atomic (dipole) polarizabilities.‖ Such atomic/molecular response properties have been shown to be accurately described by a Quantum Harmonic Oscillator (QHO) model.[49,245–249] In fact, the leading Padé approximant of the dynamic isotropic atomic dipole polarizability[250] follows the same formula as the dynamic dipole polarizability of an isotropic QHO,

$$\alpha_A^{(\mathrm{QHO})}(i\omega) \equiv \alpha_A(i\omega) = \alpha_{A,0}\left[1+\left(\frac{\omega}{\eta_A}\right)^2\right]^{-1}, \tag{34}$$

where $\alpha_{A,0} \equiv \alpha_A^{(\mathrm{QHO})}(0)$ is the effective static QHO polarizability and η_A is the characteristic excitation frequency of QHO A. Hence, the remaining step is the parametrization of such QHOs to model atoms in molecules. In MBD, the two vdW parameters are obtained from accurate atomic reference data taking into account the local chemical environment (type A non-additivity,

‖ We would like to point out that the MBD formalism does not fundamentally exclude anisotropic polarizabilities on the atomic scale. The choice of isotropic atomic polarizabilities, however, allows for an efficient, analytical evaluation of the dipole coupling.

see Section 2.3) *via*

$$x_A \approx \frac{\alpha_{A,0}}{\alpha_{A,0}^{(\mathrm{ref})}} \approx \sqrt{\frac{C_{6,AA}}{C_{6,AA}^{(\mathrm{ref})}}} \quad \text{and} \quad \eta_A = \frac{4\,C_{6,AA}}{3\,{\alpha_{A,0}}^2}, \tag{35}$$

where the rescaling factor x is derived from the electronic structure, conventionally as the ratio of the volumes of the atom in the system and the reference atom as obtained *via* Hirshfeld analysis[251] (this is further detailed for the vdW(TS) model in Section 5.5.1 below). It is worthwhile to mention, that a QHO has a natural width and thus goes beyond point-like dipoles, while the short-range dipole coupling tensor between QHOs with overlapping densities can still be evaluated analytically.[252] This short-range dipole tensor, $\mathbf{T}_{\mathrm{QHO}}^{(\mathrm{sr})}$, is then used to explicitly account for the short-range screening according to the inverted coarse-grained Dyson equation,

$$\alpha_A^{(\mathrm{sr})} \approx \tilde{\alpha}_A(i\omega) = \frac{1}{3}\mathrm{Tr}\left\{\sum_C \mathbf{B}_{AC}\right\}; \quad \mathbf{B} = \left[\mathbf{P}^{-1} + \mathbf{T}_{\mathrm{QHO}}^{(\mathrm{sr})}\right]^{-1}, \tag{36}$$

where $\mathbf{P} = \mathrm{diag}\{\alpha_A(i\omega)\cdot 1_3\}$ is a diagonal matrix containing three times $\alpha_A(i\omega)$ for each atom A, *i.e.*, the xx, yy, and zz component of the corresponding isotropic atomic polarizability tensor. The summation over all atoms C corresponds to the integration over the whole space in the Dyson equation and the factor $\frac{1}{3}$, together with the trace operator, restores an isotropic effective polarizability, $\tilde{\alpha}_A(i\omega)$. This is the model response used to define $\alpha_A^{(\mathrm{sr})}$, which already significantly improves the description of the polarizability compared to the superposition of effective atomic polarizabilities[49,253] and then enters a coarse-grained ACFD/RPA formula for the long-range correlation energy of the form of eqn (11), see also Fig. 4. For the long-range coupling there is a negligible overlap between the QHOs. Therefore, the bare point-dipole potential is applied. So, to a very good approximation, the long-range ACFD/RPA formula for an N atom system can be evaluated based on a set of N dipole coupled QHOs. Such a set of N three-dimensional QHOs can be described in terms of mass-weighted displacements, $\boldsymbol{\zeta}_A = \sqrt{m_A}(\mathbf{r}_A - \mathbf{R}_A)$ and the Hamiltonian,

$$\begin{aligned}\mathscr{H}_{\mathrm{MBD}}(\boldsymbol{\zeta}) &= \sum_{A=1}^{N} -\frac{1}{2}{\nabla_{\zeta_A}}^2 + \sum_{A=1}^{N}\frac{{\eta_A}^2}{2}\|\boldsymbol{\zeta}_A\|^2 \\ &\quad + \sum_{B=1}^{N}\frac{\eta_A\eta_B}{2}\sqrt{\tilde{\alpha}_{A,0}\tilde{\alpha}_{B,0}}\boldsymbol{\zeta}_A^{\mathrm{T}}\mathbf{T}_{AB}^{(\mathrm{lr})}\boldsymbol{\zeta}_B \end{aligned} \tag{37}$$

$$= \mathscr{T}_\zeta + \frac{1}{2}\boldsymbol{\zeta}^{\mathrm{T}}\mathscr{V}\boldsymbol{\zeta}, \tag{38}$$

with

$$\mathscr{V}_{AB}^{(i,j)} = \eta_A\eta_B\left(\delta_{ij} + \sqrt{\tilde{\alpha}_{A,0}\tilde{\alpha}_{B,0}}\mathbf{T}_{AB,\mathrm{lr}}^{(i,j)}\right),$$

where the collective variable $\boldsymbol{\zeta}$ is the direct sum of all $\boldsymbol{\zeta}_A$ and (i,j) denotes the Cartesian components of the AB-subblocks of the potential matrix $\mathscr{V}$ and the long-range dipole coupling tensor $\mathbf{T}_{AB}^{(\mathrm{lr})}$. Similar models to describe (many-body) dispersion interactions within the dipole limit were already known and used earlier.[246,254–260]

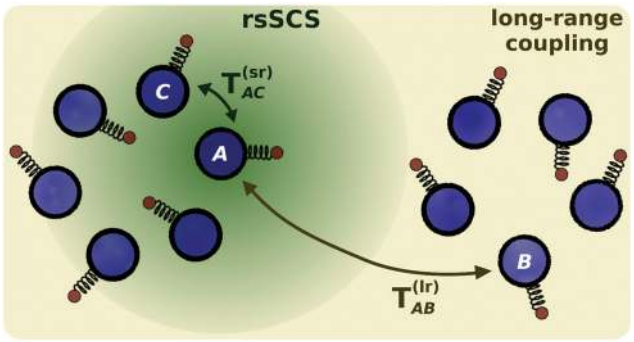

Fig. 4 Schematic illustration of the MBD model with range-separated self-consistent screening (rsSCS): Effective atomic polarizabilities are obtained from electrodynamic screening using the short-range part of the range-separated dipole tensor for quantum harmonic oscillators. The interaction between the oscillators is then obtained using the long-range part of the dipole coupling tensor.

These methods, however, were typically based on simpler model polarizabilities and did not offer general parametrization and applicability for realistic systems.

As a mathematically equivalent, yet much more efficient, alternative approach, it has been shown that the long-range RPA correlation energy of this dipole-coupled set of QHOs equals its (zero-point) interaction energy.[46,245] Thanks to the bilinear form (38), this can be obtained numerically exact *via* unitary transformation to a new collective variable, $\xi = \mathbf{C}\boldsymbol{\zeta}$, where the transformation matrix $\mathbf{C}$ diagonalizes the potential matrix:

$$\mathbf{C}\mathscr{V}\mathbf{C}^{\dagger} = \mathrm{diag}\{\tilde{\omega}_i^2\}. \tag{39}$$

With the kinetic energy operator, $\mathscr{T}$, being invariant under unitary rotations, $\mathbf{C}$ transforms the MBD Hamiltonian into an uncoupled set of $3N$ one-dimensional QHOs,

$$\begin{aligned}\mathscr{H}_{\mathrm{MBD}}(\boldsymbol{\xi}) &= \mathscr{T}_\xi + \frac{1}{2}\boldsymbol{\zeta}^{\dagger}\mathbf{C}^{\dagger}\mathbf{C}\mathscr{V}\mathbf{C}^{\dagger}\mathbf{C}\boldsymbol{\zeta} \\ &= \mathscr{T}_\xi + \frac{1}{2}\boldsymbol{\xi}^{\dagger}\mathrm{diag}\{\tilde{\omega}_i^2\}\boldsymbol{\xi} = \sum_{i=1}^{3N}\mathscr{T}_{\xi_i} + \frac{\tilde{\omega}_i^2}{2}\|\boldsymbol{\xi}_i\|^2. \end{aligned} \tag{40}$$

This set of QHOs can be solved according to textbook and its total energy is given by half the sum of its characteristic frequencies $\tilde{\omega}_i$. The (zero-point) interaction energy, ultimately corresponding to the RPA long-range correlation energy within the QHO model of electronic response, is given by

$$\begin{aligned}E_{\mathrm{vdW}}^{(\mathrm{MBD})} &= E_{\mathrm{QHO}}^{(\mathrm{coupled})} - E_{\mathrm{QHO}}^{(\mathrm{non\text{-}interacting})} \\ &= \frac{1}{2}\sum_{i=1}^{3N}\tilde{\omega}_i - \frac{3}{2}\sum_{A=1}^{N}\eta_A. \end{aligned} \tag{41}$$

The range-separation function to define $\mathbf{T}_{\mathrm{sr}}$ and $\mathbf{T}_{\mathrm{lr}}$, is chosen of Fermi-type,

$$f_{\mathrm{damp}}^{(\mathrm{MBD})}\left(R_{AB}; R_{\mathrm{vdW}}^{(AB)}\right) = \left\{1 + \exp\left[-a\left(\frac{R_{AB}}{\beta\cdot R_{\mathrm{vdW}}^{(AB)}} - 1\right)\right]\right\}^{-1}, \tag{42}$$

where $a = 6$ and the effective vdW distance, $R_{\mathrm{vdW}}^{(AB)} = \sqrt[3]{x_A} R_{\mathrm{vdW}}^{(A,\mathrm{ref})} + \sqrt[3]{x_B} R_{\mathrm{vdW}}^{(B,\mathrm{ref})}$, where one relies on a rescaling of accurate reference data of vdW radii (for further details, see Section 5.5.1). The range-separation parameter, β, is finally an empirical parameter fitted to provide optimal results in combination with a given DFA for small molecular dimers.[49] As the range-separation parameter also represents a measure of when the long-range correlation model has to be included, it gives an estimate of the range of correlation already captured by the underlying DFA.[261]

5.4.2 Practical aspects and related models. Being formally equivalent to the full long-range RPA correlation energy for a set of QHOs, the MBD formalism includes many-body interactions up to N atoms and incorporates correlation effects up to infinite order. The two main differences are the assumption of isotropic polarizabilities and that those can be modeled *via* a single QHO per atom. Relying on the QHO model polarizability, on the other side, fundamentally binds the charge fluctuations to a given atom (no electron hopping), which limits the validity and applicability of MBD for metallic systems (does not capture type C non-additivity, see Section 2.3). For a variety of non-metallic systems in different chemical environments, on the other side, the two approximations have been found to be very reliable and accurate. In fact, in various cases the MBD formalism yields the same results as the RPA-approach, while requiring only a fraction of the computational workload: The MBD method scales as $\mathcal{O}(N^3)$ with the number of atoms N for inversion and diagonalization of the $\mathbf{B}$ and $\mathscr{V}$ matrices (comparably small prefactor thanks to no integrations at runtime and only a few inversions and a single diagonalization). After its original formulation for the vdW energetics of finite-gap molecules, the applicability and efficiency of MBD was further boosted by the derivation of the analytical gradient expression[245,262] and a reciprocal space formulation,[263] which allows for efficient simulations within periodic boundary conditions and advanced the applicability of the MBD formalism to molecular crystals and layered materials.

As mentioned above, for a set of QHOs, the MBD formalism is even mathematically equivalent to the full long-range RPA correlation energy. For this to yield accurate energies for realistic systems, however, the set of QHOs has to accurately model the response properties of the system. For that, the MBD model relies on the procedure originally proposed in the vdW(TS) scheme (*vide infra*), which is based on the rescaling of accurate reference data according to Hirshfeld volume ratios. As a result, MBD can also suffer from the common shortcomings of the Hirshfeld partitioning scheme, which tends to underestimate charge transfer[264,265] and in line with that the volume ratios tend to underestimate the corresponding effect on the atomic polarizability. This can lead to considerable deficiencies in the description of the vdW parameters of ionic systems.[253,266] We would like to emphasize that this is a shortcoming of the underlying (Hirshfeld) partitioning scheme and not the MBD framework itself. Significant improvements can be achieved when relying on the computationally more demanding, but much more accurate, iterative Hirshfeld scheme[253,265] or when using a charge-dependent reference state for the polarizability,[267] for instance.

Modeling electron density fluctuations and their interactions within the so-called Drude approximation, *i.e.*, *via* negatively charged pseudo-particles harmonically oscillating around atomic centers, has already been known and used in the context of vdW interactions by London in the 1930s.[36,268,269] Based on this picture, Whitfield and Martyna[270] proposed a more general approach to model (many-body) induction and dispersion: the Quantum Drude Oscillator (QDO) model, which also largely motivated the development of the MBD framework. In the QDO model, the oscillating pseudo-particles interact *via* the full Coulomb potential, with that going beyond the typically invoked RPA or dipole approximation. The model is defined by the charge and mass of the pseudo-particles and the characteristic frequency of their oscillation. With an appropriate choice of these three parameters, the QDO model can accurately describe the response properties, many-body induction and dispersion interactions of a given system up to infinite order.[248] Direct derivation of effective parameters for realistic systems, however, represents a challenging task. Also the evaluation of the interaction energy, which is typically done *via* imaginary-time path integration[270] or Diffusion Monte-Carlo,[271] limits its applicability in terms of system size. Recently, this model has been used to showcase the relevance of many-body and multipolar vdW interactions in water and at its surfaces.[249,272]

5.4.3 Many-body dispersion formalism in select electronic structure codes. The MBD formalism is implemented in the following set of select electronic structure codes:

- ADF[273–275] features the MBD formalism with and without self-consistent electrodynamic screening.
- CASTEP:[276] being a plane-wave DFT code for periodic systems, the efficient reciprocal space formulation has been implemented.
- FHI-aims[195] allows for usage of the MBD formalism with range-separated short-range screening for periodic (reciprocal space formulation) and non-periodic calculations in a serial, MPI-parallel, and a fully memory-parallel implementation including analytical gradients.
- Q-Chem:[227] MBD contribution to total energy and optionally forces available.
- Quantum espresso:[228] MBD contribution to forces and energies has been implemented.
- VASP[197–201] features a reciprocal space formalism for periodic boundary conditions and analytical gradients (default range-separation parameter only available for the PBE xc functional). It also allows to output the first five nth-order contributions to the dispersion energy (obtained in the form of eqn (11) with short-range screened atomic polarizabilities as used within the MBD model).

5.5 Pairwise-additive van der Waals Models

Augmenting (semi-)local DFT calculations *a posteriori* with a London-type vdW term, as first put forward by Wu and Yang[277] and popularized as a general framework by Grimme,[37] represents an early and efficient approach to correct for the lack of

long-range electron correlation. As detailed in Section 2.2, the fundamental mathematical form can be derived from a coarse-grained ACFD/RPA formula. For the purpose of comparing the rich set of pairwise-additive vdW models devised to date, we will use the ACFD/RPA-derived expression (14) to define the pairwise vdW energy,

$$E_{\mathrm{vdW}}^{(\mathrm{pw})} = -\frac{1}{2}\sum_{A\neq B}\underbrace{\frac{3}{\pi}\int_0^\infty \alpha_A^{(\mathrm{sr})}\alpha_B^{(\mathrm{sr})}\mathrm{d}\omega}\frac{f_{\mathrm{damp}}\left(R_{AB};R_{\mathrm{ref}}^{(AB)}\right)}{{R_{AB}}^6} \qquad (43)$$

$$= -\frac{1}{2}\sum_{A\neq B} C_{6,AB}^{(\mathrm{eff})}\frac{f_{\mathrm{damp}}\left(R_{AB};R_{\mathrm{ref}}^{(AB)}\right)}{{R_{AB}}^6}, \qquad (44)$$

with A, B labeling atoms, f_{damp} denoting the damping function arising from range-separation, and R_{AB} as interatomic distance. Note that from our derivation, the C_6-coefficients are defined *via* the Casimir–Polder formula based on isotropic, static atomic polarizabilities, which should already include short-range screening. However, almost none of the pairwise-additive approaches explicitly accounts for the electrodynamic screening. Instead, most methods rely on effective polarizabilities or C_6-coefficients, which are meant to implicitly include such screening effects. The various pairwise models we have today basically differ in the way those effective vdW parameters are determined. As indicated in eqn (43) and (44), these typically also involve an atom-pair dependent reference distance, $R_{\mathrm{ref}}^{(AB)}$, which parametrically enters the damping function. Thereby, the actual mathematical form of this damping function has been shown to have a minor effect on the final vdW energetics.[45]

5.5.1 Electronic structure-based pairwise-additive interatomic methods. One very successful way to model the polarizability of the KS reference system without recourse to the Adler–Wiser formalism (18), is by incorporating information of the local chemical environment *via* the electron density. This represents an approximate, yet reliable and efficient method to account for type A non-additivity (see Section 2.3). A variety of successful schemes in this spirit has been devised to date, *e.g.*, the LRD model,[42] the non-local density functional for multipolar interaction coefficients by Tao *et al.*,[278,279] or the vdW-WF method.[280,281] In this work, we focus on some of the most widely used approaches: the vdW(TS) scheme[41] and the exchange-hole dipole moment model (XDM)[38,39] including the related density-dependent dispersion correction (dDsC) scheme.[44]

The vdW(TS) scheme

Just as the MBD model (see above), the vdW(TS) approach starts from the leading Padé approximant[250] based on an effective static atomic polarizability, $\alpha_{A,0}^{(\mathrm{TS})} \equiv \alpha_A^{(\mathrm{TS})}(i\omega = 0)$. While MBD subsequently explicitly accounts for screening effects (type B non-additivity), vdW(TS) directly uses this polarizability to approximate the short-range screened polarizability entering eqn (43):

$$\alpha_A^{(\mathrm{sr})}(i\omega) \approx \alpha_A^{(\mathrm{TS})}(i\omega) = \alpha_{A,0}^{(\mathrm{TS})}\left[1+\left(\frac{\omega}{\eta_A}\right)^2\right]^{-1}, \qquad (45)$$

where η_A corresponds to an effective excitation frequency as introduced in Section 5.4.[41] Inserting this into the Casimir–Polder integral in eqn (43) yields the London formula,[282] from which we can define the C_6-interaction coefficients entirely based on effective static atomic polarizabilities *via*

$$C_{6,AB}^{(\mathrm{eff})} \approx C_{6,AB}^{(\mathrm{TS})} = \frac{2C_{6,AA}^{(\mathrm{TS})}C_{6,BB}^{(\mathrm{TS})}}{\frac{\alpha_{B,0}^{(\mathrm{TS})}}{\alpha_{A,0}^{(\mathrm{TS})}}C_{6,AA}^{(\mathrm{TS})} + \frac{\alpha_{A,0}^{(\mathrm{TS})}}{\alpha_{B,0}^{(\mathrm{TS})}}C_{6,BB}^{(\mathrm{TS})}} \qquad (46)$$

$$\text{and} \qquad C_{6,AA}^{(\mathrm{TS})} = \frac{3}{4}\eta_A\left[\alpha_{A,0}^{(\mathrm{TS})}\right]^2.$$

Hence, the key quantity is the effective static atomic polarizability. To obtain this polarizability, one takes advantage of the linear correlation between the atomic volume, V_A, and the (static) atomic polarizability,[283] *i.e.*, $\alpha_A(i\omega = 0) = \kappa_A \cdot V_A$ with κ as proportionality constant. This allows the definition

$$\alpha_{A,0}^{(\mathrm{TS})} = \frac{\kappa_{\mathrm{eff}}^{(A)}V_{\mathrm{eff}}^{(A)}}{\kappa_{\mathrm{free}}^{(A)}V_{\mathrm{free}}^{(A)}}\alpha_{A,0}^{(\mathrm{free})} = \frac{\kappa_{\mathrm{eff}}^{(A)}}{\kappa_{\mathrm{free}}^{(A)}}\cdot x_V^{(A)}\cdot\alpha_{A,0}^{(\mathrm{free})}, \qquad (47)$$

where $\alpha_{A,0}^{(\mathrm{free})}$ is the static polarizability of the corresponding atom *in vacuo*.[41] The atomic volume can be determined as the expectation value of the cube of the electron-nucleus distance, r, based on the atomic density of the atom in its chemical environment or of the corresponding isolated atom, respectively. The effective atomic density is conventionally obtained *via* Hirshfeld analysis,[251] from which the rescaling factor, x_V, is given by

$$x_V^{(A)} = \frac{V_{\mathrm{eff}}^{(A)}}{V_{\mathrm{free}}^{(A)}} = \frac{\int r^3 w_A(\mathbf{r})\rho(\mathbf{r})\mathrm{d}\mathbf{r}}{\int r^3\rho_{\mathrm{free}}^{(A)}(\mathbf{r})\mathrm{d}\mathbf{r}}, \quad w_A(\mathbf{r}) = \frac{\rho_{\mathrm{free}}^{(A)}(\mathbf{r})}{\sum_B \rho_{\mathrm{free}}^{(B)}(\mathbf{r})} \qquad (48)$$

where w_A is the Hirshfeld weighting factor and $\rho(\mathbf{r})$ is the total electron density of the molecule or material. All densities, including the *in vacuo* atomic density, are evaluated at runtime with the same DFA. Finally, inserting the effective atomic polarizability into the second part of eqn (46), together with an equivalent consideration of (46) for an isolated atom, gives

$$C_{6,AA}^{(\mathrm{TS})} = \frac{\eta_A}{\eta_A^{(\mathrm{free})}}\left[\frac{\kappa_{\mathrm{eff}}^{(A)}}{\kappa_{\mathrm{free}}^{(A)}}\right]^2\left[x_V^{(A)}\right]^2 C_{6,AA}^{(\mathrm{free})} \simeq \left[x_V^{(A)}\right]^2\cdot C_{6,AA}^{(\mathrm{free})} \qquad (49)$$

where, upon closer inspection, the two prefactors involving η and κ together have been found to be well approximated by unity.[41] Relying on accurate reference data for the C_6-coefficients of the corresponding isolated atoms, $C_{6,AA}^{(\mathrm{free})}$, this approach has been shown to yield accurate effective interaction coefficients within 5.5% from values derived from experimental Dipole Oscillator Strength Distributions.[41] For the final ingredient of the energy expression (44), the damping function, a Fermi-type range-separation function was proposed,

$$f_{\mathrm{damp}}^{(\mathrm{TS})}\left(R_{AB};R_{\mathrm{vdW}}^{(AB)}\right) = \left\{1+\exp\left[-d\left(\frac{R_{AB}}{s_R\cdot R_{\mathrm{vdW}}^{(AB)}}-1\right)\right]\right\}^{-1}, \qquad (50)$$

where the steepness of the damping, d, has been found to have a negligible effect on binding energies and is therefore fixed to $d = 20$. The onset of the range-separation, finally, is determined by the DFA-dependent scaling parameter s_R (typical values: 0.94 for PBE, 0.96 for PBE0, 0.84 for B3LYP) and an effective vdW distance, $R_{\mathrm{vdW}}^{(AB)}$, given by the sum of the corresponding effective vdW radii of atoms A and B. Based on the definition of the vdW radius by Pauling and considerations from classical physics, the vdW radius of an atom is proportional to the cube-root of its volume.** This allows to define an effective vdW radius of an atom in a similar manner from its *in vacuo* counterpart:

$$R_{\mathrm{vdW}} \propto \sqrt[3]{V} \Rightarrow R_{\mathrm{vdW}}^{(A)} = \sqrt[3]{x_V^{(A)}} \cdot R_{\mathrm{vdW}}^{(A,\mathrm{free})}. \tag{51}$$

Combining eqn (44) and eqn (48)–(51), ultimately defines the vdW dispersion energy in vdW(TS),

$$E_{\mathrm{vdW}}^{(\mathrm{TS})} = -\frac{1}{2}\sum_{A\neq B} f_{\mathrm{damp}}^{(\mathrm{TS})}\left(R_{AB}; R_{\mathrm{vdW}}^{(AB)}\right)\frac{C_{6,AB}^{(\mathrm{TS})}}{{R_{AB}}^6}. \tag{52}$$

Effective, electronic structure-based vdW parameters can also be obtained *via* an alternative, yet similarly accurate and reliable, approach, which relies on net atomic populations instead of the real-space representation of the electron density as used in the Hirshfeld scheme outlined above. Atomic populations as initially classified by Mulliken, can be calculated in Fock space, *i.e.*, from the density-matrix in an atom-centered basis set representation. The alternative rescaling factor $x_{\mathbf{D}}$ is defined as,[285]

$$x_{\mathbf{D}}^{(A)} = \frac{h_A}{Z_A}; \quad h_A = \sum_a f_a \sum_{i\in A} \|\mathbf{D}_{ii}\|^2, \tag{53}$$

where Z_A is the nuclear charge (atomic number) of atom A corresponding to h_A for an atom *in vacuo*. We would like to point out that h_A, being the atom-projected trace of the Mulliken population matrix $\mathbf{D}$, does not involve off-diagonal (mixed) terms of the density matrix. As such, it does not suffer from the arbitrariness of partitioning the electron population of overlap regions, which represents the main and fundamental pitfall of Fock-space charge partitioning schemes. This approach yields interaction coefficients *en par* with the original scheme[285] and allows for the usage of the vdW(TS) model and the MBD formalism in conjunction with electronic structure methods without real-space representation of the electron density, such as the semi-empirical Density-Functional Tight-Binding method or other density matrix-based approaches. Similar in spirit, yet neglecting some hybridization effects and relying on the not well-defined full Mulliken charge, is the dDMC vdW model by Petraglia *et al.*[286] (see below).

The vdW(TS) method uses the same starting point as the MBD formalism. The interaction coefficients used in eqn (52) can thus also be adapted *via* the coarse-grained Dyson eqn (36) to account for electrodynamic (short-range) screening. Such an approach can be used to dissect the importance of screening and multi-center interactions for dispersion interactions (further sub-classifying type B non-additivity). Furthermore, the vdW(TS) scheme can be used to investigate the effect of dispersion interactions on the electronic structure and derived properties.[19] As the interaction coefficients are a functional of the electron density (or density matrix), the effective potential arising from long-range correlation forces can be derived. Inclusion of this term in the self-consistency procedure of the DFT calculation, termed self-consistent vdW(TS), has been shown to affect the work function of metals, for instance.[19] As already mentioned for the MBD model, see Section 5.4, usage of Hirshfeld analysis for the calculation of the vdW parameters can lead to a considerable underestimation of the effect of charge transfer. Also in the case of vdW(TS), this deficiency can be alleviated *via* the iterative Hirshfeld scheme[265,266] or by the use of a charge-dependent reference for the isolated atom.[267] For the simulation of hybrid organic–inorganic interfaces, an adapted version vdW$^{\mathrm{surf}}$ has been devised,[287] which accounts for the metallic screening in the substrate according to Lifshitz–Zaremba–Kohn theory.[59,60] The vdW$^{\mathrm{surf}}$ model significantly improves upon the original scheme and provides an description of the binding properties of metal surface-adsorbed organic molecules.[287–291]

The XDM model and the dDsC scheme

In the exchange-hole dipole moment (XDM) model, vdW dispersion interactions are interpreted as the interaction of electronic multipoles spanned by the moving electron and its accompanied exchange- or Fermi-hole: the instantaneous depletion of the probability to find a second electron near the position of an electron with equal spin. For a single atom the total atomic moment integrals, $\langle M_l^2\rangle$ can be calculated *via*

$$\left\langle M_l^2\right\rangle = \sum_\sigma 4\pi\int \mathrm{d}\mathbf{r}\rho_\sigma(\mathbf{r})\left\{\|\mathbf{r}-\mathbf{R}\|^l - [\|\mathbf{r}-\mathbf{R}\| - \mathscr{D}_\sigma(\mathbf{r})]^l\right\}^2, \tag{54}$$

where ρ_σ is the electron density in spin-channel σ, $\mathbf{r}$ is the spatial coordinate and $\mathbf{R}$ is the position of the nucleus. $\mathscr{D}_\sigma$ is the magnitude of the exchange-hole dipole moment, which can be obtained exactly from occupied orbitals, referred to as XDM(EXX) and typically used as post-HF method, or approximated from the Becke–Roussel model[292] for the exchange-hole, referred to as XDM(BR) and typically used in the context of DFT.[293] For an N-atom system, this is partitioned into N atomic contributions by means of the Hirshfeld scheme. The dipole moment integral of atom A in a many-atom system, for instance, is given by

$$\left\langle {M_1}^2\right\rangle_A = \sum_\sigma 4\pi\int \mathrm{d}\mathbf{r} w_A(\mathbf{r})\rho_\sigma(\mathbf{r})\mathscr{D}_\sigma{}^2(\mathbf{r}), \tag{55}$$

with w_A as Hirshfeld weighting factor, see eqn (48). Using a closure or Unsöld-approximation, as also employed in MBD or vdW(TS), one can obtain a relation between these atomic exchange-hole dipole moment integrals and the dipole–dipole

** We note that a recent study[284] predicts such classical considerations to be insufficient and that, in quantum systems, different scaling laws can apply.

interaction coefficients for pairwise vdW interactions given by

$$C_{6,AB}^{(\mathrm{XDM})} = \frac{2\langle M_1^2\rangle_A\langle M_1^2\rangle_B}{3\ \Delta_A+\Delta_B} = \frac{\alpha_{\mathrm{eff}}^{(A)}\alpha_{\mathrm{eff}}^{(B)}}{\underbrace{\alpha_{\mathrm{eff}}^{(B)}\langle M_1^2\rangle_A+\alpha_{\mathrm{eff}}^{(A)}\langle M_1^2\rangle_B}_{K_{AB}}}\langle M_1^2\rangle_A\langle M_1^2\rangle_B, \quad (56)$$

with Δ_A as average excitation energy into unoccupied orbitals of atom A, which can be expressed in terms of (effective) atomic polarizabilities by comparison to London's formula based on the first Padé approximant of the dynamic polarizability to yield the final expression.[294,295] Ultimately, effective atomic polarizabilities are obtained *via* rescaling of accurate reference data using Hirshfeld volume ratios as in the vdW(TS) model, eqn (47). The XDM model typically also involves evaluation of higher multipole vdW interactions. This gives rise to expressions similar to eqn (44) with corresponding Cn-interaction coefficients and a R^{-n}-dependence. The resulting total vdW energy is typically well-converged when accounting for n = 6, 8, 10. The $C_{8/10}$-coefficients are calculated based on the same footing using the atomic quadrupole and octopole moment integrals (l = 2, 3) and K_{AB} from eqn (56) *via*[294]

$$C_{8,AB}^{(\mathrm{XDM})} = K_{AB}\frac{3}{2}\left(\langle M_1^2\rangle_A\langle M_2^2\rangle_B+\langle M_2^2\rangle_A\langle M_1^2\rangle_B\right)$$
$$C_{10,AB}^{(\mathrm{XDM})} = K_{AB}\left[\frac{21}{5}\langle M_2^2\rangle_A\langle M_2^2\rangle_B + 2\left(\langle M_1^2\rangle_A\langle M_3^2\rangle_B+\langle M_3^2\rangle_A\langle M_1^2\rangle_B\right)\right]. \quad (57)$$

To couple the XDM approach as a long-range correlation model with (semi-)local DFAs, a rational damping was proposed, such that the final energy can be written as[39]

$$E_{\mathrm{vdW}}^{(\mathrm{XDM})} = -\frac{1}{2}\sum_{A\neq B}\frac{C_{6,AB}^{(\mathrm{XDM})}}{{R_{AB}}^6}\left[1+\left(\frac{a_1\cdot R_{\mathrm{cut}}^{(AB)}+a_2}{R_{AB}}\right)^6\right]^{-1}, \quad (58)$$

with a_1 and a_2 as DFA-dependent damping parameters.[294] In addition, three-body vdW interactions can be included according to the Axilrod–Teller–Muto formula,[296,297]

$$E_{\mathrm{vdW}}^{(\mathrm{ATM})} = \sum_{A,B,C}[\cos(\varphi)\cos(\vartheta)\cos(\theta)+1]\frac{C_{9,ABC}}{(R_{AB}R_{BC}R_{CA})^3}, \quad (59)$$

where φ, ϑ, θ are the angles enclosing the triangle spanned by the atomic positions of atoms A, B, and C. The corresponding C_9-interaction coefficients in the XDM-framework are given by,[295]

$$C_{9,ABC}^{(\mathrm{XDM})} = \frac{Q_AQ_BQ_C(Q_A+Q_B+Q_C)}{(Q_A+Q_B)(Q_B+Q_C)(Q_C+Q_A)},$$
$$\text{where } Q_A \equiv C_{9,AAA}^{(\mathrm{XDM})} = \frac{3}{4}\alpha_{\mathrm{eff}}^{(A)}C_{6,AA}^{(\mathrm{XDM})}. \quad (60)$$

In order to use the ATM expression in conjunction with (semi-)local DFAs, it is damped at short internuclear separations. Thereby, an obvious ambiguity arises in the definition of an effective distance in the damping function. Various forms have been formulated[1,298–300] and the convoluted interplay of intricate error cancellations with(in) different DFAs often leads to the sometimes unpredictable performance of adding the ATM term.[1,301–303]

As a further adaption of the XDM approach, Steinmann and Corminboeuf introduced a combination of XDM interaction coefficients with a more rigorous, density-dependent damping function based on the universal damping functions by Tang and Toennies[304] and the more robust iterative Hirshfeld partitioning scheme[265] to obtain atomic polarizabilities in eqn (56).[305] As in the case of the vdW(TS) scheme, this model, termed dDXDM, has been shown to provide significant improvements in particular for ionic systems thanks to the more reliable and robust partitioning scheme.[305] Building ontop of this approach, a simplification of the Becke–Roussel model tailored for the derivation of long-range interaction coefficients has been derived by the same authors and has been given the name dDsC.[306] It typically employs an (iterative) Hirshfeld-dominant partitioning scheme[306,307] and has been shown to yield accurate results for a variety of benchmark sets for vdW complexes, ionic systems, and reactions while affording rather low computational costs in comparison to vdW-optimized (non-local) density functionals.[44,306] With the C_6-coefficients and the damping function being a functional of the electron density, the dDsC model can also be used self-consistently in order to investigate vdW effects on the electronic structure at acceptable computational cost.[18]

The dDsC scheme has also been adapted for use in Tight-Binding approaches, where the Hirshfeld partitioning has been replaced by Mulliken charge analysis. Despite neglecting important hybridization effects (vdW parameters of homonuclear systems correspond to *in vacuo* parameters, for instance), the resulting dDMC model has been shown to substantially augment the semi-empirical Density-Functional Tight-Binding method for the description of non-covalent interactions.[286]

5.5.2 (Semi-)empirical pairwise approaches. The first widely used vdW model in the context of DFT was the DFT-D approach by Grimme, which followed the form of eqn (44) and featured effective, but fixed C_6-interaction coefficients and a Fermi-type damping function.[37] The applicability was later (DFT-D2) extended by deducing effective interaction coefficients from atomic properties.[40] It is worthwhile to mention that both approaches did not account for any effects of the chemical environment (type A non-additivity) nor did they yield the correct asymptotic behavior.[43] These obsolete methods can thus not be recommended for use in electronic structure calculations today. After careful numerical investigation of the effect of the local chemical environment, a new semi-empirical variant, termed D3, was devised. The scheme is based on atom-pair specific C_6 coefficients and includes local information in the form of geometry-motivated, fractional coordination numbers,[43]

$$\mathrm{CN_A} = \sum_{B\neq A}\left\{1+\exp\left[-p_1\cdot\left(p_2\cdot\frac{R_{\mathrm{cov}}^{(A)}+R_{\mathrm{cov}}^{(B)}}{R_{AB}}-1\right)\right]\right\}^{-1}, \quad (61)$$

where the parameters p_1 = 16 and p_2 = 4/3 have been chosen based on a set of organic molecules, R_{AB} is the distance between atoms A and B, and $R_{\mathrm{cov}}^{(A)}$ is the (scaled) covalent radius of atom A. The final procedure has been shown to yield chemically sensible coordination numbers for a variety of organic and non-organic systems.[43] The interaction coefficient for atoms A and B is then calculated for a number of different coordination numbers, which are achieved by considering the corresponding hydrides and approximately decomposed to provide reference values for $C_{6,\mathrm{AB}}$. This collection of coordination number-dependent C_6 coefficients then serves as a reference database and the final effective interaction coefficient, $C_{6,AB}^{(\mathrm{D3})}$, which enters eqn (44), is obtained from interpolation of the reference coefficients based on their coordination numbers *via*

$$C_{6,AB}^{(\mathrm{D3})}(\mathrm{CN}_A, \mathrm{CN}_B) = \frac{1}{\mathscr{L}} \sum_{A_{\mathrm{ref}}} \sum_{B_{\mathrm{ref}}} C_{6,A_{\mathrm{ref}}B_{\mathrm{ref}}} L(A_{\mathrm{ref}}, B_{\mathrm{ref}}), \quad (62)$$

where

$$L(A_{\mathrm{ref}}, B_{\mathrm{ref}}) = \mathrm{e}^{-p_3\left[\left(\mathrm{CN}_A - \mathrm{CN}_{A_{\mathrm{ref}}}\right)^2 + \left(\mathrm{CN}_B - \mathrm{CN}_{B_{\mathrm{ref}}}\right)^2\right]} \quad (63)$$

and $\mathscr{L}$ is the sum of all Gaussian distances $L(A_{\mathrm{ref}},B_{\mathrm{ref}})$, The last global *ad hoc* parameter p_3 = 4 to assure smooth behavior at integer coordination numbers.[43] Thus, the effective interaction coefficients are interpolated from reference values based on their local coordination. The general procedure for the definition of coordination numbers and the interpolation scheme is thereby, in principle, completely arbitrary and was motivated by numerical results.[43] The geometry-based D3 model neglects any electronic structure and explicit screening effects, but at the same time models dispersion interactions beyond the dipole approximation and allows for a vdW correction for any given total energy method including molecular mechanics. As showcased by Ehrlich *et al.* strong electronic structure effects like far-from-neutral species, can be incorporated by a suitable choice of reference systems for the interpolation scheme.[308] For general applications however, such an approach introduces a certain degree of empiricism and requires a careful choice and testing. Recently, also a more straightforward approach to include such effects *via* rescaling of interaction coefficients based on atom-in-a-molecule charges was proposed (D4) and shown to significantly improve transferability and general applicability.[309] The D3 scheme also involves an additional term for pairwise dipole–quadrupole vdW interactions, which scales as $1/R^8$ (derived from perturbation theory). The C_8-interaction coefficients, *i.e.*, the equivalent of C_6 for dipole–quadrupole vdW interactions, are computed recursively[304,310,311] based on the corresponding C_6-coefficients.[43] For the damping two mathematical forms are commonly used: the original scheme employed a formulation proposed by Chai and Head-Gordon.[312] Including the quadrupolar interaction term, this defines the vdW energy in D3 as

$$E_{\mathrm{vdW}}^{(\mathrm{D3})} = -\frac{1}{2} \sum_{A \neq B} \sum_{m=6,8} \frac{p_4^{(m)} C_{m,AB}^{(\mathrm{D3})} \Big/ R_{AB}^m}{1 + 6\left(p_5^{(m)} \cdot R_{\mathrm{D3}}^{(AB)} \Big/ R_{AB}\right)^{2n_{\mathrm{b}}+m+4}} \quad (64)$$

respectively. Above, n_{b} = 2 for two-body interaction and m = 6, 8 denotes dipole–dipole and dipole–quadrupole interaction. p_4 is a rescaling factor for the dipole–quadrupole interaction (p_4 = 1 for m = 6), while p_5 is a DFA-dependent damping parameter, which together with the atom pair-dependent cutoff radius, R_{D3}, determines the onset of the vdW correction. The cutoff radius R_{D3} is determined from the attenuation of the DFT interaction energy below a certain threshold for the corresponding dimer.[43] Such a choice of cutoff parameters instead of vdW radii in the damping function can conceptually be justified as the appropriate range-separation is not necessarily a function of vdW radii, but depends on the range of electron correlation captured by the underlying DFA. This, however, is highly system-dependent and a rigorous and seamless scheme for arbitrary systems has not been derived so far. As an alternative range-separation, Becke and Johnson proposed to use a rational damping as in the XDM model (*cf.* eqn (58)) also in D3, which is widely used and referred to as D3-BJ.[38,39,45] The cutoff radius entering the damping function in the case of D3-BJ is defined by[45]

$$R_{\mathrm{D3\text{-}BJ}}^{(AB)} = \sqrt{C_{8,AB}^{(\mathrm{D3})} \Big/ C_{6,AB}^{(\mathrm{D3})}}. \quad (65)$$

A nowadays common extension of the DFT-D3 framework is to also include beyond-pairwise terms in the form of the three-body term according to Axilrod and Teller[296] and Muto,[297] eqn (59). In the context of D3, the effective three-body C_9-interaction coefficients are approximated *via* the effective two-body C_6-coefficients according to

$$C_{9,ABC}^{(\mathrm{D3})} = -\sqrt{C_{6,AB}^{(\mathrm{D3})} C_{6,BC}^{(\mathrm{D3})} C_{6,CA}^{(\mathrm{D3})}}. \quad (66)$$

Finally, the three-body term is damped at short distances equivalently to the two-body interaction in eqn (64) using p_4 = 4/3, n_{b} = 3 and m = 6. As mentioned above in the context of the XDM model, formulating a rigorous damping function for the three-body ATM energy in terms of internuclear distances leads to an obvious ambiguity and can give rise to a considerable uncertainty whether the additional three-body term improves the final vdW energies.[302,303]

5.5.3 Pairwise-additive vdW models in select electronic structure codes. As of today most electronic structure packages feature pairwise-additive vdW models to correct for the lack of long-range correlation in common (semi-)local DFAs. Among others the following approaches are available:

- ABINIT[191–193] features the D3 dispersion correction (64), D3-BJ, and the three-body D3-ATM term, eqn (59) with definition (66).
- ADF[273–275] allows for inclusion of D3, D3-BJ, and dDsC as post-DFT vdW models.
- CASTEP:[276] pairwise-additive vdW models can be included in an *a posteriori* fashion. Available methods include vdW(TS), vdW$^{\mathrm{surf}}$, and D3.
- DFTD3:[313] being independent of the electronic structure, the D2, D3 and D3-ATM models can be employed *a posteriori* to any electronic-structure calculation *via* a standalone calculator.

For instance, a library version of Grimme's DFTD3 code is available at https://github.com/aradi/dftd3-lib.

• FHI-aims:[195] the vdW(TS) model can be applied for periodic and non-periodic systems in an *a posteriori* manner as well as self-consistently, which accounts for long-range correlation effects on the self-consistent solution for the electron density and derived properties.

• Gaussian:[314] D3 and D3-BJ can be included natively. For the XDM model, Otero de la Roza and co-workers, developed the post-processing program *postg*[315,316] available as free software on https://github.com/aoterodelaroza/postg. Further information on the usage of the program and damping parameters are available at http://schooner.chem.dal.ca/wiki/XDM.

• NWChem[317] features the original dispersion model by Wu and Yang[277] and Grimme's D1, D2, D3, and D3-BJ including default parameters for a variety of xc functionals. The XDM model is available. As of the time of this publication, this requires manual specification of the damping parameters a_1 and a_2 for a given xc functional, which can be obtained from ref. 316 or at http://schooner.chem.dal.ca/wiki/XDM.

• Q-Chem[227] allows for inclusion of several (semi-)empirical dispersion corrections including the scheme by Chai and Head-Gordon[312] as well as Grimme's D3 with a number of options for the damping function. In addition, the ATM three-body term can be included. Also, the electronic structure-based XDM (post-DFT and self-consistent) and vdW(TS) models are available.

• Quantum espresso:[228] the XDM model can be used (only together with PAW pseudopotentials, however). The corresponding a_1 and a_2 parameters can again be obtained, for instance, at http://schooner.chem.dal.ca/wiki/XDM. The vdW(TS) scheme is implemented as post-DFT model as well for self-consistent inclusion of vdW interactions.

• TURBOMOLE:[196] the D3, D3-BJ and the D3-ATM vdW model can be added.

• VASP:[197–201] the pairwise-additive models D3, D3-BJ, or vdW(TS) can be enabled. Also, the extension of the vdW(TS) model by using iterative Hirshfeld partitioning as well as Ewald summation of the vdW(TS) energy for periodic systems is implemented and the dDsC scheme is available with conventional Hirshfeld-dominant partitioning.

6 Performance

With the exception of the fully first-principles EXX/cRPA approach, all of the above methods involve minimum one empirical parameter and in the end all of the practical methods outlined above rely on a given model for the non-local density–density response and approximations to the evaluation of the ACFD formula. Therefore, the importance of careful analysis of the transferability and validity of the employed approximations cannot be overestimated. However, the applicability of highly accurate quantum-chemical approaches, including (local) coupled cluster theory, Quantum Monte-Carlo (QMC), and SAPT, as reference methods is limited to a maximum of a few hundred atoms in the best case. Due to the often still substantial gap between experimentally and theoretically accessible length-scales, comparison to experimental data also does not represent a seamless and adequate way of assessing the accuracy of vdW models in all but a few cases. As a result, most of the practical approaches for modeling vdW interactions are parametrized and tested against benchmark sets of small (and medium) size complexes or simple molecular materials. As we shall see in the following section, the majority of schemes provides comparable accuracy for these standard test sets. Yet, long-range correlation forces show a far from trivial, strongly non-linear behavior with increasing system size due to their inherently quantum-mechanical and non-local character. As such, the performance of different models often strongly depends on the size and complexity of the systems under consideration (see Section 6.2). A careful analysis and comparison among models that rely on different approximations can provide tremendous insight into the failure of certain models or approximations and is invaluable for further methodological developments. In the following we will present a few exemplary test sets and reference systems to illustrate such cases. Please note, that most of the numerical data presented herein has not been based on maximally accurate DFT calculations (consistent improvements of up to 1% possible, yet negligible for the relative accuracy of the vdW models). Instead, we have used settings as they are employed in typical production calculations, which in our opinion offers an optimal way to discuss general trends and features of the models and particular systems in the context of practical applications.

6.1 Benchmark sets with high-level reference data

Typically, vdW models are judged based on the interaction energies they provide in comparison to high-level quantum-chemical calculations. An important advantage of such an approach is that it allows to evaluate the different models based on a given (fixed) geometry of the test system and does not involve an intricate interplay of the interaction energy and, *e.g.*, finite-temperature effects, which can be hard to disentangle. At the same time, it allows to evaluate the accuracy of interaction energies as a function of nuclear positions, *i.e.*, the overall shape of the potential energy surface.

Over the last decade, especially the group of Hobza has designed and obtained a number of benchmark sets in this spirit. Among others,[321–324] this includes sets of small molecular dimers in equilibrium configuration (S22, S66)[318,320] featuring a variety of types of intermolecular interactions (vdW-bound, hydrogen-bonded, mixed) and the corresponding dissociation curves (S22x5, S66x8).[319,325] The remaining empirical (damping) parameter(s) in almost all of the above practical models, have been obtained based on an optimal performance for these benchmark sets. As a result, the different vdW models overall perform comparably well on these sets of molecular dimers (*cf.* Table 2) and as a main conclusion it underlines the importance of vdW interactions for a reasonable description (accuracy of bare PBE more than four times worse than any vdW-inclusive method!). Upon closer inspection, we see that, as one might expect, the

Table 2 Mean absolute deviations (MADs) of interaction energies obtained by MBD, vdW(TS), XDM, D2, D3, and D3-ATM in conjunction with the PBE-GGA density functional for the S22, S66, and S66x8 benchmark sets in kJ mol^{-1}. The calculations have been performed using standard production settings in FHI-Aims,[195] NWChem,[317] and the DFTD3 code.[313] Reference data from CCSD(T)/CBS calculations[318–320]

		S22	S66	S66x8	Average
PBE		10.88	9.00	6.44	8.77
PBE +	MBD	2.01	1.55	1.34	1.63
	vdW(TS)	1.42	1.42	1.38	1.41
	XDM	1.72	1.59	1.72	1.67
	D2	2.13	2.34	1.76	2.08
	D3	1.80	1.26	1.13	1.39
	D3-ATM	2.01	1.38	1.26	1.55
vdW-DF2[a,b]		2.13	2.01		2.07
VV10[a,c]		1.30	1.26		1.28
LC-VV10[a,c]		0.88	0.63		0.75

[a] Data taken from ref. 220. [b] Data taken from ref. 214. [c] Data taken from ref. 219.

empirical D2 scheme with its neglect of the local chemical environment typically yields the least accurate results. Nevertheless, employing any of the vdW models drastically improves upon the bare (semi-)local description with PBE or other DFAs for that fact. When testing such combined approaches of a (semi-)local DFA and a given vdW model, one should also consider the error in the short-range description associated with the chosen DFA. Any discussion or optimization of dispersion methods beyond this intrinsic error is not physical and should be avoided.

For years, small organic dimers as discussed above represented the only class of systems, where accurate reference data was available. The accuracy of simple, pairwise vdW models for these systems motivated their wide-spread use and even gave rise to the impression that dispersion interactions can universally be well approximated by pairwise-additive interatomic potentials as still concluded in many standard textbooks. A first step to go beyond these typical reference sets was the investigation of molecular crystals, where an accurate treatment of dispersion interactions is vital.[3,4,301,303,326] As a test suite, the C21 benchmark set[327] and its extended version X23[328] have been proposed. Here one relies on lattice energies derived from experimental sublimation enthalpies. For such an approach and the comparison to experimentally derived reference data, in general, it is important to keep in mind possible experimental errors or uncertainties - both in the experimental measurement and for the derivation of (electronic) interaction energies, where one typically relies on some (simple) model to account for the experimental conditions. As can be seen from Fig. 5, many modern vdW models (MBD, XDM, D3, D3-ATM) almost reach this experimental accuracy of roughly 4.3% (4.6 kJ mol^{-1}), while vdW(TS) and rVV10 give a mean absolute relative error (MARE) of 17.2 and 15.0%. This divergence between the pairwise models and in particular the poor performance of the vdW(TS) model can be explained by two major points. First, the (Hirshfeld) rescaling procedure does not sufficiently capture the effect of the local environment due to the strong anisotropy in the system, which is exemplified by the significant improvement when explicitly accounting for short-range screening (see "with SCS" in Fig. 5). Second, as pointed out by Otero de la Roza and Johnson, the neglect of higher multipole vdW interactions can lead to an overestimation due to a spurious damping/range separating function for the dipolar C_6/R^6-interaction.[295,329] Neglecting higher multipole vdW interactions in the D3 model, for instance, leads to a similar performance as for the C_6/R^6-only vdW(TS) scheme (*cf.* "only dip." in Fig. 5). The performance of rVV10 for these systems can mainly be traced down to the neglect of screening effects (type-B non-additivity, see Section 5.2), which have been shown to be important for anisotropic systems. In addition, experience has shown that rVV10, and VV09 for that matter,[218] perform best with more "repulsive" semi-local functionals, *i.e.*, functionals capturing a sufficient portion of exchange-repulsion. Hence, the PBE functional might not represent an optimal choice for combination with rVV10. For consistency with the remaining calculations, however, we will stick to the PBE xc-functional throughout this work.

In another approach to study vdW interactions in larger-scale systems, Grimme and Risthaus[330,331] made use of experimentally

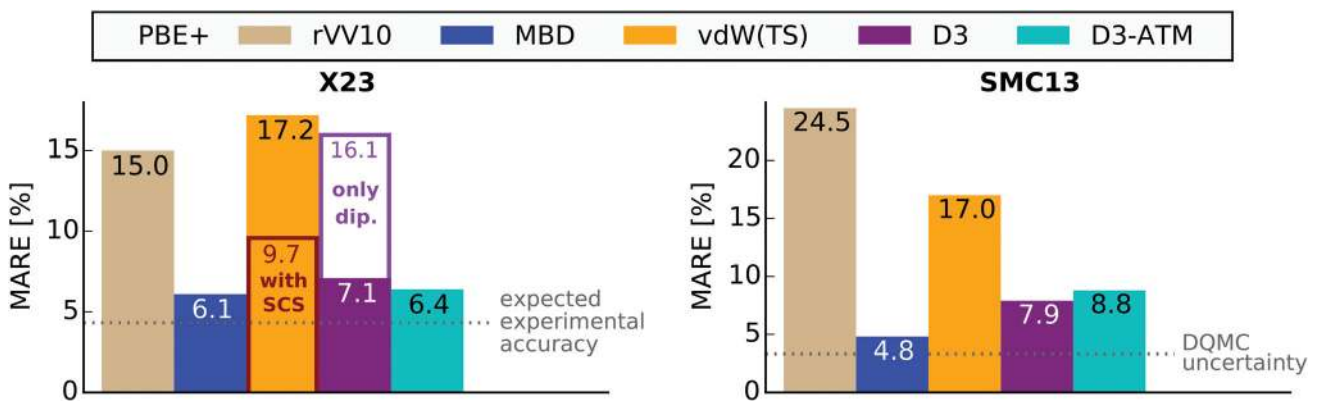

Fig. 5 Mean absolute relative error (MARE) of PBE in conjunction with van der Waals models. Left: With respect to experimentally derived lattice energies for X23 set of molecular crystals[327,328] (rVV10 result taken from ref. 261). Results for D3 with neglect of higher multipole interactions and vdW(TS) with account for electrodynamic screening shown as empty bars. Right: Interaction energies as compared to Diffusion Quantum Monte-Carlo (DQMC) results for the SMC13 set of supramolecular complexes (see Fig. 6). Note that the MARE for plain PBE is 61% and 128% for X23 and SMC13, respectively.

derived association energies, when they compiled the S12L benchmark set of supramolecular guest–host complexes. The reference data was derived from experimental Gibb's free energies in solution. Thanks to ongoing methodological developments in the quantum-chemistry community and the ever-growing computational power, accurate QMC results are also available for a subset of S12L. These calculations provide a reliable benchmark at a given geometry, which is free of any thermal or solvation effects. Noteworthy, these results show that the approximations in the ''back-correction'' from experimental free energies can introduce errors of up to 16% (or 15 kJ mol^{-1}).[8] In addition to the subset of S12L set covered in ref. 8, Hermann *et al.* obtained QMC reference results for additional guest–host complexes of the C_{70} fullerene.[9] For the purpose of this work, we compiled 13 supramolecular complexes for which QMC reference data is available. This set, to which we will refer to as ''SMC13'', is shown in Fig. 6. The complexes are characterized by strongly anisotropic molecular polarizabilities and represent showcase examples for the non-additivity of (short-range) screening and multi-center interactions. It also shows the absolute inapplicability of bare (semi-)local DFAs for non-covalently bound systems with increasing size. In fact, PBE predicts attractive interaction for only three of the 13 complexes and yields a MARE of 128%.

Including vdW forces in form of the atom-pairwise vdW(TS) model or two-point non-local rVV10 density functional already drastically improves the description of supramolecular complexes as contained in the SMC13 set down to a MARE of 17–25% (see Fig. 5). One main part of the remaining error can be traced down to the strong anisotropy of the systems. This gives rise to significant many-body effects in form of (short-range) screening, which are not captured by the Hirshfeld rescaling procedure in vdW(TS) and the semi-local polarizability functional in rVV10. Thanks to an improved description of screening effects *via* additional gradient information, the still pairwise XDM model yields significantly better results.[329] Also in the case of D3, considerable improvements can be obtained. How much of the improvements in XDM and D3 stem from the inclusion of higher-multipolar interactions is still often under debate. Inclusion of the ATM three-body term, for example, in both cases reduces the accuracy. This might be connected to the ambiguous definition of the damping function for the three-body energy, but on the other side might raise the question in how far the increased functional space in form of multipolar interactions facilitates error cancellation and overfitting. In the case of VV10, on the other side, it has been shown, that inclusion of the ATM vdW energy leads to considerable improvements in the description of supramolecular complexes.[332] Accounting for (short-range) dielectric screening as well as (long-range) electron correlation to all orders in the MBD formalism, ultimately, yields mean deviations just above the uncertainty of the reference method.

Overall, the X23 and SMC13 test sets allow to get a glimpse at the non-additivity of vdW interactions in systems beyond the typically considered simple dimers and further benchmark sets

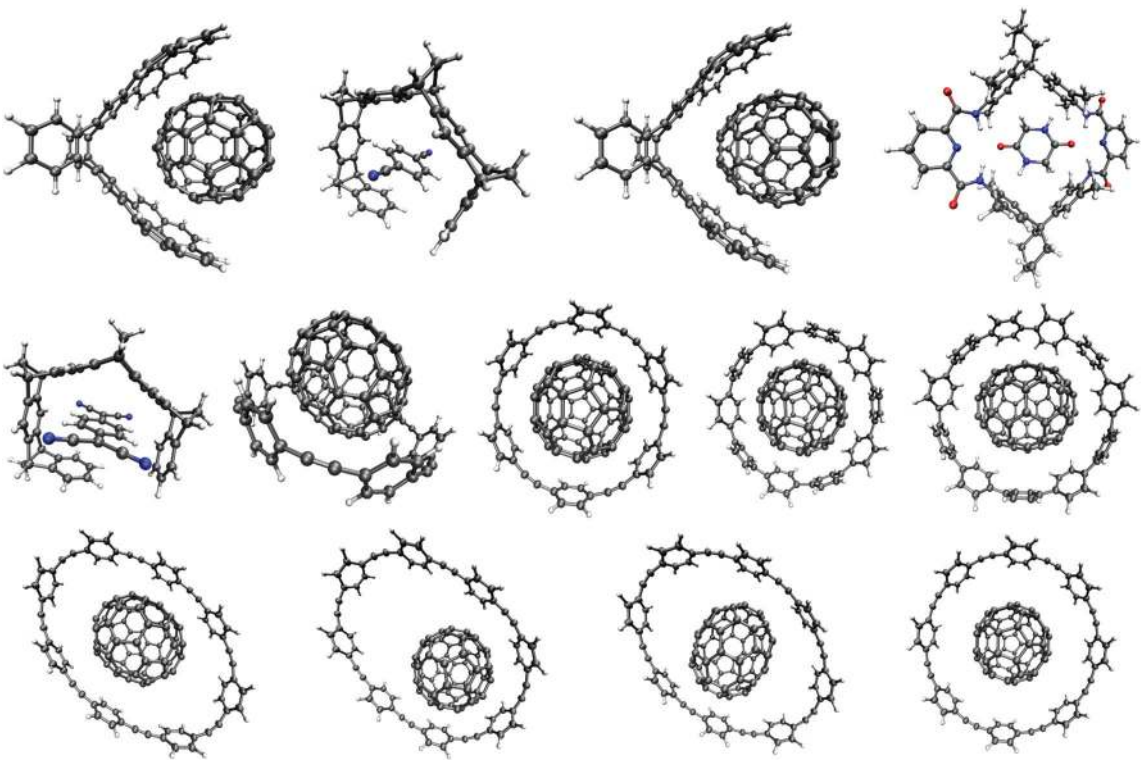

Fig. 6 SMC13 complexes. First row, left to right: C_{60}@catcher, 1,4-dicyano benzene@tweezer, C_{70}@catcher, and gycine anhydride@macrocycle. Second row: tetracyano quinone@tweezer, two configurations of C_{70}@[6]-CPPA (cycloparaphenylacetelyne), C_{70}@[10]-CPP (cycloparaphenylene), and C_{70}@[11]-CPP. Third row: four configurations of C_{70}@[8]-CPPA.

in this direction are being compiled and have already been proposed, *e.g.*, the S8 or L7 set.[333,334] It is worthwhile to point out that this can be assumed to only be the tip of the iceberg of the many-body nature of long-range correlation forces, which are expected to occur in more complex systems and materials.

6.2 Beyond typical benchmarking

Above, we outlined the general benchmarking scheme for (vdW) approaches in electronic structure modeling: Determining and discussing the overall deviation from high-level reference data of interaction energies based on a select set of hopefully diverse systems, which then serves as an estimate for the expected accuracy. For many studies in molecular and materials modeling, however, the average performance in terms of electronic interaction energies does not represent an optimal testing ground for the accuracy of the studied quantity or property. For studying the critical points on a potential energy surface, for example, the average accuracy of interaction energies in equilibrium geometries provides only limited information. Therefore, it is worthwhile to also analyze more specific quantities a given (combined) electronic structure method yields. In recent years a number of studies showed that while providing similar accuracies for the common benchmark sets, the results for specific applications can substantially differ when employing different vdW models. In the following we will showcase some of these findings.

6.2.1 Precision and reproducibility. As a first important point, we would like to remind about one of the fundamental necessities of science: the replicability of results. One major concern in molecular and materials modeling in general is that by now we have a wide array of software available to perform computational studies. Typically, each of these (electronic structure) codes uses a different computational and sometimes theoretical framework in order to perform calculations (different approaches to diagonalization, integration, *etc.*). Additionally, there exists a variety of potential basis set representations for the wavefunction or electron density. As a result of all this, it has been shown for DFT calculations that careful testing is needed such that different implementations of the same theoretical approach also yield the same results.[335] In the same way, different implementations of vdW models have to be carefully checked and compared in terms of consistency. Experience has shown that, different codes can yield different results for the same vdW approach. This especially holds true for electronic structure-based methods, as different electronic structure codes are typically tested and benchmarked with respect to energies and not for the parameters entering the vdW model. Thus, a collective effort to unify the results from different implementations is of utmost importance and on-going work.

6.2.2 Beyond (single) equilibrium structures. Another important point, which remains largely under-explored in the typical benchmark procedure outlined above, is the performance of vdW-inclusive electronic structure methods beyond individual equilibrium geometries.

Relative energies of (meta-)stable states. Predicting a correct energetic ranking is of utmost importance in the field of crystal structure prediction, for instance.[4,303] Molecular crystals are often characterized by a variety of possible and meta-stable polymorphs (crystalline systems with equivalent composition, but different crystal packing), which are mainly governed by non-covalent interactions. Knowing the thermodynamically most stable form is quintessential in, *e.g.*, pharmacy or organic electronics, as a given drug or functional organic material might loose its solubility or functionality upon phase transition to a thermodynamically more stable form as regretfully discovered in the case of the HIV protease inhibitor Ritonavir.[336] As such, predicting the correct energetic order in vdW-bound systems is an important capability. One well-studied example is oxalic acid, for which a majority of vdW-inclusive methods does not predict the correct relative stabilities of the two polymorphs. The vdW-DF2 approach and accounting for exact exchange and explicit or implicit many-body effects in PBE0+MBD or PBE0+D3, respectively, finally yields the correct energetic order. Thereby, only PBE+MBD agrees well with experimental findings both in a qualitative and quantitative sense.[3] A similar example is the Coumarin crystal, where inclusion of many-body dispersion effects significantly improves the prediction of the most stable polymorphs and their energetic order compared to the pairwise vdW(TS) method.[56]

In the case of supramolecular complexes, Hermann *et al.* investigated the relative interaction energies of the C_{70}-fullerene with [*N*]-cycloparaphenylene ([*N*]-CPP) as also contained in the SMC13 set (*vide supra*). Accurate QMC reference calculations show that the binding energies of C_{70} to [10]- and [11]-CPP are degenerate (within QMC uncertainty).[9] However, DFT calculations in conjunction with pairwise or two- and three-body vdW models, including PBE+vdW(TS), PW6B95+D3, PW6B95+D3-ATM, and rVV10, show a clear preference for the 10-membered ring and only explicit account for the many-body character of vdW interactions correctly predicts an energetic degeneracy.[9,333]

General trends in (binding) energetics. Overall, the divergence between the different vdW models significantly increases with increasing system size and complexity, when going from small organic dimers to organic crystals and supramolecular complexes. This trend is continued when going even beyond this regime to layered materials, such as graphene and boronitride (BN).[337] The adsorption energy of water on a BN-flake with increasing size nicely showcases the increasing spread of the energetics predicted by the different models: for the simple borazine ($H_6B_3N_3$), all considered vdW-inclusive methods provide good agreement with QMC and CCSD(T) reference data, while the results start to strongly deviate for boronene ($H_{12}B_{12}N_{12}$). For hexagonal boronitride (h-BN) finally, RPA+SOSEX is the only DFT-based method found, that yields accurate results. Noteworthy, the strongly constrained and appropriately normalized (SCAN) functional[338] provides a fairly good agreement compared to the remaining DFT-based methods. Even more importantly, when comparing the adsorption of water on borazine, boronene, and h-BN, the authors showed that the tested vdW-DFs (vdW-DF2 and optB86b-vdW) predict an increase in the interaction energy with increasing size, which is not obtained in QMC, RPA, PBE+MBD, or PBE+D3. This has been assigned to the inherent isotropy in

non-local vdW-DFs conflicting the strong anisotropy of h-BN.[337] For layered materials, detailed tests showed that different flavors of vdW-DFs show a wide spread in terms of the predicted interlayer binding energy. The deviations can thereby reach up to 80% with respect to RPA calculations and 100% among the various vdW-DFs when considering different systems.[339]

Another clear difference between semi-local DFAs in combination with a vdW model and non-local vdW-DFs can be shown for the adsorption on and inside carbon nanostructures. While both approaches yield similar results for the extended 2D-analogue (graphene), vdW-DFs have been shown to significantly overestimate the adsorption energy inside carbon nanotubes.[340] This can be traced down to electron correlation at medium-ranges between the regimes of covalent bonds and the asymptotic London-type limit, which turned out to be strongly overestimated for nanostructures in the case of vdW-DFs. It is the highly complex, non-linear scaling of vdW interactions with increasing system size, which makes the accurate, quantitative description across all length scales a very demanding task. For a more qualitative description, one often relies on the power law a given kind of interaction follows with increasing separation. In the case of dispersion interactions, even this poses an intricate issue: As shown by Ambrosetti *et al.*, the power law exponent for the interaction between carbyne-like atomic wires varies strongly with the interwire separation before reaching its (very) long-range value and a very similar behavior has been observed for layered structures, nanotubes, and even nanostructure–protein complexes. Moreover, the distinct many-body character of vdW interactions gives rise to a strong dependence of power law exponents on the geometrical and response properties of the respective interaction partners.[50]

Asymptotic behavior. Despite the often complex variations before reaching the long-range scaling law, the long-range decay in itself represents a very strong qualitative benchmark for intermolecular interactions. Especially in this regard, collective electronic behavior and the quantum-mechanical many-body character of long-range correlation forces have been shown to have a pivotal influence. The summation of R^{-6}-terms does yield the correct power laws for the decay of the interaction of atoms, small molecular systems, insulating 2D-materials, and thick metal slabs. The results for more complex systems such as thin (semi-)metallic layers, on the other side, can be qualitatively wrong.[23] For instance, the interaction of two two-dimensional metallic systems (in parallel alignment) decays in the long range as $D^{-5/2}$ with distance D and the interaction between undoped graphene layers as D^{-3} according to RPA calculations (an even more complex scaling laws once considering many-body effects beyond the RPA).[23,341,342] Simple pairwise-additive vdW models, on the other side, predict a D^{-4}-dependence in all cases of parallel sheets.

Reaction barriers, rates, and mechanisms. An accurate description of vdW interactions in non-equilibrium structures is, of course, also essential for determining and evaluating reactive pathways. For a wide variety of configurational changes of small organic compounds, Steinmann and Corminboeuf showed that most vdW-inclusive methods including non-local vdW-DFs and pairwise dispersion models provide accurate relative energies for the respective equilibrium geometries, while they found mixed performances for reaction barriers.[44] For more complex reactions and transitions, this aspect is in general hardly explored. Nevertheless, the accuracy of vdW models out of equilibrium (in a structural sense) can be pivotal, especially for systems that form a vdW-bound precursor as it is often the case in bimolecular reactions[343,344] or (catalytic) surface reactions,[345] for example. Also, the role of vdW interactions for the reaction path (ensemble) and the sensitivity of reaction mechanisms with respect to the accuracy of the vdW model remain open questions.

6.2.3 Beyond (electronic) interaction energies. Above we outlined some important deviations between and short-comings of the various vdW models in terms of interaction energies for specific systems. In actual studies, however, we are often not only interested in interaction energies, but also several connected or derived properties, which can also be significantly affected by long-range correlation forces.

Effect on free energy contributions. For proper comparison to experiment and realistic modeling, for instance, one usually needs to account for thermal effects and obtain free energies. An interesting example of vdW interactions modifying such a derived quantity is the polymorphism of aspirin. While most electronic structure methods (both with and without vdW model) predict two polymorphs to be energetically degenerate, only one of them (''form I'') prevails in nature. By explicitly accounting for many-body dispersion effects, it has been shown in ref. 346 that an intricate interplay of phonons and long-range electronic fluctuations can explain the abundance of form I *via* entropic stabilization (emergence of low-frequency phonon modes).

Equilibrium geometries. One of the central steps in almost all studies in molecular and materials modeling is an (initial) geometry optimization. Hence, one of the most important tasks of an electronic structure method is to provide accurate structures. Nevertheless, the performance of vdW models is only rarely assessed based on geometrical features. In an extensive study, Witte *et al.* covered a wide range of popular (vdW-inclusive) methods in terms of their ability to reproduce accurate geometries for molecular reference systems. Non-local vdW-DFs, in particular ωB97X-V and (LC-)VV10, turned out to provide excellent agreement with accurate reference geometries over a wide range of system sizes.[347] The good performance of vdW-DFs in terms of geometries was also found for layered materials.[339] For the adsorption of water on two-dimensional structures, on the other side, it has been shown that with the exception of RPA many vdW-inclusive DFT approaches underestimate the equilibrium adsorption height by about 0.2 Å, which is in line with their overestimation of the adsorption energy (see above).[337] Comparing pairwise-additive vdW models and the MBD formalism, Blood-Forsythe *et al.* showed that the pairwise vdW(TS) and D3 approach yield considerably larger deviations from benchmark geometries of different benzene configurations, small peptides, and supramolecular complexes.[262] This is especially pronounced for π–π-stacked systems and can thus mainly be attributed to an

insufficient account of anisotropy in the systems.[27,262] In many cases, however, pairwise approaches such as vdW(TS) or D3 are known to give good geometries, despite the sometimes poor performance for the corresponding energies.

Molecular dynamics and dynamic properties. Connected to finding the (meta-)stable configurations of a given system, is the exploration of extended regions of the potential energy surface in (*ab initio*) molecular dynamics simulations. For many structural changes that do not involve breaking covalent bonds, vdW dispersion interactions represent the main source of interatomic forces and thus govern the dynamics of the system. A well-known example is the folding process of peptides and proteins in the gas phase. In the absence of solvent effects, non-covalent interactions between the residues are responsible for the adaption of a secondary structure. Hence, (accurate) inclusion of vdW interactions is pivotal as even small errors might be propagated to qualitatively wrong results during the dynamics. As such, inclusion of long-range correlation forces in form of a vdW model substantially improves the formation of helical entities in polypeptides.[348–352] Another example is liquid water, where vdW forces have been shown to considerably affect the obtained equilibrium radial distribution and diffusion coefficients.[353–357] The overall effect, however, strongly depends on the choice of the xc-functional and the vdW model and no final conclusion about an physically correct combination has been agreed upon. An accurate (first principles-based) treatment of dispersion interactions is also important for the dynamics of liquid water on 2D-materials, where minimal changes in microscopic geometrical features give rise to significant differences in macroscopic properties.[358]

Polarizabilities and effective interaction coefficients. Atomic and molecular (dipole) polarizabilities are one of the fundamental properties in the context of vdW interactions, which nevertheless are equally relevant in many more fields like spectroscopy and solvation. It has been shown that both explicit account for electrodynamic screening[49] as well as an appropriate determination of the initial, unscreened atomic polarizabilities can significantly improve the description of the (dipole) polarizabilities of molecules and (ionic) materials.[49,267] In this regard, it has been shown that the MBD framework does provide accurate polarizabilities for close to neutral molecular systems, its predictve power for ionic systems, however, is strongly limited by the employed Hirshfeld scheme to obtain the initial unscreened polarizabilities. This can be overcome by employing an iterative partitioning scheme, which has been shown to substantially improve the description of polarizabilities in ionic systems.[267] Also in the case of two-dimensional systems it was found that accounting for anisotropy has an important effect on the polarizability and correspondingly on the derived (anisotropic) C_6-interaction coefficients.[337] Similar collective effects can be found for effective C_6-coefficients. Inclusion of the self-consistent electrodynamic screening polarizabilities, *i.e.*, account for type-B non-additivity, reveals a highly non-trivial scaling of atom-atom interaction coefficients with respect to system size; a behavior that is not observed for coefficients based on a more local description as in vdW(TS) or D3.[2]

Effects on electronic properties. As pointed out earlier, the correlation energy is part of the electronic Hamiltonian and as such they, in principle, affect the self-consistent electronic charge density. However, as the correlation energy is typically around five orders of magnitude smaller than the total energy, its effect on the electron density is negligible in most cases and the vdW energy can be evaluated as an *a posteriori* correction. Mostly, inclusion of a vdW model in the KS self-consistency procedure only leads to a small polarization of the electron density towards intermolecular regions.[27] Yet, in-depth testing of the self-consistent vdW(TS) scheme revealed a striking exception: It has been shown that for several metal surfaces, long-range electron correlation can indeed affect the electronic structure and introduce a highly system-specific change in the work function due to charge polarization effects.[19] Small effects of self-consistent inclusion of long-range correlation have also been found for the radial distribution in liquid water.[357]

7 Conclusion

Above we gave a general introduction to a wide variety of current approaches to model vdW dispersion interactions in electronic structure calculations and presented a general overview of the performance on select showcase examples. We will now draw some general conclusions, provide what we think are some best-practice tips, and give a short outlook on some major open problems in the field.

7.1 The *Status quo* of van der Waals modeling

As can be seen from Section 6.1, most modern models provide an apparently reliable description of vdW interactions in select test systems. Thereby, the main focus in almost all benchmarking studies is on intermolecular interaction energies. For the assessment of the performance of a given methodology, however, we highly suggest to consider, first, systems beyond the typical benchmark sets (as these are often considered in the parametrization of vdW models) and, second, quantities beyond plain (intermolecular) interaction energies. Fig. 5 and Section 6.2 highlight the non-trivial scaling with size and complexity of the system and the implications of modeling vdW interactions for derived properties. As a result of this, careful choice and analysis of the applicability and suitability of a given approach for the system and property of interest is recommended.

Our current understanding of vdW interactions is mainly motivated by an atom-pairwise picture, which is in clear contrast to the fundamental physics behind dispersion interactions (see Section 2.1) and a growing number of experimental and theoretical studies show a failure of the pairwise-additive approximation. Unfortunately, our conceptual understanding beyond this simple approximation is still in its infancy and only a few studies (mostly employing the RPA approach or the MBD formalism) shed some light on the quantum nature of dispersion interactions and collective electronic behavior in systems of practical interest.[3,9,23,50,342,359] Due to this limited understanding

there are no general guidelines for the validity of a given approximation and the applicability of the corresponding model, when going beyond typical benchmark systems. Hence, we suggest to always test different approaches on representative reference systems. Comparison amongst approaches, which rely on fundamentally different approximations, helps to assess the validity of calculations. Comparing models, which are based on the same fundamental approximations, allows conclusions about the result within a given framework and limits the danger of fortuitous error cancellation in a select flavor of the model.

The *Status quo* can be summarized as follows: Current vdW methods significantly improve upon dispersion-less (semi-local) DFAs and are imperative to model realistic systems due to the ubiquitous nature of long-range correlation forces. The results from different models, however, can be wide spread and there is no universal method applicable to practically relevant systems. On the upside, the current situation is like ''different horses for different courses'' – mostly one of the many devised models is applicable to the system of interest and after careful testing reliable results can be obtained for a broader class of systems. Nevertheless, a few important points in terms of accuracy and physical completeness remain to be addressed, some of which we will outline below.

7.2 Open problems and outlook

While vdW-inclusive modeling has become routine in electronic-structure calculations by now, a variety of experimental observations can still not be fully explained within current vdW models.[61–65,67–69] Thus a lot of methodological research is still put into the improvement of current models and the development of new models. In the following we will outline some of the currently open problems, categorized as aspects of practical application or concerning the fundamental physics, which are neglected or only approximately present in current interatomic vdW models.

• Aspects connected to practical application

Combining a vdW model with DFT. A certain degree of empiricism is (maybe inevitably) introduced by coupling a (semi-)local DFA with a given vdW model. Introducing a range-separation of the coupling tensor as shown in Section 2.1 provides a solid and, in principle, exact framework for the typically *ad hoc* employed damping function in vdW approaches. For practical applications then, we assume that short-range correlation forces are captured by the underlying DFA and hence limit the dispersion model to the long-range regime. So, in order to obtain a seamless description of the total system, the range-separating function would need to describe the range of correlation that is captured in the DFA and correspondingly switch on the vdW method beyond that. This range captured by the DFA is in general not known and thus one relies on empirical switching functions of fixed form with some parametrical dependence on the system. This complicates the range-separated combination of (semi-)local DFT with a (long-range) vdW model and impedes a clear-cut analysis of the vdW model For instance, using CCSD(T) and SAPT, Shahbaz and Szalewicz have recently shown, that most (semi-)local DFAs lack several, considerable contributions to the interaction energy of molecular dimers at distances less than the vdW equilibrium,[360,361] where the DFA is assumed to capture all terms. By fitting the combined DFT + vdW method to total interaction energies, the range-separation function is pushed to (unphysically) also correct for several non-vdW effects including contributions from electrostatics, exchange, induction, and different higher-order correlation terms. An important point, when treating metallic systems with a vdW model in conjunction with DFT, is that most DFAs are designed to be exact for the homogeneous electron gas. As such, the DFA already captures a large extend of long-range correlation in metallic systems (especially alkali-metals). This contribution to electron correlation and the polarizability further complicates the development of a seamless and clear-cut combination of vdW models with a given DFA and, to the best of our knowledge, no accurate solution with universal applicability has been put forward to date. An intriguing early work in the context of damping pairwise interatomic and intermolecular potentials are the so-called universal damping functions by Tang and Toennies.[304] For practical application in the context of DFT, this approach, unfortunately, still lacks some universality due to the limited sensitivity to capture the shortcomings of a given DFA in describing intermediate- and short-range correlation.

In contrast to a clear-cut separation of the DFT- and vdW-description, non-local vdW-DFs represent a very promising approach by simply avoiding such a separation altogether and explicitly incorporating long-range correlation into the DFT-description. As can be seen from Section 6, however, the vdW-DF approach is still in the earlier stages of development and, in our opinion, needs further methodological refinement, especially in order to account for many-body effects and for the description of the intermediate range between the asymptotic limits.

Determination of an atomic density response from KS-DFT. In the context of combining a given dispersion model with DFT, all vdW models rely on some representation of the (effective) density–density response or correspondingly the polarizability of the KS reference system. While the Adler–Wiser formula (18) provides a seamless and accurate description, it is not very useful in practical applications as it requires explicit evaluation of all KS states. In addition, most of the efficient techniques are formulated in an atomistic framework. This requires additional mapping to effective atoms-in-molecules response properties and such partitioning is never unambiguous. Despite several successful schemes have been proposed, none can be universally applied in an efficient manner to neutral and ionic molecular, solid, and metallic systems. First works in this direction combine ideas from non-local density functionals and electronic structure-based interatomic frameworks.

Account for geometrical characteristics. Typically, benchmarking and parametrization of a vdW model focuses on the reproduction of interaction energies for a given geometry. However, the starting point of almost all modeling studies is an initial optimization/relaxation of the systems structure. Any subsequent calculations therefore rely on this very first step to give an accurate configuration. Yet, very little attention is given

to this pivotal capability when parameterizing or testing a vdW-inclusive total energy method. Despite some models by now account for the reproduction of intermolecular equilibrium distances to some extent, this is still far from testing if a given approach provides accurate geometries in a practical work flow.

Benchmark references for (more) complex systems. As mentioned above, our understanding of vdW interactions is currently still mainly based on a pairwise-additive framework. As showcased in Sections 2.3, 3.2, and 6, however, strong many-body effects and other complex phenomena arise with increasing system size and complexity. What is known for small organic dimers, might therefore not apply to practically relevant systems. Conceptual understanding usually roots from a profound basis of accurate observations or reference data. Our hope is, that with the growing computational capacities and ongoing methodological improvements, further accurate benchmark calculations will guide our conceptual understanding and shed some light on the non-additivity of long-range correlation forces and its implications for derived properties.

vdW interactions in comprehensive modeling techniques. For many of the tasks in molecular and materials modeling, specialized methods have been developed for an accurate and efficient simulation, *e.g.*, continuum solvation models, subsystem DFT, methods to account for nuclear quantum effects, and others. Only few examples among those techniques accurately account for dispersion interactions, however. Incorporation of vdW models might help to elucidate some of the more comprehensive ramifications of long-range correlation. On the same note, the cross-over and borderland between vdW interactions (microscopic) and Casimir forces (meso- to macroscopic) remains to be fully explored.

• Physics incorporated in interatomic vdW models

Beyond atomic dipoles in interatomic frameworks. As shown in Section 2.1, an dipole formulation of vdW interaction can, in principle, be exact. This, however, would require a continuous description in the form of infinite, infinitesimal polarizability centers. For the formulation of an exact interatomic framework, a given set of infinitesimal dipoles would need to be combined into an, in principle infinite, set of atomic multipoles, in order to represent the exact, continuous description within the dipole formulation. It is evident from the asymptotic behavior, that the neglect of higher-order atomic multipoles can in particular affect the description at intermediate separations. Nevertheless, the importance of explicitly including such higher-order atomic multipoles in the description of long-range vdW interactions and how much the effect of higher-order contributions can be mimicked by an appropriate form of the damping/range-separation function is still often under debate. On the other side, the contribution of higher-order multipoles to the short-range part of the coupling tensor, which is relevant for electrodynamical screening, is indisputable in our view. Instead of following up on any of the discussions, we here would like to give our general perspective on a framework to include vdW dispersion interactions between higher-order multipoles: all contributions should root from the same (range-separated) coupling tensor, such that the multipolar expansion is asymptotically exact, and all coupling parameters should be derived on the same footing. Otherwise, one could arbitrarily define effective damping functions and coupling parameters, which in the end boils down to providing a larger functional space with different ranges to be fit to interaction profiles much like in a molecular mechanics approach. Any improvement in such a formalism would not necessarily stem from improved physics, but simply from an increased parameter space for fitting and the physical meaning of individual terms would be highly limited.

As a complimentary approach, inclusion of higher-order multipoles can also be achieved by means of perturbation theory based on the quantum Drude oscillator model[248] or directly on the corresponding dipole-coupled state as presented in ref. 362, for instance. Such contributions beyond dipolar coupling and/or second-order perturbation theory can introduce qualitatively new features in confined structures[362] or electric fields (also due to the presence of ionic species)[363] and the implications for realistic and practically relevant systems remain to be fully explored.

Polarizability anisotropy on atomic level. Polarizability anisotropy on a molecular level has been shown to be of high importance for the description of vdW interactions especially with increasing system size and complexity. This can be further strengthened by anisotropies on an atomic level. While this is naturally accounted for in non-local functionals, all interatomic vdW models outlined above rely on isotropic atomic polarizabilities and therefore neglect the intrinsically different in-plane and out-of-plane polarizabilities of a carbon atom in graphene, for instance. Including atomically anisotropic polarizabilities is not fundamentally excluded in most vdW models, evaluation of the resulting anisotropic dipole coupling tensor, however, represents a prohibitive computational bottleneck.

Interatomic approaches and type C non-additivity. Furthermore, all of the above interatomic models are formulated in terms of dipole fluctuations on atomic sites. As a result, none of those is able to capture charge displacements that exceed atom-atom distances, *i.e.*, intrinsic electron hopping within electronic fluctuations. Such a phenomenon would cause very large multipolar terms and can give rise to very long-ranged correlation forces.[48] This effect was labeled type C non-additivity by Dobson and is so far only well-studied within the RPA formulation.

• Understanding van der Waals interactions from experiment

All in all, understanding the nature and complex scaling of vdW interactions requires pushing both theoretical and experimental boundaries in order to merge the conclusions from both sides into one consistent picture. A very promising approach in that regard are the recent advances in the field of (2D-)THz spectroscopy, which allows to study more collective vibrations and dynamics. In contrast to most previous measurements, it also enables a direct investigation of the underlying (non-local) dielectric/polarization response of the system, see *e.g.*, ref. 364 and 365. Finally, further exploration of the frequency spectrum in (multi-dimensional) electronic spectroscopy can open up a new route towards exploring the nature of vdW interactions. Such an approach could directly probe the underlying collective electronic fluctuations (with wave lengths

expected in the vacuum ultra-violet region around 50–150 nm) and their potential connection to the Rydberg states (or Rydberg series) of condensed matter. This, of course, requires careful and accurate disentanglement from other (photo-)ionization and excitation processes.

Author contribution

MS compiled, calculated, and formulated the results, theory, and discussion presented in this work and all three authors wrote the paper.

Conflicts of interest

There are no conflicts of interest to declare.

Acknowledgements

MS acknowledges financial support from the Fonds National de la Recherche, Luxembourg (AFR PhD Grant CNDTEC) and AT support from the European Research Council (ERC-CoG Grant BeStMo). TV's contribution to this work was funded by a grant from the US National Science Foundation (CHE-1464804). The authors thank Johannes Hoja and Yasmine S. Al-Hamdani for helpful discussions on the presentation of parts of this publication.

References

1 A. Otero-de-la-Roza and E. R. Johnson, *J. Chem. Phys.*, 2012, **136**, 174109.
2 V. V. Gobre and A. Tkatchenko, *Nat. Commun.*, 2013, **4**, 2341.
3 A. M. Reilly and A. Tkatchenko, *Chem. Sci.*, 2015, **6**, 3289–3301.
4 J. Hoja, A. M. Reilly and A. Tkatchenko, *Wiley Interdiscip. Rev.: Comput. Mol. Sci.*, 2017, **7**, e1294.
5 S. Grimme, *Wiley Interdiscip. Rev.: Comput. Mol. Sci.*, 2011, **1**, 211–228.
6 J. Klimeš and A. Michaelides, *J. Chem. Phys.*, 2012, **137**, 120901.
7 T. Björkman, A. Gulans, A. V. Krasheninnikov and R. M. Nieminen, *Phys. Rev. Lett.*, 2012, **108**, 235502.
8 A. Ambrosetti, D. Alfè, R. A. DiStasio and A. Tkatchenko, *J. Phys. Chem. Lett.*, 2014, **5**, 849–855.
9 J. Hermann, D. Alfè and A. Tkatchenko, *Nat. Commun.*, 2017, **8**, 14052.
10 D. A. Egger and L. Kronik, *J. Phys. Chem. Lett.*, 2014, **5**, 2728–2733.
11 A. Tkatchenko, *Adv. Funct. Mater.*, 2015, **25**, 2054–2061.
12 Y. V. Shtogun and L. M. Woods, *J. Phys. Chem. Lett.*, 2010, **1**, 1356–1362.
13 W. Gao and A. Tkatchenko, *Phys. Rev. Lett.*, 2015, **114**, 096101.
14 R. J. Maurer, W. Liu, I. Poltavsky, T. Stecher, H. Oberhofer, K. Reuter and A. Tkatchenko, *Phys. Rev. Lett.*, 2016, **116**, 146101.
15 W. Gao and A. Tkatchenko, *Phys. Rev. Lett.*, 2013, **111**, 045501.
16 D. A. Egger, L. Kronik and A. M. Rappe, *Angew. Chem., Int. Ed.*, 2015, **54**, 12437–12441.
17 A. Fabrizio and C. Corminboeuf, *J. Phys. Chem. Lett.*, 2018, 464–470.
18 E. Brémond, N. Golubev, S. N. Steinmann and C. Corminboeuf, *J. Chem. Phys.*, 2014, **140**, 18A516.
19 N. Ferri, R. A. DiStasio, A. Ambrosetti, R. Car and A. Tkatchenko, *Phys. Rev. Lett.*, 2015, **114**, 176802.
20 O. Sinanoğlu, *Many-Electron Theory of Atoms, Molecules and Their Interactions, Adv. Chem. Phys.*, John Wiley & Sons, Ltd, 1964, vol. 6, pp. 315–412.
21 S. Wilson, *Electron Correlation in Molecules*, Dover Publications, New York, Dover edn, 1984.
22 *Recent Advances in Multireference Methods*, ed. K. Hirao, World Scientific, 1999, vol. 4 of Recent Advances in Computational Chemistry.
23 J. F. Dobson, A. White and A. Rubio, *Phys. Rev. Lett.*, 2006, **96**, 073201.
24 J. Chen, A. Zen, J. G. Brandenburg, D. Alfè and A. Michaelides, *Phys. Rev. B*, 2016, **94**, 220102.
25 L. M. Woods, D. A. R. Dalvit, A. Tkatchenko, P. Rodriguez-Lopez, A. W. Rodriguez and R. Podgornik, *Rev. Mod. Phys.*, 2016, **88**, 045003.
26 S. Y. Buhmann, *Dispersion Forces I*, Springer Berlin Heidelberg, Berlin, Heidelberg, 2012, vol. 247.
27 J. Hermann, R. A. DiStasio and A. Tkatchenko, *Chem. Rev.*, 2017, **117**, 4714–4758.
28 L. D. Landau and E. M. Lifshitz, *Statistical Physics*, Pergamon Press, Oxford, 2nd edn, 1970, vol. 5 of Course of Theoretical Physics.
29 M. Born and V. Fock, *Z. Phys.*, 1928, **51**, 165–180.
30 T. Kato, *J. Phys. Soc. Jpn.*, 1950, **5**, 435–439.
31 S. L. Adler, *Phys. Rev.*, 1962, **126**, 413–420.
32 N. Wiser, *Phys. Rev.*, 1963, **129**, 62–69.
33 J. Toulouse, F. Colonna and A. Savin, *Phys. Rev. A: At., Mol., Opt. Phys.*, 2004, **70**, 062505.
34 H. B. G. Casimir and D. Polder, *Phys. Rev.*, 1948, **73**, 360–372.
35 H. Hamaker, *Physica*, 1937, **4**, 1058–1072.
36 F. London, *Z. Phys. Chem., Abt. B*, 1930, **11**, 222–251.
37 S. Grimme, *J. Comput. Chem.*, 2004, **25**, 1463–1473.
38 E. R. Johnson and A. D. Becke, *J. Chem. Phys.*, 2005, **123**, 024101.
39 A. D. Becke and E. R. Johnson, *J. Chem. Phys.*, 2005, **122**, 154104.
40 S. Grimme, *J. Comput. Chem.*, 2006, **27**, 1787–1799.
41 A. Tkatchenko and M. Scheffler, *Phys. Rev. Lett.*, 2009, **102**, 73005.
42 T. Sato and H. Nakai, *J. Chem. Phys.*, 2009, **131**, 224104.
43 S. Grimme, J. Antony, S. Ehrlich and H. Krieg, *J. Chem. Phys.*, 2010, **132**, 154104.

44 S. N. Steinmann and C. Corminboeuf, *J. Chem. Theory Comput.*, 2011, **7**, 3567–3577.
45 S. Grimme, S. Ehrlich and L. Goerigk, *J. Comput. Chem.*, 2011, **32**, 1456–1465.
46 A. Tkatchenko, A. Ambrosetti and R. A. DiStasio, *J. Chem. Phys.*, 2013, **138**, 074106.
47 A. J. Stone, *The Theory of Intermolecular Forces*, Oxford University Press, Oxford, 2nd edn, 2016.
48 J. F. Dobson, *Int. J. Quantum Chem.*, 2014, **114**, 1157–1161.
49 A. Tkatchenko, R. A. DiStasio, R. Car and M. Scheffler, *Phys. Rev. Lett.*, 2012, **108**, 236402.
50 A. Ambrosetti, N. Ferri, R. A. DiStasio and A. Tkatchenko, *Science*, 2016, **351**, 1171–1176.
51 J. R. Reimers, M. J. Ford, S. M. Marcuccio, J. Ulstrup and N. S. Hush, *Nat. Rev. Chem.*, 2017, **1**, 0017.
52 R. Pollice, M. Bot, I. J. Kobylianskii, I. Shenderovich and P. Chen, *J. Am. Chem. Soc.*, 2017, **139**, 13126–13140.
53 A. Noy, *Surf. Interface Anal.*, 2006, **38**, 1429–1441.
54 F. Biedermann and H.-J. Schneider, *Chem. Rev.*, 2016, **116**, 5216–5300.
55 A. Zen, J. G. Brandenburg, J. Klimeš, A. Tkatchenko, D. Alfè and A. Michaelides, *Proc. Natl. Acad. Sci. U. S. A.*, 2018, **115**, 1724–1729.
56 A. G. Shtukenberg, Q. Zhu, D. J. Carter, L. Vogt, J. Hoja, E. Schneider, H. Song, B. Pokroy, I. Polishchuk, A. Tkatchenko, A. R. Oganov, A. L. Rohl, M. E. Tuckerman and B. Kahr, *Chem. Sci.*, 2017, **8**, 4926–4940.
57 M. Becucci and S. Melandri, *Chem. Rev.*, 2016, **116**, 5014–5037.
58 C. E. H. Dessent and K. Müller-Dethlefs, *Chem. Rev.*, 2000, **100**, 3999–4022.
59 E. M. Lifshitz, *Sov. Phys. - JETP*, 1956, **2**, 73–83.
60 E. Zaremba and W. Kohn, *Phys. Rev. B: Solid State*, 1976, **13**, 2270–2285.
61 C. Wagner, N. Fournier, V. G. Ruiz, C. Li, K. Müllen, M. Rohlfing, A. Tkatchenko, R. Temirov and F. S. Tautz, *Nat. Commun.*, 2014, **5**, 5568.
62 C. Wagner, D. Kasemann, C. Golnik, R. Forker, M. Esslinger, K. Müllen and T. Fritz, *Phys. Rev. B: Condens. Matter Mater. Phys.*, 2010, **81**, 035423.
63 C. Kleimann, B. Stadtmüller, S. Schröder and C. Kumpf, *J. Phys. Chem. C*, 2014, **118**, 1652–1660.
64 X. Liu, Y. Wei, J. E. Reutt-Robey and S. W. Robey, *J. Phys. Chem. C*, 2014, **118**, 3523–3532.
65 G. A. Rance, D. H. Marsh, S. J. Bourne, T. J. Reade and A. N. Khlobystov, *ACS Nano*, 2010, **4**, 4920–4928.
66 C. A. S. Batista, R. G. Larson and N. A. Kotov, *Science*, 2015, **350**, 1242477.
67 P. Loskill, H. Hähl, T. Faidt, S. Grandthyll, F. Müller and K. Jacobs, *Adv. Colloid Interface Sci.*, 2012, **179–182**, 107–113.
68 P. Loskill, J. Puthoff, M. Wilkinson, K. Mecke, K. Jacobs and K. Autumn, *J. R. Soc., Interface*, 2012, **10**, 20120587.
69 S. Tsoi, P. Dev, A. L. Friedman, R. Stine, J. T. Robinson, T. L. Reinecke and P. E. Sheehan, *ACS Nano*, 2014, **8**, 12410–12417.
70 G. N. Lewis, *J. Am. Chem. Soc.*, 1916, **38**, 762–785.
71 R. F. W. Bader, *Atoms in Molecules: A Quantum Theory*, Clarendon Press, 1990.
72 A. D. Becke and K. E. Edgecombe, *J. Chem. Phys.*, 1990, **92**, 5397–5403.
73 B. Silvi and A. Savin, *Nature*, 1994, **371**, 683–686.
74 P. de Silva, J. Korchowiec and T. A. Wesolowski, *ChemPhysChem*, 2012, **13**, 3462–3465.
75 P. de Silva, J. Korchowiec, N. Ram J. S. and T. A. Wesolowski, *Chimia*, 2013, **67**, 253–256.
76 B. Honig and A. Nicholls, *Science*, 1995, **268**, 1144–1149.
77 P. Hohenberg and W. Kohn, *Phys. Rev.*, 1964, **136**, B864–B871.
78 E. R. Johnson, S. Keinan, P. Mori-Sanchez, J. Contreras-Garcia, A. J. Cohen and W. Yang, *J. Am. Chem. Soc.*, 2010, **132**, 6498–6506.
79 J. Contreras-Garcia, E. R. Johnson, S. Keinan, R. Chaudret, J.-P. Piquemal, D. N. Beratan and W. Yang, *J. Chem. Theory Comput.*, 2011, **7**, 625–632.
80 B. J. Miller, J. R. Lane and H. G. Kjaergaard, *Phys. Chem. Chem. Phys.*, 2011, **13**, 14183.
81 E. Sanna, E. C. Escudero-Adán, A. Bauzá, P. Ballester, A. Frontera, C. Rotger and A. Costa, *Chem. Sci.*, 2015, **6**, 5466–5472.
82 A. Vargas-Caamal, S. Pan, F. Ortiz-Chi, J. L. Cabellos, R. A. Boto, J. Contreras-Garcia, A. Restrepo, P. K. Chattaraj and G. Merino, *Phys. Chem. Chem. Phys.*, 2016, **18**, 550–556.
83 L. A. H. van Bergen, M. Alonso, A. Palló, L. Nilsson, F. De Proft and J. Messens, *Sci. Rep.*, 2016, **6**, 30369.
84 P. de Silva and C. Corminboeuf, *J. Chem. Theory Comput.*, 2014, **10**, 3745–3756.
85 T. Kato, *Communications on Pure and Applied Mathematics*, 1957, **10**, 151–177.
86 M. M. Morrell, R. G. Parr and M. Levy, *J. Chem. Phys.*, 1975, **62**, 549.
87 S. Mebs, *Chem. Phys. Lett.*, 2016, **651**, 172–177.
88 S. Mebs and J. Beckmann, *J. Phys. Chem. A*, 2017, **121**, 7717–7725.
89 A. P. de Lima Batista, A. G. S. de Oliveira-Filho and S. E. Galembeck, *ChemistrySelect*, 2017, **2**, 4648.
90 M. Zheng, J. A. Kuriappan and M. P. Waller, *Int. J. Quantum Chem.*, 2017, **117**, e25336.
91 T. Lu and F. Chen, *J. Comput. Chem.*, 2012, **33**, 580–592.
92 J. Contreras-Garcia, E. R. Johnson, S. Keinan and W. Yang, *NCI*, http://www.lct.jussieu.fr/pagesperso/contrera/nciplot.html.
93 W. Humphrey, A. Dalke and K. Schulten, *J. Mol. Graphics*, 1996, **14**, 33–38.
94 J.-P. Piquemal, A. Marquez, O. Parisel and C. Giessner-Prettre, *J. Comput. Chem.*, 2005, **26**, 1052–1062.
95 Z. Lu, N. Zhou, Q. Wu and Y. Zhang, *J. Chem. Theory Comput.*, 2011, **7**, 4038–4049.
96 K. Morokuma, *J. Chem. Phys.*, 1971, **55**, 1236–1244.
97 K. Kitaura and K. Morokuma, *Int. J. Quantum Chem.*, 1976, **10**, 325–340.
98 T. Ziegler and A. Rauk, *Theor. Chim. Acta*, 1977, **46**, 1–10.
99 P. S. Bagus, K. Hermann and C. W. Bauschlicher, *J. Chem. Phys.*, 1984, **80**, 4378–4386.

100 W. J. Stevens and W. H. Fink, *Chem. Phys. Lett.*, 1987, **139**, 15–22.
101 E. Gianinetti, M. Raimondi and E. Tornaghi, *Int. J. Quantum Chem.*, 1996, **60**, 157–166.
102 T. Nagata, O. Takahashi, K. Saito and S. Iwata, *J. Chem. Phys.*, 2001, **115**, 3553–3560.
103 R. Z. Khaliullin, M. Head-Gordon and A. T. Bell, *J. Chem. Phys.*, 2006, **124**, 204105.
104 E. D. Glendening and A. Streitwieser, *J. Chem. Phys.*, 1994, **100**, 2900–2909.
105 E. D. Glendening, *J. Phys. Chem. A*, 2005, **109**, 11936–11940.
106 W. Chen and M. S. Gordon, *J. Phys. Chem.*, 1996, **100**, 14316–14328.
107 Q. Wu, P. W. Ayers and Y. Zhang, *J. Chem. Phys.*, 2009, **131**, 164112.
108 Y. Imamura, T. Baba and H. Nakai, *Int. J. Quantum Chem.*, 2008, **108**, 1316–1325.
109 P. Su and H. Li, *J. Chem. Phys.*, 2009, **131**, 014102.
110 R. J. Azar and M. Head-Gordon, *J. Chem. Phys.*, 2012, **136**, 024103.
111 S. N. Steinmann, C. Corminboeuf, W. Wu and Y. Mo, *J. Phys. Chem. A*, 2011, **115**, 5467–5477.
112 W. Gao, H. Feng, X. Xuan and L. Chen, *J. Mol. Model.*, 2012, **18**, 4577–4589.
113 P. Su, Z. Jiang, Z. Chen and W. Wu, *J. Phys. Chem. A*, 2014, **118**, 2531–2542.
114 M. J. S. Phipps, T. Fox, C. S. Tautermann and C.-K. Skylaris, *Chem. Soc. Rev.*, 2015, **44**, 3177–3211.
115 L. Shirkov and V. Sladek, *J. Chem. Phys.*, 2017, **147**, 174103.
116 B. Jeziorski, R. Moszynski and K. Szalewicz, *Chem. Rev.*, 1994, **94**, 1887–1930.
117 K. Szalewicz, *Wiley Interdiscip. Rev.: Comput. Mol. Sci.*, 2012, **2**, 254–272.
118 H. L. Williams and C. F. Chabalowski, *J. Phys. Chem. A*, 2001, **105**, 646–659.
119 A. Heßelmann and G. Jansen, *Chem. Phys. Lett.*, 2002, **357**, 464–470.
120 A. Heßelmann and G. Jansen, *Chem. Phys. Lett.*, 2002, **362**, 319–325.
121 A. Heßelmann and G. Jansen, *Chem. Phys. Lett.*, 2003, **367**, 778–784.
122 A. J. Misquitta and K. Szalewicz, *Chem. Phys. Lett.*, 2002, **357**, 301–306.
123 A. J. Misquitta, B. Jeziorski and K. Szalewicz, *Phys. Rev. Lett.*, 2003, **91**, 033201.
124 A. J. Misquitta, R. Podeszwa, B. Jeziorski and K. Szalewicz, *J. Chem. Phys.*, 2005, **123**, 214103.
125 A. Heßelmann and F. R. Manby, *J. Chem. Phys.*, 2005, **123**, 164116.
126 G. Jansen and A. Heßelmann, *J. Phys. Chem. A*, 2001, **105**, 11156–11157.
127 A. J. Misquitta and K. Szalewicz, *J. Chem. Phys.*, 2005, **122**, 214109.
128 A. Tekin and G. Jansen, *Phys. Chem. Chem. Phys.*, 2007, **9**, 1680–1687.
129 A. Szabo and N. S. Ostlund, *Modern quantum chemistry: Introduction to advanced electronic structure theory*, McGraw-Hill, New York, 1989.
130 M. Pitoňák and A. Heßelmann, *J. Chem. Theory Comput.*, 2010, **6**, 168–178.
131 G. R. Jenness, O. Karalti, W. A. Al-Saidi and K. D. Jordan, *J. Phys. Chem. A*, 2011, **115**, 5955–5964.
132 E. G. Hohenstein, H. M. Jaeger, E. J. Carrell, G. S. Tschumper and C. D. Sherrill, *J. Chem. Theory Comput.*, 2011, **7**, 2842–2851.
133 X. Li, A. V. Volkov, K. Szalewicz and P. Coppens, *Acta Crystallogr., Sect. D: Biol. Crystallogr.*, 2006, **62**, 639–647.
134 A. J. Stone and A. J. Misquitta, *Int. Rev. Phys. Chem.*, 2007, **26**, 193–222.
135 R. Podeszwa, B. M. Rice and K. Szalewicz, *Phys. Chem. Chem. Phys.*, 2009, **11**, 5512.
136 J. R. Schmidt, K. Yu and J. G. McDaniel, *Acc. Chem. Res.*, 2015, **48**, 548–556.
137 M. Jeziorska, B. Jeziorski and J. Čižek, *Int. J. Quantum Chem.*, 1987, **32**, 149–164.
138 R. Moszynski, T. Heijmen and B. Jeziorski, *Mol. Phys.*, 1996, **88**, 741–758.
139 R. Moszynski, P. E. S. Wormer, B. Jeziorski and A. van der Avoird, *J. Chem. Phys.*, 1995, **103**, 8058–8074.
140 R. Podeszwa and K. Szalewicz, *J. Chem. Phys.*, 2007, **126**, 194101.
141 R. Podeszwa, B. M. Rice and K. Szalewicz, *Phys. Rev. Lett.*, 2008, **101**, 115503.
142 T. Korona, A. Heßelmann and H. Dodziuk, *J. Chem. Theory Comput.*, 2009, **5**, 1585–1596.
143 J. P. Heindel, E. S. Knodel and D. P. Schofield, *J. Phys. Chem. A*, 2018, **122**, 6724–6735.
144 L. D. Jacobson and J. M. Herbert, *J. Chem. Phys.*, 2011, **134**, 094118.
145 K. U. Lao and J. M. Herbert, *J. Phys. Chem. A*, 2015, **119**, 235–252.
146 K. Carter-Fenk, K. U. Lao, K.-Y. Liu and J. M. Herbert, *J. Phys. Chem. Lett.*, 2019, **10**, 2706–2714.
147 I. Mayer, *Int. J. Quantum Chem.*, 1983, **23**, 341–363.
148 J. F. Gonthier and C. Corminboeuf, *J. Chem. Phys.*, 2014, **140**, 154107.
149 R. M. Parrish, J. F. Gonthier, C. Corminbœuf and C. D. Sherrill, *J. Chem. Phys.*, 2015, **143**, 051103.
150 H. Stoll, G. Wagenblast and H. Preuβ, *Theor. Chim. Acta*, 1980, **57**, 169–178.
151 E. Pastorczak, A. Prlj, J. F. Gonthier and C. Corminboeuf, *J. Chem. Phys.*, 2015, **143**, 224107.
152 C. R. Jacob and L. Visscher, *J. Chem. Phys.*, 2008, **128**, 155102.
153 A. Goez, C. R. Jacob and J. Neugebauer, *Comput. Theor. Chem.*, 2014, **1040–1041**, 347–359.
154 A. Goez and J. Neugebauer, *J. Chem. Theory Comput.*, 2016, **12**, 4843–4855.
155 R. M. Parrish and C. D. Sherrill, *J. Chem. Phys.*, 2014, **141**, 044115.
156 D. Bohm and D. Pines, *Phys. Rev.*, 1953, **92**, 609–625.
157 M. Gell-Mann and K. A. Brueckner, *Phys. Rev.*, 1957, **106**, 364–368.
158 J. Harris and R. O. Jones, *J. Phys. F: Met. Phys.*, 1974, **4**, 1170–1186.

159 D. C. Langreth and J. P. Perdew, *Solid State Commun.*, 1975, **17**, 1425–1429.
160 D. C. Langreth and J. P. Perdew, *Phys. Rev. B: Solid State*, 1977, **15**, 2884–2901.
161 J. F. Dobson, in *Time-Dependent Density Functional Theory*, ed. M. Marques, F. Nogueira, A. Rubio, K. Burke and E. K. U. Gross, Springer, Berlin, 2006, pp. 443–462.
162 A. Marini, P. García-González and A. Rubio, *Phys. Rev. Lett.*, 2006, **96**, 136404.
163 F. Furche, *J. Chem. Phys.*, 2008, **129**, 114105.
164 G. E. Scuseria, T. M. Henderson and D. C. Sorensen, *J. Chem. Phys.*, 2008, **129**, 231101.
165 J. Harl and G. Kresse, *Phys. Rev. Lett.*, 2009, **103**, 056401.
166 J. Paier, B. G. Janesko, T. M. Henderson, G. E. Scuseria, A. Grüneis and G. Kresse, *J. Chem. Phys.*, 2010, **132**, 094103.
167 J. Toulouse, I. C. Gerber, G. Jansen, A. Savin and J. G. Ángyán, *Phys. Rev. Lett.*, 2009, **102**, 096404.
168 B. G. Janesko, T. M. Henderson and G. E. Scuseria, *J. Chem. Phys.*, 2009, **130**, 081105.
169 W. Zhu, J. Toulouse, A. Savin and J. G. Ángyán, *J. Chem. Phys.*, 2010, **132**, 244108.
170 A. Grüneis, M. Marsman, J. Harl, L. Schimka and G. Kresse, *J. Chem. Phys.*, 2009, **131**, 154115.
171 X. Ren, A. Tkatchenko, P. Rinke and M. Scheffler, *Phys. Rev. Lett.*, 2011, **106**, 153003.
172 A. M. Burow, J. E. Bates, F. Furche and H. Eshuis, *J. Chem. Theory Comput.*, 2014, **10**, 180–194.
173 K. S. Singwi, M. P. Tosi, R. H. Land and A. Sjölander, *Phys. Rev.*, 1968, **176**, 589–599.
174 H.-V. Nguyen and S. de Gironcoli, *Phys. Rev. B: Condens. Matter Mater. Phys.*, 2009, **79**, 205114.
175 G. E. Scuseria, T. M. Henderson and I. W. Bulik, *J. Chem. Phys.*, 2013, **139**, 104113.
176 J. Toulouse, W. Zhu, A. Savin, G. Jansen and J. G. Ángyán, *J. Chem. Phys.*, 2011, **135**, 084119.
177 H. Eshuis, J. E. Bates and F. Furche, *Theor. Chem. Acc.*, 2012, **131**, 1084.
178 A.-S. Hehn, D. P. Tew and W. Klopper, *J. Chem. Phys.*, 2015, **142**, 194106.
179 G. Jansen, R.-F. Liu and J. G. Ángyán, *J. Chem. Phys.*, 2010, **133**, 154106.
180 S. Kurth and J. P. Perdew, *Phys. Rev. B: Condens. Matter Mater. Phys.*, 1999, **59**, 10461–10468.
181 Z. Yan, J. P. Perdew and S. Kurth, *Phys. Rev. B: Condens. Matter Mater. Phys.*, 2000, **61**, 16430–16439.
182 H. Jiang and E. Engel, *J. Chem. Phys.*, 2007, **127**, 184108.
183 F. Furche, *Phys. Rev. B: Condens. Matter Mater. Phys.*, 2001, **64**, 195120.
184 J. Paier, X. Ren, P. Rinke, G. E. Scuseria, A. Grüneis, G. Kresse and M. Scheffler, *New J. Phys.*, 2012, **14**, 043002.
185 X. Ren, P. Rinke, G. E. Scuseria and M. Scheffler, *Phys. Rev. B: Condens. Matter Mater. Phys.*, 2013, **88**, 035120.
186 J. E. Bates and F. Furche, *J. Chem. Phys.*, 2013, **139**, 171103.
187 M. Beuerle and C. Ochsenfeld, *J. Chem. Phys.*, 2017, **147**, 204107.
188 J. Klimeš, M. Kaltak, E. Maggio and G. Kresse, *J. Chem. Phys.*, 2015, **143**, 102816.
189 J. Klimeš, *J. Chem. Phys.*, 2016, **145**, 094506.
190 G. P. Chen, M. M. Agee and F. Furche, *J. Chem. Theory Comput.*, 2018, **14**, 5701–5714.
191 The ABINIT Group, *ABINIT*, https://www.abinit.org, date accessed: 2018-08-16.
192 X. Gonze, *et al.*, *Zeitschrift für Kristallographie - Crystalline Materials*, 2005, **220**, 558–562.
193 X. Gonze, *et al.*, *Comput. Phys. Commun.*, 2009, **180**, 2582–2615.
194 The CP2K developers Group, *CP2K Open Source Molecular Dynamics*, https://www.cp2k.org, date accessed: 2018-12-03.
195 V. Blum, R. Gehrke, F. Hanke, P. Havu, V. Havu, X. Ren, K. Reuter and M. Scheffler, *Comput. Phys. Commun.*, 2009, **180**, 2175–2196.
196 TURBOMOLE GmbH, *TURBOMOLE: Program Package for ab initio Electronic Structure Calculations*, http://www.turbomole.com/, date accessed: 2018-08-16.
197 G. Kresse and J. Hafner, *Phys. Rev. B: Condens. Matter Mater. Phys.*, 1993, **47**, 558–561.
198 G. Kresse and J. Hafner, *Phys. Rev. B: Condens. Matter Mater. Phys.*, 1994, **49**, 14251–14269.
199 G. Kresse and J. Furthmüller, *Comput. Mater. Sci.*, 1996, **6**, 15–50.
200 G. Kresse and J. Furthmüller, *Phys. Rev. B: Condens. Matter Mater. Phys.*, 1996, **54**, 11169–11186.
201 VASP Software GmbH, *The VASP site*, https://www.vasp.at/, date accessed: 2018-08-16.
202 J. F. Dobson and B. P. Dinte, *Phys. Rev. Lett.*, 1996, **76**, 1780–1783.
203 J. F. Dobson and J. Wang, *Phys. Rev. Lett.*, 1999, **82**, 2123–2126.
204 Y. Andersson, D. C. Langreth and B. I. Lundqvist, *Phys. Rev. Lett.*, 1996, **76**, 102–105.
205 E. Hult, Y. Andersson, B. I. Lundqvist and D. C. Langreth, *Phys. Rev. Lett.*, 1996, **77**, 2029–2032.
206 W. Kohn, Y. Meir and D. E. Makarov, *Phys. Rev. Lett.*, 1998, **80**, 4153–4156.
207 O. A. Vydrov and T. Van Voorhis, *Phys. Rev. A: At., Mol., Opt. Phys.*, 2010, **81**, 062708.
208 H. Rydberg, N. Jacobson, P. Hyldgaard, S. Simak, B. I. Lundqvist and D. C. Langreth, *Surf. Sci.*, 2003, **532–535**, 606–610.
209 M. Dion, H. Rydberg, E. Schröder, D. C. Langreth and B. I. Lundqvist, *Phys. Rev. Lett.*, 2004, **92**, 246401.
210 D. C. Langreth, M. Dion, H. Rydberg, E. Schröder, P. Hyldgaard and B. I. Lundqvist, *Int. J. Quantum Chem.*, 2005, **101**, 599–610.
211 D. C. Langreth, B. I. Lundqvist, S. D. Chakarova-Käck, V. R. Cooper, M. Dion, P. Hyldgaard, A. Kelkkanen, J. Kleis, L. Kong, S. Li, P. G. Moses, E. Murray, A. Puzder, H. Rydberg, E. Schröder and T. Thonhauser, *J. Phys.: Condens. Matter*, 2009, **21**, 084203.
212 J. Klimeš, D. R. Bowler and A. Michaelides, *J. Phys.: Condens. Matter*, 2010, **22**, 022201.
213 J. Klimeš, D. R. Bowler and A. Michaelides, *Phys. Rev. B: Condens. Matter Mater. Phys.*, 2011, **83**, 195131.

214 K. Lee, E. D. Murray, L. Kong, B. I. Lundqvist and D. C. Langreth, *Phys. Rev. B: Condens. Matter Mater. Phys.*, 2010, **82**, 081101.
215 K. Berland, V. R. Cooper, K. Lee, E. Schröder, T. Thonhauser, P. Hyldgaard and B. I. Lundqvist, *Rep. Prog. Phys.*, 2015, **78**, 066501.
216 K. Berland and P. Hyldgaard, *Phys. Rev. B: Condens. Matter Mater. Phys.*, 2013, **87**, 205421.
217 O. A. Vydrov, Q. Wu and T. Van Voorhis, *J. Chem. Phys.*, 2008, **129**, 014106.
218 O. A. Vydrov and T. Van Voorhis, *Phys. Rev. Lett.*, 2009, **103**, 063004.
219 O. A. Vydrov and T. Van Voorhis, *J. Chem. Phys.*, 2010, **133**, 244103.
220 O. A. Vydrov and T. Van Voorhis, *J. Chem. Theory Comput.*, 2012, **8**, 1929–1934.
221 W. Hujo and S. Grimme, *J. Chem. Theory Comput.*, 2011, **7**, 3866–3871.
222 N. Mardirossian and M. Head-Gordon, *J. Chem. Phys.*, 2015, **142**, 074111.
223 N. Mardirossian and M. Head-Gordon, *J. Chem. Phys.*, 2016, **144**, 214110.
224 N. Mardirossian and M. Head-Gordon, *Phys. Chem. Chem. Phys.*, 2014, **16**, 9904.
225 G. Román-Pérez and J. M. Soler, *Phys. Rev. Lett.*, 2009, **103**, 096102.
226 R. Sabatini, T. Gorni and S. de Gironcoli, *Phys. Rev. B: Condens. Matter Mater. Phys.*, 2013, **87**, 041108.
227 Y. Shao, *et al.*, *Mol. Phys.*, 2015, **113**, 184–215.
228 P. Gianozzi, *et al.*, *J. Phys.: Condens. Matter*, 2009, **21**, 395502.
229 T. Thonhauser, V. R. Cooper, S. Li, A. Puzder, P. Hyldgaard and D. C. Langreth, *Phys. Rev. B: Condens. Matter Mater. Phys.*, 2007, **76**, 125112.
230 B. Kolb and T. Thonhauser, *Phys. Rev. B: Condens. Matter Mater. Phys.*, 2011, **84**, 045116.
231 J. M. Soler, E. Artacho, J. D. Gale, A. García, J. Junquera, P. Ordejón and D. Sánchez-Portal, *J. Phys.: Condens. Matter*, 2002, **14**, 2745–2779.
232 R. T. Sharp and G. K. Horton, *Phys. Rev.*, 1953, **90**, 317.
233 R. Colle and O. Salvetti, *Theor. Chim. Acta*, 1975, **37**, 329–334.
234 A. Görling and M. Levy, *Phys. Rev. A: At., Mol., Opt. Phys.*, 1994, **50**, 196–204.
235 T. Grabo and E. K. U. Gross, *Chem. Phys. Lett.*, 1995, **240**, 141–150.
236 L. Fritsche and J. Yuan, *Phys. Rev. A: At., Mol., Opt. Phys.*, 1998, **57**, 3425–3432.
237 O. A. von Lilienfeld, I. Tavernelli, U. Rothlisberger and D. Sebastiani, *Phys. Rev. Lett.*, 2004, **93**, 153004.
238 C. Hartwigsen, S. Goedecker and J. Hutter, *Phys. Rev. B: Condens. Matter Mater. Phys.*, 1998, **58**, 3641–3662.
239 O. A. von Lilienfeld, I. Tavernelli, U. Rothlisberger and D. Sebastiani, *Phys. Rev. B: Condens. Matter Mater. Phys.*, 2005, **71**, 195119.
240 A. Tkatchenko and O. A. von Lilienfeld, *Phys. Rev. B: Condens. Matter Mater. Phys.*, 2006, **73**, 153406.
241 I.-C. Lin, M. D. Coutinho-Neto, C. Felsenheimer, O. A. von Lilienfeld, I. Tavernelli and U. Rothlisberger, *Phys. Rev. B: Condens. Matter Mater. Phys.*, 2007, **75**, 205131.
242 E. Tapavicza, I.-C. Lin, O. A. von Lilienfeld, I. Tavernelli, M. D. Coutinho-Neto and U. Rothlisberger, *J. Chem. Theory Comput.*, 2007, **3**, 1673–1679.
243 I.-C. Lin, A. P. Seitsonen, M. D. Coutinho-Neto, I. Tavernelli and U. Rothlisberger, *J. Phys. Chem. B*, 2009, **113**, 1127–1131.
244 IBM Corporation and Max-Planck-Institut für Festkörperforschung, Stuttgart, *CPMD*, http://www.cpmd.org/, date accessed: 2018-12-03.
245 A. Ambrosetti, A. M. Reilly, R. A. DiStasio and A. Tkatchenko, *J. Chem. Phys.*, 2014, **140**, 18A508.
246 W. L. Bade, *J. Chem. Phys.*, 1957, **27**, 1280–1284.
247 F. Wang and K. D. Jordan, *J. Chem. Phys.*, 2001, **114**, 10717–10724.
248 A. P. Jones, J. Crain, V. P. Sokhan, T. W. Whitfield and G. J. Martyna, *Phys. Rev. B: Condens. Matter Mater. Phys.*, 2013, **87**, 144103.
249 V. P. Sokhan, A. P. Jones, F. S. Cipcigan, J. Crain and G. J. Martyna, *Proc. Natl. Acad. Sci. U. S. A.*, 2015, **112**, 6341–6346.
250 K. T. Tang and M. Karplus, *Phys. Rev.*, 1968, **171**, 70–74.
251 F. L. Hirshfeld, *Theor. Chim. Acta*, 1977, **44**, 129–138.
252 R. A. DiStasio, V. V. Gobre and A. Tkatchenko, *J. Phys.: Condens. Matter*, 2014, **26**, 213202.
253 T. Bucko, S. Lebègue, J. G. Ángyán and J. Hafner, *J. Chem. Phys.*, 2014, **141**, 034114.
254 W. L. Bade and J. G. Kirkwood, *J. Chem. Phys.*, 1957, **27**, 1284–1288.
255 G. D. Mahan, *J. Chem. Phys.*, 1965, **43**, 1569–1574.
256 A. A. Lucas, *Physica*, 1967, **35**, 353–368.
257 M. Renne and B. Nijboer, *Chem. Phys. Lett.*, 1967, **1**, 317–320.
258 A. G. Donchev, *J. Chem. Phys.*, 2006, **125**, 074713.
259 H.-Y. Kim, J. O. Sofo, D. Velegol, M. W. Cole and A. A. Lucas, *J. Chem. Phys.*, 2006, **124**, 074504.
260 M. W. Cole, D. Velegol, H.-Y. Kim and A. A. Lucas, *Mol. Simul.*, 2009, **35**, 849–866.
261 J. Hermann and A. Tkatchenko, *J. Chem. Theory Comput.*, 2018, **14**, 1361–1369.
262 M. A. Blood-Forsythe, T. Markovich, R. A. DiStasio, R. Car and A. Aspuru-Guzik, *Chem. Sci.*, 2016, **7**, 1712–1728.
263 T. Bučko, S. Lebègue, T. Gould and J. G. Ángyán, *J. Phys.: Condens. Matter*, 2016, **28**, 045201.
264 P. W. Ayers, *J. Chem. Phys.*, 2000, **113**, 10886–10898.
265 P. Bultinck, C. Van Alsenoy, P. W. Ayers and R. Carbó-Dorca, *J. Chem. Phys.*, 2007, **126**, 144111.
266 T. Bučko, S. Lebègue, J. Hafner and J. G. Ángyán, *J. Chem. Theory Comput.*, 2013, **9**, 4293–4299.
267 T. Gould, S. Lebègue, J. G. Ángyán and T. Bučko, *J. Chem. Theory Comput.*, 2016, **12**, 5920–5930.
268 F. London, *Trans. Faraday Soc.*, 1937, **33**, 8b.
269 F. London, *Z. Phys.*, 1930, **63**, 245–279.
270 T. W. Whitfield and G. J. Martyna, *Chem. Phys. Lett.*, 2006, **424**, 409–413.

271 A. P. Jones, A. Thompson, J. Crain, M. H. Müser and G. J. Martyna, *Phys. Rev. B: Condens. Matter Mater. Phys.*, 2009, **79**, 144119.
272 A. P. Jones, F. S. Cipcigan, V. P. Sokhan, J. Crain and G. J. Martyna, *Phys. Rev. Lett.*, 2013, **110**, 227801.
273 C. Fonseca Guerra, J. G. Snijders, G. te Velde and E. J. Baerends, *Theor. Chem. Acc.*, 1998, **99**, 391–403.
274 G. te Velde, F. M. Bickelhaupt, E. J. Baerends, C. Fonseca Guerra, S. J. A. van Gisbergen, J. G. Snijders and T. Ziegler, *J. Comput. Chem.*, 2001, **22**, 931–967.
275 E. J. Baerends *et al.*, *ADF, SCM, Theoretical Chemistry, Vrije Universiteit, Amsterdam, The Netherlands*, https://www.scm.com, date accessed: 2018-12-03.
276 S. J. Clark, M. D. Segall, C. J. Pickard, P. J. Hasnip, M. I. J. Probert, K. Refson and M. C. Payne, *Z. Kristallogr. – Cryst. Mater.*, 2005, **220**, 567–570.
277 Q. Wu and W. Yang, *J. Chem. Phys.*, 2002, **116**, 515–524.
278 J. Tao, J. P. Perdew and A. Ruzsinszky, *Phys. Rev. B: Condens. Matter Mater. Phys.*, 2010, **81**, 233102.
279 J. Tao, J. P. Perdew and A. Ruzsinszky, *Proc. Natl. Acad. Sci. U. S. A.*, 2012, **109**, 18–21.
280 P. L. Silvestrelli, *Phys. Rev. Lett.*, 2008, **100**, 053002.
281 P. L. Silvestrelli, K. Benyahia, S. Grubisiĉ, F. Ancilotto and F. Toigo, *J. Chem. Phys.*, 2009, **130**, 074702.
282 K. T. Tang, *Phys. Rev.*, 1969, **177**, 108–114.
283 T. Brinck, J. S. Murray and P. Politzer, *J. Chem. Phys.*, 1993, **98**, 4305–4306.
284 D. V. Fedorov, M. Sadhukhan, M. Stöhr and A. Tkatchenko, *Phys. Rev. Lett.*, 2018, **121**, 183401.
285 M. Stöhr, G. S. Michelitsch, J. C. Tully, K. Reuter and R. J. Maurer, *J. Chem. Phys.*, 2016, **144**, 151101.
286 R. Petraglia, S. N. Steinmann and C. Corminboeuf, *Int. J. Quantum Chem.*, 2015, **115**, 1265–1272.
287 V. G. Ruiz, W. Liu, E. Zojer, M. Scheffler and A. Tkatchenko, *Phys. Rev. Lett.*, 2012, **108**, 146103.
288 J. Carrasco, W. Liu, A. Michaelides and A. Tkatchenko, *J. Chem. Phys.*, 2014, **140**, 084704.
289 W. Liu, F. Maaß, M. Willenbockel, C. Bronner, M. Schulze, S. Soubatch, F. S. Tautz, P. Tegeder and A. Tkatchenko, *Phys. Rev. Lett.*, 2015, **115**, 036104.
290 R. J. Maurer, V. G. Ruiz, J. Camarillo-Cisneros, W. Liu, N. Ferri, K. Reuter and A. Tkatchenko, *Prog. Surf. Sci.*, 2016, **91**, 72–100.
291 V. G. Ruiz, W. Liu and A. Tkatchenko, *Phys. Rev. B*, 2016, **93**, 035118.
292 A. D. Becke and M. R. Roussel, *Phys. Rev. A: At., Mol., Opt. Phys.*, 1989, **39**, 3761–3767.
293 A. D. Becke and E. R. Johnson, *J. Chem. Phys.*, 2005, **123**, 154101.
294 A. D. Becke and E. R. Johnson, *J. Chem. Phys.*, 2007, **127**, 154108.
295 A. Otero-de-la-Roza and E. R. Johnson, *J. Chem. Phys.*, 2013, **138**, 054103.
296 B. M. Axilrod and E. Teller, *J. Chem. Phys.*, 1943, **11**, 299–300.
297 Y. Muto, *Phys.-Math. Soc. Jpn.*, 1943, **17**, 629.
298 M. T. Cvitaš, P. Soldán and J. M. Hutson, *Mol. Phys.*, 2006, **104**, 23–31.
299 W. Cencek, M. Jeziorska, O. Akin-Ojo and K. Szalewicz, *J. Phys. Chem. A*, 2007, **111**, 11311–11319.
300 O. Anatole von Lilienfeld and A. Tkatchenko, *J. Chem. Phys.*, 2010, **132**, 234109.
301 A. M. Reilly and A. Tkatchenko, *J. Chem. Phys.*, 2013, **139**, 024705.
302 J. Řezáč, Y. Huang, P. Hobza and G. J. O. Beran, *J. Chem. Theory Comput.*, 2015, **11**, 3065–3079.
303 G. J. O. Beran, *Chem. Rev.*, 2016, **116**, 5567–5613.
304 K. T. Tang and J. P. Toennies, *J. Chem. Phys.*, 1984, **80**, 3726–3741.
305 S. N. Steinmann and C. Corminboeuf, *J. Chem. Theory Comput.*, 2010, **6**, 1990–2001.
306 S. N. Steinmann and C. Corminboeuf, *J. Chem. Phys.*, 2011, **134**, 044117.
307 P. Bultinck, D. L. Cooper and R. Ponec, *J. Phys. Chem. A*, 2010, **114**, 8754–8763.
308 S. Ehrlich, J. Moellmann, W. Reckien, T. Bredow and S. Grimme, *ChemPhysChem*, 2011, **12**, 3414–3420.
309 E. Caldeweyher, C. Bannwarth and S. Grimme, *J. Chem. Phys.*, 2017, **147**, 034112.
310 G. Starkschall and R. G. Gordon, *J. Chem. Phys.*, 1972, **56**, 2801–2806.
311 A. J. Thakkar, H. Hettema and P. E. S. Wormer, *J. Chem. Phys.*, 1992, **97**, 3252–3257.
312 J.-D. Chai and M. Head-Gordon, *Phys. Chem. Chem. Phys.*, 2008, **10**, 6615.
313 B. Aradi, *GitHub – aradi/dftd3-lib: Library version of S. Grimmes DFTD3 code*, https://github.com/aradi/dftd3-lib.
314 M. J. Frisch *et al.*, *Gaussian 16*, 2016, http://gaussian.com/.
315 F. O. Kannemann and A. D. Becke, *J. Chem. Theory Comput.*, 2010, **6**, 1081–1088.
316 A. Otero-de-la-Roza and E. R. Johnson, *J. Chem. Phys.*, 2013, **138**, 204109.
317 M. Valiev, E. Bylaska, N. Govind, K. Kowalski, T. Straatsma, H. Van Dam, D. Wang, J. Nieplocha, E. Apra, T. Windus and W. de Jong, *Comput. Phys. Commun.*, 2010, **181**, 1477–1489.
318 P. Jurečka, J. Šponer, J. Černý and P. Hobza, *Phys. Chem. Chem. Phys.*, 2006, **8**, 1985–1993.
319 J. Řezáč, K. E. Riley and P. Hobza, *J. Chem. Theory Comput.*, 2011, **7**, 2427–2438.
320 J. Řezáč, K. E. Riley and P. Hobza, *J. Chem. Theory Comput.*, 2011, **7**, 3466–3470.
321 K. Berka, R. Laskowski, K. E. Riley, P. Hobza and J. Vondrášek, *J. Chem. Theory Comput.*, 2009, **5**, 982–992.
322 J. Řezáč and P. Hobza, *J. Chem. Theory Comput.*, 2012, **8**, 141–151.
323 J. Řezáč, K. E. Riley and P. Hobza, *J. Chem. Theory Comput.*, 2012, **8**, 4285–4292.
324 J. Řezáč and P. Hobza, *J. Chem. Theory Comput.*, 2013, **9**, 2151–2155.
325 L. Gráfová, M. Pitoňák, J. Řezáč and P. Hobza, *J. Chem. Theory Comput.*, 2010, **6**, 2365–2376.

326 J. Moellmann and S. Grimme, *Phys. Chem. Chem. Phys.*, 2010, **12**, 8500.
327 A. Otero-de-la-Roza and E. R. Johnson, *J. Chem. Phys.*, 2012, **137**, 054103.
328 A. M. Reilly and A. Tkatchenko, *J. Phys. Chem. Lett.*, 2013, **4**, 1028–1033.
329 A. Otero-de-la-Roza and E. R. Johnson, *J. Chem. Theory Comput.*, 2015, **11**, 4033–4040.
330 S. Grimme, *Chem. – Eur. J.*, 2012, **18**, 9955–9964.
331 T. Risthaus and S. Grimme, *J. Chem. Theory Comput.*, 2013, **9**, 1580–1591.
332 J. Calbo, E. Ortí, J. C. Sancho-García and J. Aragó, *J. Chem. Theory Comput.*, 2015, **11**, 932–939.
333 J. Antony, R. Sure and S. Grimme, *Chem. Commun.*, 2015, **51**, 1764–1774.
334 R. Sedlak, T. Janowski, M. Pitoňák, J. Řezáč, P. Pulay and P. Hobza, *J. Chem. Theory Comput.*, 2013, **9**, 3364–3374.
335 K. Lejaeghere, *et al.*, *Science*, 2016, **351**, aad3000.
336 D.-K. Bučar, R. W. Lancaster and J. Bernstein, *Angew. Chem., Int. Ed.*, 2015, **54**, 6972–6993.
337 Y. S. Al-Hamdani, M. Rossi, D. Alfè, T. Tsatsoulis, B. Ramberger, J. G. Brandenburg, A. Zen, G. Kresse, A. Grüneis, A. Tkatchenko and A. Michaelides, *J. Chem. Phys.*, 2017, **147**, 044710.
338 J. Sun, A. Ruzsinszky and J. P. Perdew, *Phys. Rev. Lett.*, 2015, **115**, 036402.
339 T. Björkman, *J. Chem. Phys.*, 2014, **141**, 074708.
340 Y. S. Al-Hamdani, D. Alfè and A. Michaelides, *J. Chem. Phys.*, 2017, **146**, 094701.
341 J. F. Dobson, K. McLennan, A. Rubio, J. Wang, T. Gould, H. M. Le and B. P. Dinte, *Aust. J. Chem.*, 2001, **54**, 513–527.
342 J. F. Dobson, T. Gould and G. Vignale, *Phys. Rev. X*, 2014, **4**, 021040.
343 L. N. Krasnoperov, J. Peng and P. Marshall, *J. Phys. Chem. A*, 2006, **110**, 3110–3120.
344 Y. Georgievskii and S. J. Klippenstein, *J. Phys. Chem. A*, 2007, **111**, 3802–3811.
345 M. Bowker, *Top. Catal.*, 2016, **59**, 663–670.
346 A. M. Reilly and A. Tkatchenko, *Phys. Rev. Lett.*, 2014, **113**, 55701.
347 J. Witte, M. Goldey, J. B. Neaton and M. Head-Gordon, *J. Chem. Theory Comput.*, 2015, **11**, 1481–1492.
348 M. Rossi, V. Blum, P. Kupser, G. von Helden, F. Bierau, K. Pagel, G. Meijer and M. Scheffler, *J. Phys. Chem. Lett.*, 2010, **1**, 3465–3470.
349 A. Tkatchenko, M. Rossi, V. Blum, J. Ireta and M. Scheffler, *Phys. Rev. Lett.*, 2011, **106**, 118102.
350 F. Schubert, K. Pagel, M. Rossi, S. Warnke, M. Salwiczek, B. Koksch, G. von Helden, V. Blum, C. Baldauf and M. Scheffler, *Phys. Chem. Chem. Phys.*, 2015, **17**, 5376–5385.
351 F. Schubert, M. Rossi, C. Baldauf, K. Pagel, S. Warnke, G. von Helden, F. Filsinger, P. Kupser, G. Meijer, M. Salwiczek, B. Koksch, M. Scheffler and V. Blum, *Phys. Chem. Chem. Phys.*, 2015, **17**, 7373–7385.
352 C. Baldauf and M. Rossi, *J. Phys.: Condens. Matter*, 2015, **27**, 493002.
353 J. Schmidt, J. VandeVondele, I.-F. W. Kuo, D. Sebastiani, J. I. Siepmann, J. Hutter and C. J. Mundy, *J. Phys. Chem. B*, 2009, **113**, 11959–11964.
354 A. Møgelhøj, A. K. Kelkkanen, K. T. Wikfeldt, J. Schiøtz, J. J. Mortensen, L. G. M. Pettersson, B. I. Lundqvist, K. W. Jacobsen, A. Nilsson and J. K. Nørskov, *J. Phys. Chem. B*, 2011, **115**, 14149–14160.
355 R. Jonchiere, A. P. Seitsonen, G. Ferlat, A. M. Saitta and R. Vuilleumier, *J. Chem. Phys.*, 2011, **135**, 154503.
356 Y. Wang, C.-Y. Yam, T. Frauenheim, G. Chen and T. Niehaus, *Chem. Phys.*, 2011, **391**, 69–77.
357 R. A. DiStasio, B. Santra, Z. Li, X. Wu and R. Car, *J. Chem. Phys.*, 2014, **141**, 084502.
358 G. Tocci, L. Joly and A. Michaelides, *Nano Lett.*, 2014, **14**, 6872–6877.
359 W. Gao, Y. Chen and Q. Jiang, *Phys. Rev. Lett.*, 2016, **117**, 246101.
360 M. Shahbaz and K. Szalewicz, *Phys. Rev. Lett.*, 2018, **121**, 113402.
361 M. Shahbaz and K. Szalewicz, *Theor. Chem. Acc.*, 2019, **138**, 25.
362 M. Sadhukhan and A. Tkatchenko, *Phys. Rev. Lett.*, 2017, **118**, 210402.
363 A. Kleshchonok and A. Tkatchenko, *Nat. Commun.*, 2018, **9**, 3017.
364 J. T. Kindt and C. A. Schmuttenmaer, *J. Chem. Phys.*, 1999, **110**, 8589–8596.
365 C. A. Schmuttenmaer, *Chem. Rev.*, 2004, **104**, 1759–1780.

